POLITECNICO DI TORINO

Department of Electronics and Telecommunications

Master's Degree Course

in Electronic Engineering

Master's Degree Thesis

Advanced waveguide antennas for automotive radar

Supervisor

Riccardo Maggiora

Co-supervisor

Giuseppe Virone

Candidate

Andi Aga (281743)

Academic Year 2022/2023

Declaration

I attest that I am the sole author of this thesis and that all the work included in it is original and entirely my own, unless stated otherwise. I further declare that I am the rightful owner of the copyright to the work, and that I have not submitted it previously in full or in part to obtain any other qualification.

Abstract

The objective of this thesis work is to look into the design and development a 3D slotted waveguide antenna for automotive radar application working at around 77-81 GHz. The antenna is based on the WR10 of reduced height rectangular waveguide with longitudinal slots cut on top of it, which provide the apertures through which the EM energy can be radiated. Different types of feedings for the antenna are presented, including a microstrip and a waveguide feeding, in which an L-transition between a WR12 and WR10 with reduced height is also designed to satisfy the Launcher On Package technology. Ultimately, an array of antennas is designed taking in consideration the L-transition, the dimensions of the single antennas and the characteristics of arrays for radar application. The proposed designs are done using CST Microwave Studio simulation tool, which is a reliable and widely used EM design software. The results yielded from the software, among other parameters, include the s-parameters, radiation efficiencies, and the radiation pattern.
An optimization process followed the designs, which involved an extensive adjustment of various dimensions and structures of the antenna, together with continuous simulations of these adjustments. Based on the simulation results, the design is tweaked to fit automotive radar requirements and usage.

Acknowledgments

The author expresses gratitude to the individuals listed below for their valuable contribution to this project.

- Prof. Riccardo Maggiora for giving me the opportunity to work on this topic.
- Prof. Giuseppe Virone for providing the initial design of the slotted waveguide antenna.
- Gianluca Dassano for being always ready to assist whenever asked and for helping with the different features of the CST Microwave software.

List of Figures

Table of Contents

Abbreviations

CST – CST Microwave Studio (Electromagnetic simulation tool)

EM - Electromagnetic

TE – Transverse Electric

TM – Transverse Magnetic

TEM – Transverse Electro-Magnetic

λ_0 – Free-Space Wavelength

f_0 – Operating Frequency

f_c – Cutoff Frequency

λ_g – Guiding Wavelength

SLR – Side Lobe Ratio (Measure of the level of radiation from the side lobes relative to the main lobe)

LOP – Launcher On Package

Chapter 1: Introduction

"Radio detection and ranging", most commonly known as radar is one of the most important inventions of the last century. Most of the work on developing the radar began in the 1930s, but the idea behind it was posed much before by Hertz in the 1880s. Hertz was proving the ideas formulated by Maxwell that radio waves and light waves are actually ruled by the same EM laws but have different operating frequencies. This work concluded that radio waves can be reflected and refracted from objects in the same way that the light waves do.

This discovery was so important that in fact it went on to determine the fate of the second World War. It played a critical role in detecting enemy aircrafts and ships, which was a major factor in the outcome of the conflict.

The radar works on the principle of wave scattering. Basically, radio waves are transmitted into a desired direction and when they hit an obstacle, part of the waves are reflected back (called echo) and collected by the radar antenna as in Fig. 1.1.

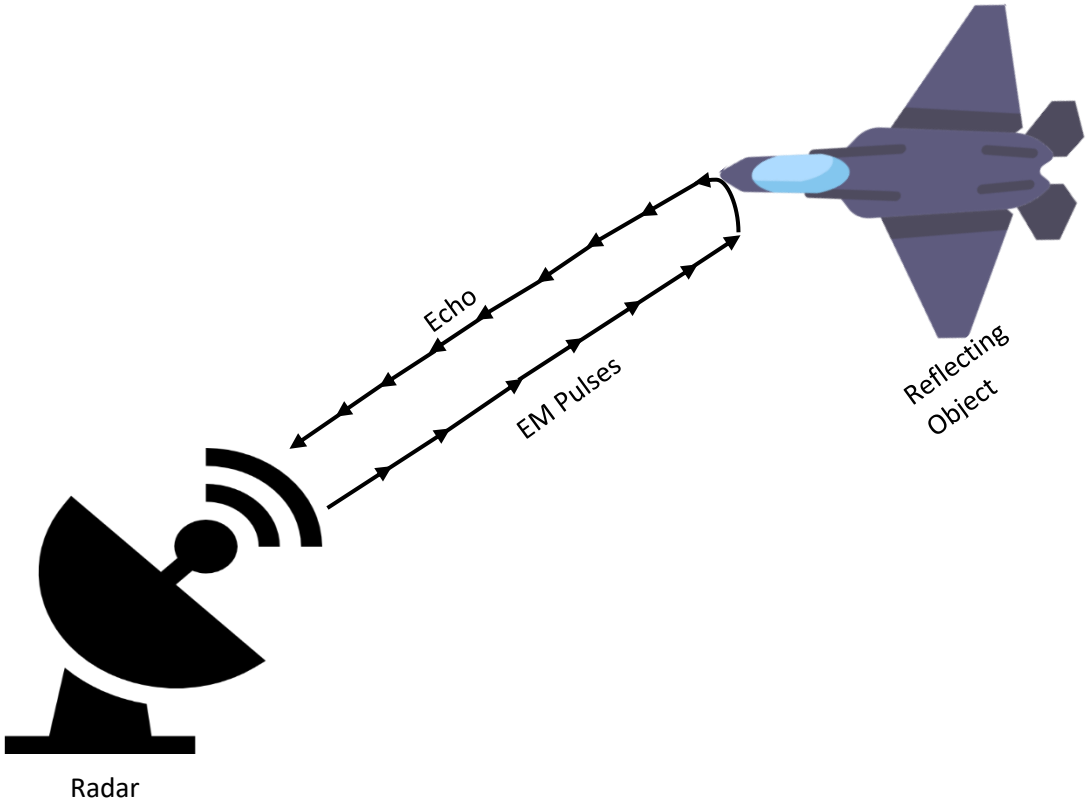

Figure 1.1: Working principle of a radar.

The echoes' characteristics, including the time it takes for the signal to travel to the object and back, as well as the strength of the reflection, can be processed in such a way that you can obtain useful information about the object, such as:

- distance (range)
- angle
- velocity

Despite it initially being used for military purposes, radars went on to evolve and be used on many other fields, including:

- Meteorology (Doppler weather radar) by measuring the speed and direction of winds and precipitation.
- Satellite-surveillance by tracking satellites, debris, and other objects in the orbit.
- Archeology, mineral exploration by using ground-probing radars to investigate subsurface structures and features like rock formations.
- Geographical mapping by imaging the surface of planets.
- Air-traffic control by tracking aircrafts
- Ground-traffic control by monitoring and controlling the movement of vehicles on roads and highways, such that you can control the traffic flow and detect collisions and congestions.
- Space

Overall, radar is a powerful and versatile technology that has played a vital role in shaping the world we live in today, offering a wide range of applications. It continues to evolve and advance by having more sophisticated and efficient ways of detecting and locating objects, making it an integral part of our daily lives.

1.1 Automotive radars

Automotive radars have nowadays become an integral part of newly produced vehicles. They are the most important sensor used in the adaptive cruise control (ACC) as well as in autonomous driving assistance systems (ADAS). With the advancement in technology, automotive radars have become able to not only detect vehicles, but also pedestrians, animals and other road obstacles. These capacities play a major role in collision-avoidance and in making the driver more conscious of the surrounding environment. The ability of the automotive radar to detect and track objects in the vicinity of the vehicle as well as in long distances ensures the safety and comfort of the driver and reduces the number of accidents on the road.

Depending on the usage, automotive radars are divided into two groups:

- Short-range radar (SRR): These radar applications include parking assistance with a range of 1.8m, sensing before crash, blind spot detection, lane change assistant, obstacle detection, etc. The latter operations can be performed within a 30m range. They are typically mounted on the rear, front and sides of the vehicle to have a full 360° view of the surroundings, avoiding blind spots and are often used in conjunction with other sensors like cameras. They have a large field of view and a high resolution (ability to distinguish objects that are in close proximity to each other). [1]
- Long-range radar (LRR): They have a longer range of application of around 80-200m and a smaller resolution, which is enough for operations like automatic emergency breaking, adaptive cruise control (maintain a safe following distance and stay within the speed limit), or forward collision

warning. They have a small field of view and are typically mounted in the front of the vehicle.

The frequency of operation for automotive radar systems can vary, with some systems using frequencies around 24 GHz, while others use frequencies around 77 GHz. [2] It's important to note that the resolution of the radar is inversely proportional to the wavelength of operation, meaning that higher frequency radars have a higher resolution. Moreover, the size of the radar antenna is directly proportional to the wavelength, which means that higher frequency radars can have smaller antennas (as shown in Figure 1.2). This can make it easier to mount the radar device on a vehicle without adding significant weight or bulk. The shorter wavelength of 77 GHz systems can lead also to less propagation losses due to rainfall and dust. However, there are some trade-offs to consider, such as the increased cost and complexity associated with higher frequency radar systems. Nonetheless, the benefits of improved resolution and smaller antenna size make higher frequency radar systems a promising technology for enhancing automotive safety and improving driver assistance features.

The different ranges of automotive radars are given in Fig. 1.3.

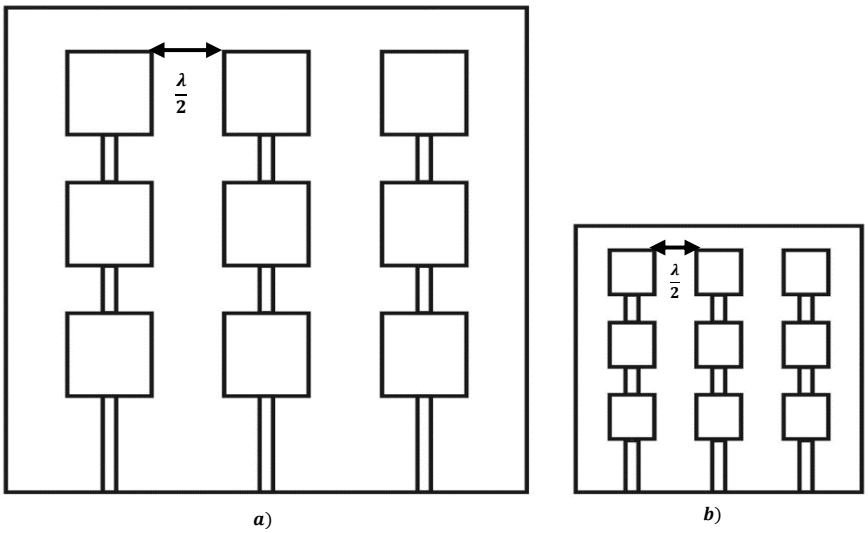

Figure 1.2: Schematic of an array antenna configuration. (a) 24 GHz, (b) 77 GHz.

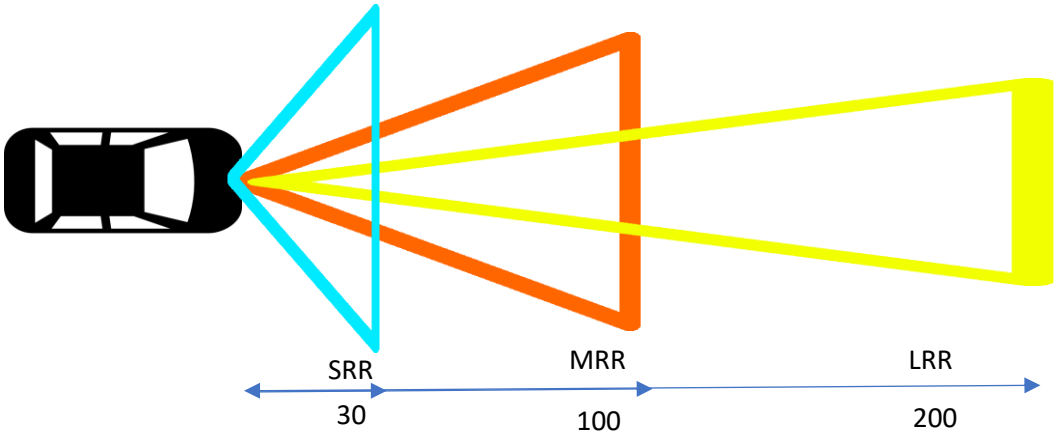

Figure 1.3 (a): Different operating ranges of automotive radars.

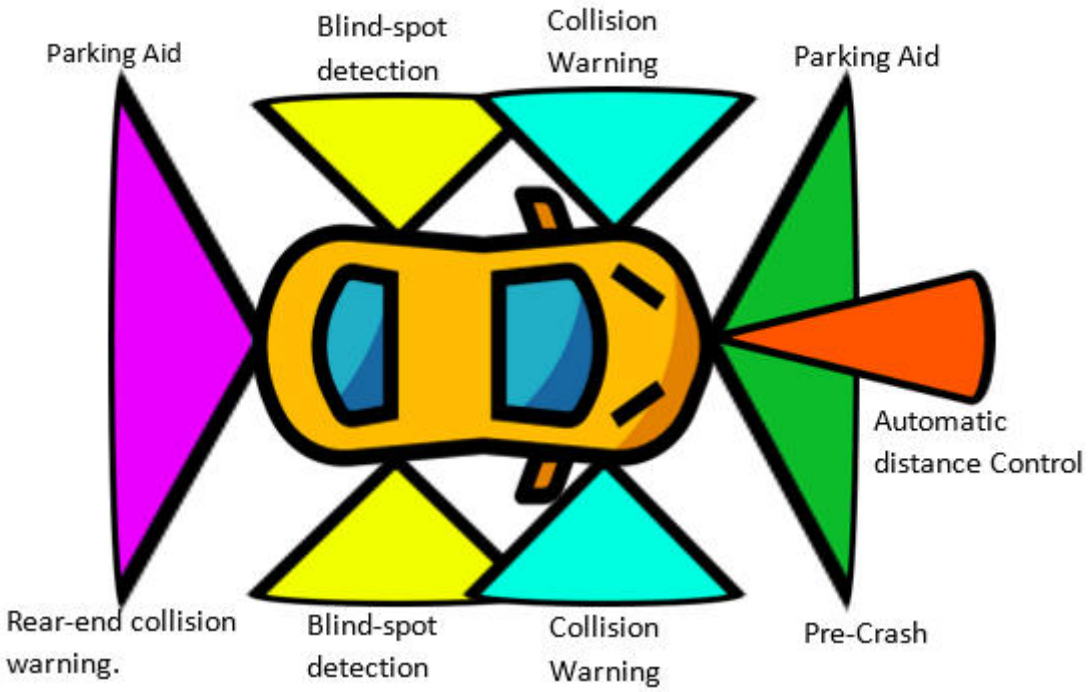

Figure 1.3 (b):Different operations of an automotive radar.

In fact, it is decided that by the year 2022, the 24 GHz operating frequency will be phased out in both Europe and the US due to spectrum regulation by the Federal Communications Commission and the European Telecommunications Standards Institute. This shift is being made in order to promote the use of 77 GHz automotive radar systems, which offer superior performance and are supported by an international standard. While this change does bring some design complexities that can make production challenging, the long-term benefits of using 77 GHz radar systems outweigh these challenges and make them a good choice for the future.

Considering all of these details, this thesis work aims at the design of an antenna for automotive radar working at high frequencies (77-81 GHz).

Chapter 2: Printed antenna vs 3D antenna radars

Radar antennas can be classified in two main categories: printed antennas and 3D waveguide antennas. Each of these types of antennas have unique characteristics and are used in numerous different applications. They will be discussed in more detail in the following chapters. But first, an introductory description of the main antenna properties is needed.

2.1 Main antenna properties

The following gives a definition of the main antenna properties that will be discussed and studied.

- ***Antenna pattern***: It is often called the radiation pattern or far field pattern or directivity and is a graphical representation of the radiation properties of an antenna, showing how the antenna receives/radiates energy in certain direction. In other words, it displays a directional dependance of the radiation/reception strength of the antenna. The radiation happens in every direction, even though very little in some parts, so an amplitude and phase description of the emission is done [3]. It can be represented in a 2D, or a three-dimensional format. In the 3D format, one parameter defines the amplitude and the other two define the angles of operation. To have a full understanding of the description, 2 terms have to be introduced: azimuth plane and elevation plane.
  When describing an antenna pattern, the antenna is assumed mounted in the direction that it will be used. The *azimuthal* plane refers to the horizontal plane with respect to the plane of mounting, whereas the *elevation* plane refers to the vertical plane. As shown in Fig. 2.1, the azimuthal plane is comprised of angles θ of the horizontal plane, varying from 0 to 360°. On the other hand, the elevation plane has angles φ. The antenna patterns for the azimuthal and elevation planes are usually given in polar plots, besides the cartesian one. The azimuth and elevation parameters can be controlled by using mechanisms (such as motors) to adjust the position of the antenna. The ability to control these parameters is important in allowing to have a specific direction of the beam, and to detect targets in a specific area.

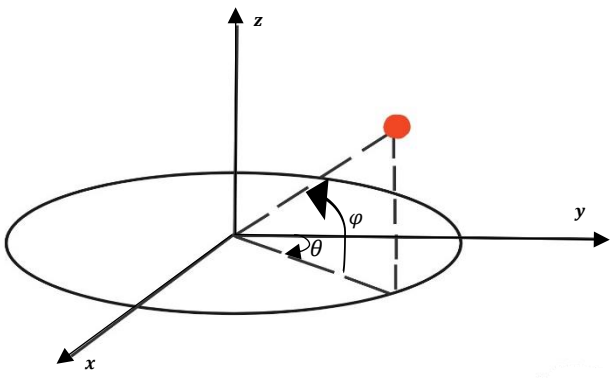

Figure 2. 1: Azimuthal and elevation angles.

The directivity measures the concentration of radiated power in a particular direction. It is given in a plot, where the x-axis shows the direction, and the y-axis shows the intensity, The directivity pattern in working antennas has a peak (main lobe) and is surrounded by lower ones (side lobes) in the sides. Usually, the side lobes are preferred to be small in order to minimize interferences and reduce false positives. An example is given in Fig. 2.2

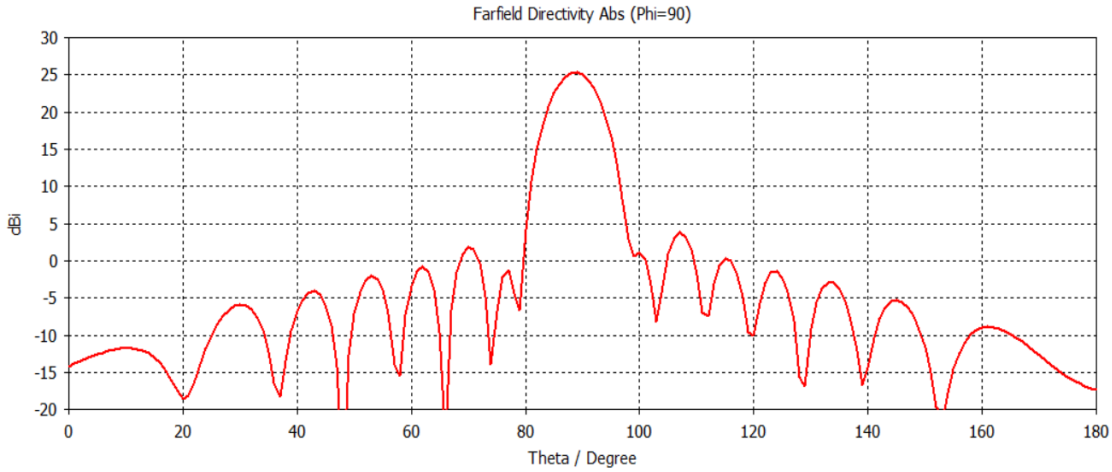

Figure 2.2: Directivity pattern, showing the main lobe and side lobes for angles theta from 0 to 180°

- The ***operating frequency*** is very important as it determines the wavelength of operation of the radar, which in turn affects the range and resolution, as well as the interactions with the environment.
- The ***range*** of a radar defines the ability to detect targets at a certain distance. Most of automotive radar systems go up to 200m (LRR).
- The ***spatial resolution*** defines the ability to distinguish between two objects that are close to each other. Usually, automotive radar systems have a high spatial resolution in order to detect multiple targets. The spatial resolution is affected by the antenna beamwidth. The beamwidth is a measure of the main lobe of the antenna radiation pattern. A narrow beamwidth corresponds to a more directional radar system and a higher resolution.
- The ***gain*** is also a parameter which depends on the direction. It is given as the ratio of the power density radiated by the antenna in a certain direction to the power density that would be radiated by a reference antenna, which is an isotropic one (same power radiation in all directions). The gain expressed in dBi units is often employed, which means decibels with respect to the isotropic antenna.
- The ***power output*** affects the range of the system. Usually, automotive radars have a lower power output than other types of radars to comply with regulations, have safety and minimize the power density of the signal.
- ***Signal-to-noise ratio (SNR)*** is the ratio between the amplitude of the desired signal to that of the noise signals. Higher the SNR, better the antenna.
- ***Radiation efficiency*** is a measure of how well an antenna converts the input fed power into radiated power. Low radiation efficiency is usually due to internal losses, such as dielectric and magnetic losses, as well as the design techniques, materials, size and shape of the antenna.

- ***Reflection coefficient*** (s-parameter) quantifies how much of an EM wave is reflected from the antenna. The s-parameter is simulated beforehand to predict the performance of the system and tune it to achieve the desired performance.
- ***Insertion loss*** is the loss that occurs when a signal is travelling through a component. The main causes of insertion loss are reflected losses, dielectric losses (power dissipated in dielectric materials) and copper losses (due to conducting surfaces).
- The ***immunity to interferences*** is very important in the functioning of an antenna system in presence of unwanted interferences. Automotive radars have a high immunity to interferences such as dust, wind, rain. This immunity can be achieved through techniques such as frequency diversity, time diversity and spatial diversity.
- ***Adaptability*** includes the ability of the radar system to adjust their radiation pattern, frequency, output in response to the environment and situation. This way the performance can be optimized in different cases and scenarios.

2.1.1 Note about the scattering parameters

In this work, a huge interest will be shown on the optimization of the scattering parameters. A small introduction to these parameters will be given in the following.

The scattering parameters give a description of the behavior of an N-port network in response to incident signals. These parameters represent the amount of energy that is transferred from one port to another. In their definition, they have two subscripts, each referring to a port. The first one refers to the receiving port, whereas the second one refers to the incident port.

The main scattering parameter that will be discussed in this thesis work is the S11 parameter, also known as the "reflection coefficient", which measures the amount of power that is reflected back to the input port. The S11 parameter is desired to be as close to 0 as possible at the desired frequency of operation, thus having a very small reflected power. The majority of the input power is transmitted over the network. Example: If 20 dB of power is delivered to a network through port 1, and the s11 parameter is equal to -18 dB, 2 dB correspond to the reflected power.

Another widely discussed scattering parameter is the S12 or S21 parameter. These parameters, also known as the "insertion loss", represents the amount of energy a signal loses when it passes through a network. Ideally, the S12 parameter is desired to be as close to 1 as possible, meaning that the network has a good level of isolation, and there is minimal interference or coupling between its ports.

2.2 Introduction to printed antennas

Printed antennas, as the name suggests, use printed circuits like:

- microstrip lines
- coplanar lines
- slot lines

to achieve radiation. The general fabrication technique of these type of antennas is by using optical lithography, meaning using light to produce thin films of desired materials over a substrate (usually dielectric), which on the other side is bounded by a metal layer acting as a ground plane. Printed antennas are of different types and usually differ on their geometry and the feeding which excites the radiating element.

A general description of the advantages and disadvantages of printed antennas is given below.

Advantages include:

- small dimensions (proportional to the wavelength), meaning a light weight.
- ease of integrability with other electronic components since they have a low profile and are lightweight.
- possibility to use them in arrays (multiple antenna elements on a common substrate) to achieve much higher gains.
- ease of manufacturing with today's technology, meaning large quantities can be produced at low prices.
- robustness, making it suitable for numerous applications.

On the other hand, some of the downsides include:

- low efficiency, due to losses in the substrate (dielectric losses) and losses on the feeding.
- usually narrow bandwidth (some percent of the operating frequency).
- inability to have high polarization levels, due to the need of large ground planes or good conducting surfaces and the need of precision shaping.
- susceptibility to nearby objects.

Although these disadvantages, printed antennas have found use in many fields, including mobile communication, television, medicine, telecommunication, space, radars, and are still being used today in frequencies ranging from radio (UHF: 300-3000 MHz) up to millimeter wave (EHF: 30-300 GHz).

The most used microstrip antenna in printed circuit boards is the rectangular patch antenna. It consists of a conducting patch of length L and width W, placed on top of a substrate (dielectric) of thickness h and relative permittivity ε_r, as shown in Fig. 2.3. It should be noted that the thickness should be much smaller than the operating wavelength, but not be too small to not have a degraded efficiency. The frequency of

operation of the patch antenna is inversely proportional to the length of the patch, and is given by the following formula:

$$f_c = \frac{c}{2*L*\sqrt{\varepsilon_r}}$$

, where c is the speed of light, L is the length of the patch and ε_r is the relative permittivity. There are fringing fields underneath the patch, which become responsible for the radiation. These fields also cause a shift on the operating frequency of the antenna, making the patch seem a higher length [4], thus reducing the operating frequency. Small trimming of the patch may be required in order to have a resonance in the desired frequency.

The feeding is usually done through a microstrip transmission line (feedline), as illustrated in Fig. 2.3. Current flows through it and becomes maximum at the middle of the patch, and zero at the start and end of it. This rectangular shape results in a broadside radiation pattern, meaning a maximum radiation of energy perpendicular to the surface of the patch.

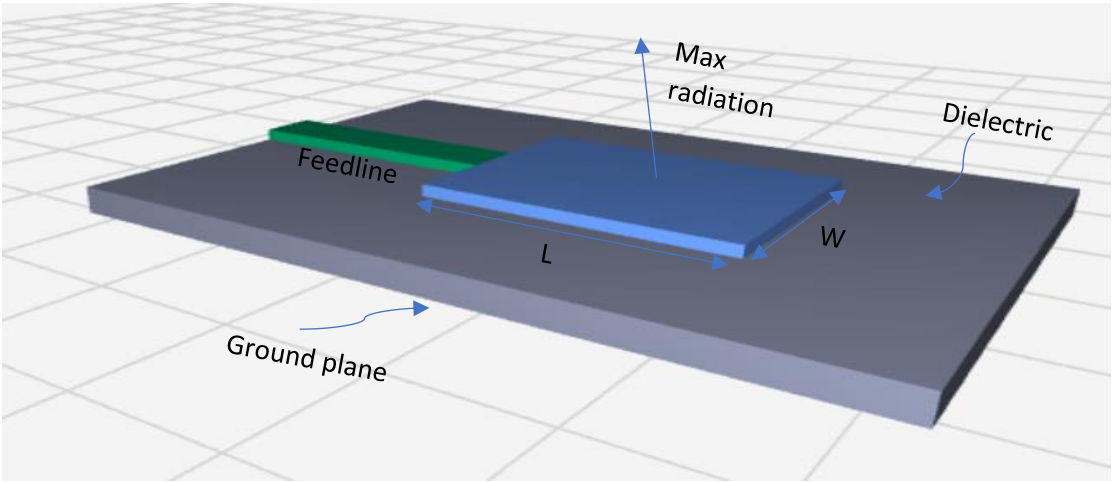

Figure 2.3: Rectangular patch antenna

2.2.1 Note about the relative permittivity

The relative permittivity of a dielectric material, also known as the dielectric constant or the electric constant, is a measure of its ability to store electrical energy in an electric field. Mathematically, it can be expressed as a ratio:

$$\varepsilon_r = \frac{\varepsilon}{\varepsilon_0}$$

, where ε_r is the relative permittivity, ε is the permittivity of the material, and ε_0 is the permittivity on free space (also known as the vacuum permittivity). These two parameters are given in units of Farad/meter. Being a ratio of two same types of parameters, the relative permittivity is a dimensionless quantity. Materials with high relative permittivity can store more electrical energy in an electric field than materials with low relative permittivity.

The relative permittivity of a dielectric material can vary depending on factors such as temperature, frequency, and the composition of the material. For example, the relative

permittivity of common dielectric materials used in electrical insulation can range from close to 1 for air or vacuum, to several thousand for materials such as ceramics or certain polymers.

Another important aspect of the relative permittivity is its effect on the speed of propagation of a wave through a medium. The speed of propagation is given by the following formula:

$$v = \frac{1}{\sqrt{\varepsilon\mu}} = \frac{1}{\sqrt{\varepsilon_r \varepsilon_0 \mu}} = \frac{c}{\sqrt{\varepsilon_r}}$$

Hence, a higher relative permittivity results in a smaller speed of propagation for the wave. A slower wave propagation results in a smaller wavelength, as shown in the equation below, which might affect the dimensions of the antennas you are building.

$$\lambda = \frac{v}{f} = \frac{c}{f\sqrt{\varepsilon_r}}$$

2.2.2 Note about the electric tangent delta

The electric tangent delta, usually given as the dielectric loss tangent, is a measure of the dissipation factor of a dielectric material. It is defined as the ratio between the imaginary part and the real part of the absolute permittivity of the material. It is thus a dimensionless quantity that can mathematically be expressed as:

$$tan\ \delta\ = \frac{Im(\varepsilon)}{Re(\varepsilon)}$$

The value of tangent delta depends directly on the permittivity, so the properties discussed on the previous sub-chapter will affect this parameter. Generally, high tangent delta values indicate high energy losses and poor insulation properties. Its value can range from 0 to infinity. The most common tangent delta values for dielectric materials used in electrical insulation range from less than 0.001 for high-quality materials, to 0.1 or higher for lower quality materials [5]. It should be noted that this parameter varies for different conditions and can change over long periods of time due to stress, exposure and aging.

2.2.3 AWR2243 by Texas Instruments

Antenna arrays formed by joining simple microstrip patches can be easily implemented. In the following section, the commercially available, printed antenna radar developed by Texas Instruments will be discussed.

The radar in question is the “AWR2243”, shown in Fig. 2.4.

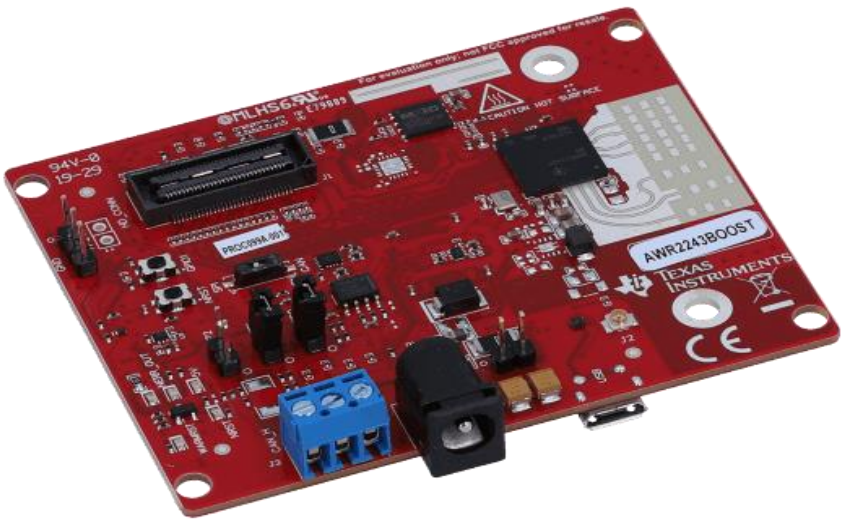

Figure 2.4: AWR2243 by Texas Instruments

On the top-right corner of the board, the printed antenna can be noticed. Focusing solely on the antenna, given in Fig.2.5, there can be noticed the patches which compose the different antennas. There are 3 transmitter modules, and 4 receiver ones, with the distance between the transmitter antennas being of one wavelength, whereas that of the receiving antennas being of one-half of wavelength. On the other hand, the distance between patches of the same array is of one-half wavelength.

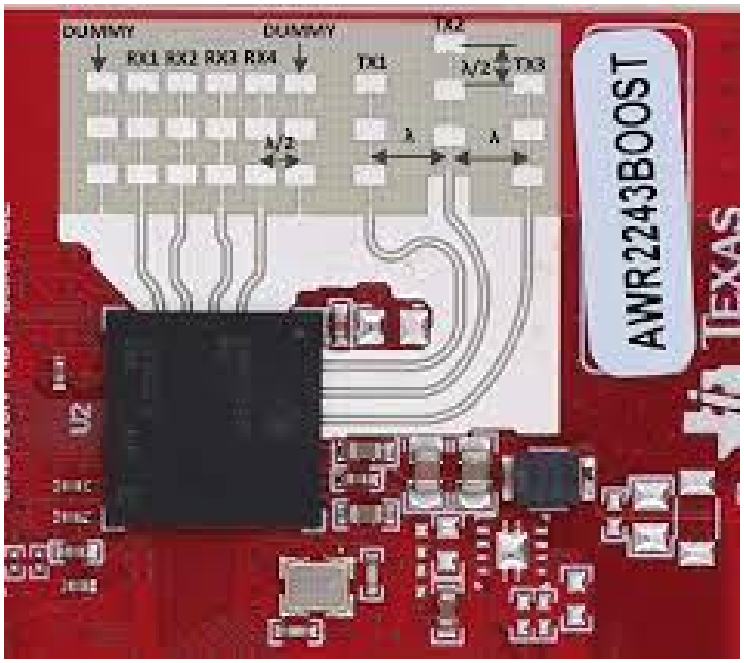

Figure 2.5: View of the printed antenna on the AWR2243 by Texas Instruments

2.3 Introduction to 3D waveguide antennas

To explore a new approach, the next strategy being considered involves using a 3D waveguide antenna instead of a printed antenna on a PCB. However, before going on with the details of the antenna, it is important to comprehend some fundamentals about waveguides.

A waveguide is a hollow metallic structure which can propagate EM waves by reflecting them off the conducting sides, while having a net electric or magnetic field component in the propagation direction. The rectangular waveguide is of particular interest. It supports 2 types of modes, which give a description of the EM field pattern, each characterized by its unique pattern, frequency, polarization, and direction:

- TE mode: It is the transverse electric mode in which the electric field is transverse to the direction of propagation (perpendicular to the direction of the advancement of waves), whereas the magnetic field is not transverse.
- TM mode: It is the transverse magnetic mode in which the magnetic field is transverse to the direction of propagation, whereas the electric field is not.

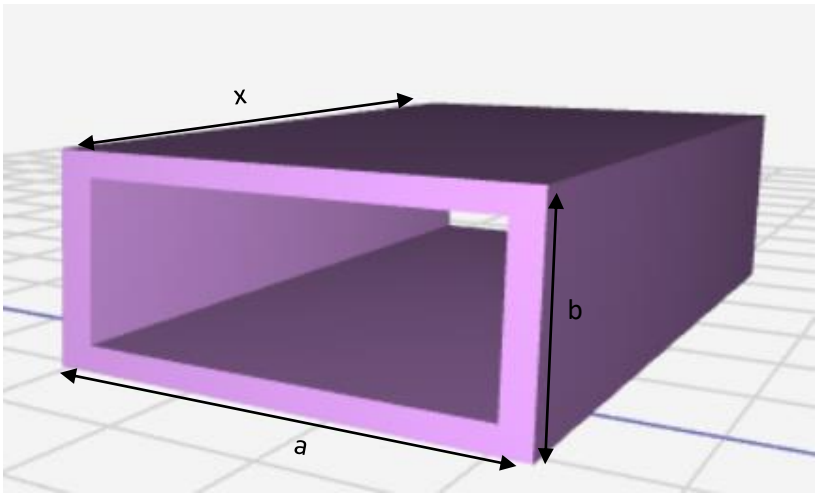

Figure 2.6: Hollow rectangular waveguide

As seen in Fig. 2.6, the rectangular waveguide is characterized by 2 main parameters, namely the width $\boldsymbol{a}$ and the height $\boldsymbol{b}$, which also determine the cutoff frequency of the waveguide. Usually a is bigger than b, with it often being twice its value. Moreover, the thickness of the walls is related to the wavelength of the signal being transmitted through the waveguide. Thin walls, compared to the wavelength may bring to energy losses due to radiation. Thick walls, on the other hand, can make the structure bulky and heavy. In this context, the cutoff frequency can be defined as the point at which waves begin to propagate, effectively functioning as a high pass filter by allowing frequencies above the threshold to pass through.

It should be noted that the TEM mode is not supported in rectangular waveguides. Modes which are not supported include:

- TEM mode: It is the transverse electromagnetic mode in which the electric and magnetic field are perpendicular to each other and perpendicular to the

direction of propagation. It exists on structures which have 2 excited conductors surrounded by dielectric material (coaxial cable). In the coaxial cables, the electric field is in a radial direction, whereas the magnetic field is around in form of concentric circles, with the propagation direction being the length of the cable.

- Quasi-TEM mode: Quasi, because it resembles the TEM mode. It exists in microstrips, in which the top and bottom are conductors, and the middle is dielectric. There is a propagation through the air above the top strip and the dielectric substrate. Having different resistivities, the wave propagates with different speed in both regions.

The number of TE and TM modes that can propagate along these waveguides is infinite, but the most dominant mode is the TE10. The subscripts in the mode definition indicate the field pattern. The first subscript indicates the number of half wave patterns in the direction a, whereas the second subscript indicates the number of half wave patterns in the direction b. In fact, these two parameters play a role in the cutoff frequency calculation, as follows:

$$f_{c,m,n} = \frac{c}{2\pi}\sqrt{\left(\frac{m\pi}{a}\right)^2 + \left(\frac{n\pi}{b}\right)^2}$$

, where a and b are the lengths of the waveguide, c is the speed of light, m and n are the mode subscripts.

The rectangular waveguide was selected, due to its advantages over the printed lines, including:

- Wide bandwidth for single mode propagation
- Low attenuation due to the geometry and the materials used.
- Mode stability for the fundamental propagating modes, since they have a well-defined cutoff frequency.
- Higher power rating which is related to the waveguide conductor (walls) and the distance between them.
- Fields completely contained within the waveguide (shielded), so the radiation losses are small.

Slotted waveguide antennas consist of a waveguide with one or more holes (rectangular or elliptical) cut on their surface, as shown in Fig. 2.7. They are used in very high frequencies. In lower frequencies, a simple metallic surface with holes in it can be used.

The slots can be either on the upper wall, or on the narrow ones, and can be of various shapes, as rectangular, elliptical, or tapered. When an EM wave propagating through the waveguide encounters a slot, portion of the wave is scattered and radiated into free space. The shape and the size of the slots determines the radiation pattern. The slots are typically smaller than a tenth of the wavelength of propagation in width, and smaller than a half of the wavelength of propagation in length. It should be noted that increasing the width, you increase the bandwidth of the radiation.

Rectangular slots produce a radiation pattern which is directed and has a sharp peak in the direction perpendicular to the surface of the slots, whereas elliptical or circular slots will produce a more symmetrical radiation pattern.

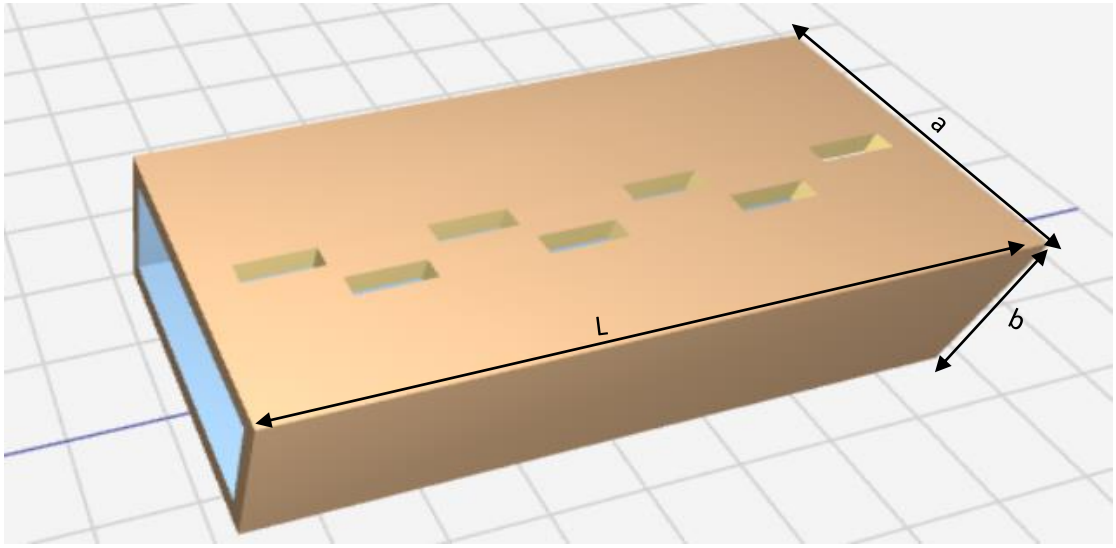

Figure 2.7: Slotted waveguide antenna

The front is the part of the antenna that is driven, whereas the far end is usually enclosed in metal and short circuited.

These types of antennas:

- have a low loss (high antenna efficiency).
- radiate linear polarizations with a low cross-polarization. However, increasing the bandwidth, you can have higher degrees of cross-polarization.
- can transmit high power levels, which is suitable for radars.
- are directional.
- can be manufactured to embody the surface in which they will be attached to
- can be mass produced with ease.

Selecting the appropriate antenna type is not very straightforward and often requires a careful consideration of various trade-offs. Both types of antennas have their own set of strengths and weaknesses, and it is important to carefully evaluate them before making a decision. After careful consideration, it was decided that the 3D waveguide antenna is more suitable than the printed antenna for the design of an automotive radar. This choice will have significant impact on the performance and effectiveness of the system and overall, it is expected to deliver a good performance and contribute on the successful implementation of the automotive radar system.

Chapter 3: Design of a waveguide automotive radar antenna

This chapter describes the design of the 3D waveguide antenna based on the slotted waveguide technology. There will be 2 solutions proposed for this design, defined by the feeding type for the waveguide. A step-by-step procedure will be given for each design.

3.1 Microstrip fed antenna

For this type of antenna, the feeding is done through a microstrip line, which couples the energy into the waveguide. A microstrip line is a thin metal strip placed on the surface of a dielectric substrate, which in turn is bounded by a ground metal layer. This microstrip line is connected to an EM energy source on one end, like a microwave generator and introduces this EM energy into the waveguide antenna on the other end. It is designed to match the characteristic impedance of the waveguide, such that an efficient energy transfer from one side to the other is ensured. It must be noted that the position of the microstrip feed line plays a crucial role in the radiation pattern and gain of the antenna, so its position, along with the number and placement of the slots of the antenna, must be carefully set to achieve the desired characteristics.

This type of feeding and antenna is widely used in millimeter-wave applications due to the compact size, its ease of fabrication and high-gain. The following subchapters give a detailed review of each step.

3.1.1 Microstrip to SIW transition

Initially, the input from the microstrip line must be contained and then fed to the waveguide antenna. In order to do this, a simple SIW (Substrate Integrated Waveguide) can be used as in Fig. 3.1.

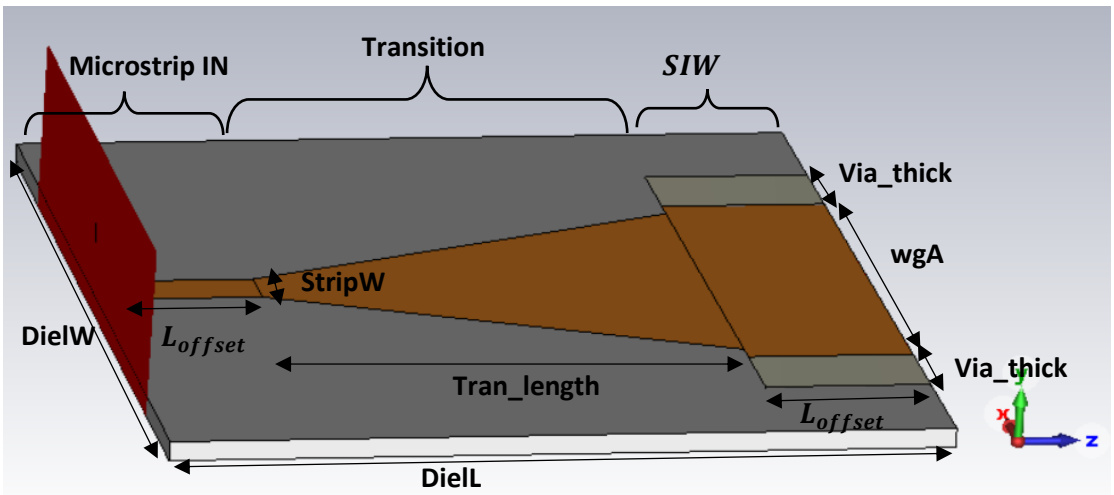

Figure 3.1: Microstrip to SIW transition design in CST

A SIW is a waveguide, which consists of a dielectric layer (grey color) and 2 parallel rows of metallic vias in the dielectric, used to guide the wave propagation. This type of waveguide is integrated into the substrate of a circuit board and commonly used in

millimeter-wave applications. In this initial phase, instead of rows of vias, 2 metal rows (light grey color) of length $\boldsymbol{L_{offset}}$ have been used. Due to these side rows, TM modes don't exist in the SIW. TE10 is the dominant mode.

The dielectric used as a substrate has:

- $\boldsymbol{\varepsilon_r = 3}$
- $\boldsymbol{electric\ tangent\ delta = 0.001\ @\ 78.5\ GHz}$
- $\boldsymbol{\mu_r = 1}$
- $\boldsymbol{thickness\ hDiel = 0.127mm\ << \lambda}$

To interface the signal and couple the energy between the microstrip (orange color), which has been chosen to be copper, and the SIW, a transition stage is used. The microstrip has a length of around half-wavelength to ensure no phase changes for the desired frequency of operation. The wavelength, in this case, will depend on the dielectric constant by:

$$\lambda_g = \frac{c}{f * \sqrt{\varepsilon_r}} \approx 2\ mm$$

So, the microstrip has a length of around 1 mm and it was chosen to have a height of around 0.0039 mm.

The design is realized on the same substrate (dielectric). The transition is not rectangular, but rather a trapezoidal one. Its purpose is to have a transformation of the quasi-TEM mode of the microstrip into the dominant TE10 mode of the SIW [6]. It also ensures an impedance matching between the microstrip line and the SIW, such that the return loss will be very small. The design of the transition structure, such as the width and height of the microstrip, the distance between the microstrip and the SIW, the size of the metal filling the SIW, can affect the impedance matching, the loss and the reflection of the energy between the microstrip line and the SIW. Note that the impedance Z0 for the microstrip is dependent on the width of the trace, its height, the dielectric constant of the substrate material and the height between the trace and the reference plane.

For the 3D antenna, it was decided to use a WR10 waveguide of reduced height. The conventional WR10 waveguide has a width *a=2.54mm*, and a height *b=1.27mm.* Its recommended frequency band is from 75 to 110 GHz, with the cutoff frequency of lowest order mode equal to 59.015 GHz and the cutoff frequency of the highest order mode equal to 118.03 GHz. The reduction of height for the WR10 waveguide has the effect of increasing the cutoff frequency, since the cutoff frequency and the height are inversely proportional.

The choice of that waveguide forces the SIW metals to have a distance equal to the width of the WR10 waveguide. So, the two metal rows will be separated by a distance ***wgA=2.54mm.*** The transition stage between the microstrip and the SIW will also be dependent on this parameter.

It should be noted that the end position of the transition stage on the SIW side changes depending on the parameter called ***EndRatio***, which varies from 0 to 1. If it is equal to

1, then the transition stage ends on the point where the metallic rows are supposed to start. If it is lower, then it ends on a point which is before the metallic rows.

The parameters, which were modified during the simulation phase to achieve the desired result are the length of the transition stage and the ***EndRatio***. The desired operation is around 78.5 GHz. To this end, the final parameters used are:

- $\boldsymbol{DielW = 5mm}$
- $\boldsymbol{L_{offset} = 1mm}$
- $\boldsymbol{Tran_{length} = 2.8 * \left(\frac{76}{78.5}\right)^2 mm}$
- $\boldsymbol{EndRatio = 0.8}$
- $\boldsymbol{wgA = 2.54mm}$
- $\boldsymbol{DielH = 0.127mm}$
- $\boldsymbol{StripW = 0.3mm}$
- $\boldsymbol{DielL = 2 * L_{offset} + Tran_{length}}$

There are 2 ports defined, one on each end: the microstrip input and the SIW output as seen in Fig. 3.2.

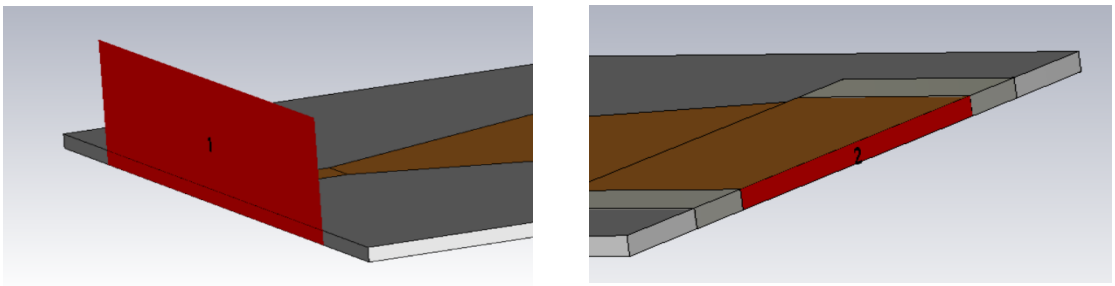

Figure 3.2 (a): View of the ports for the Microstrip to SIW topology

The simulations have been performed using CST Microwave Studio 2022. The following images show the results of this simulation:

Port1 e1	
Frequency	77.5 GHz
Phase	0 °
Mode type	Quasi TEM
Line Imp.	50.8609 Ω
Wave Imp.	285.646 Ω
Beta	2568.35 1/m
Accuracy	1.46556e-11
Maximum (Plot)	138749 V/m

Port2 e1	
Frequency	77.5 GHz
Phase	0 °
Mode type	TE
Wave Imp.	242.173 Ω
Beta	2526.77 1/m
Fcutoff	34.0685 GHz
Accuracy	3.74463e-11
Maximum (Plot)	38748.7 V/m

Figure 3.2 (b): EM result of the ports for the Microstrip to SIW topology

As stated on the theoretical description of this structure, the transition stage transforms the quasi-TEM mode of the microstrip line into the dominant TE mode of the SIW.

As for the s-parameters, Fig. 3.3 shows that the reflection coefficient S11 is lowest at around 78.5GHz, which is the desired one, whereas the inter-port coefficients S21 and S12 are equal and close to 1 in linear scale on the desired frequency.

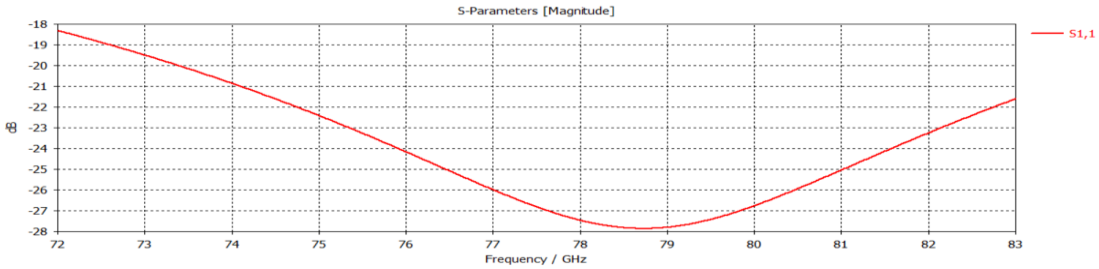

Figure 3.3 (a): S11 parameter result for the Microstrip to SIW topology.

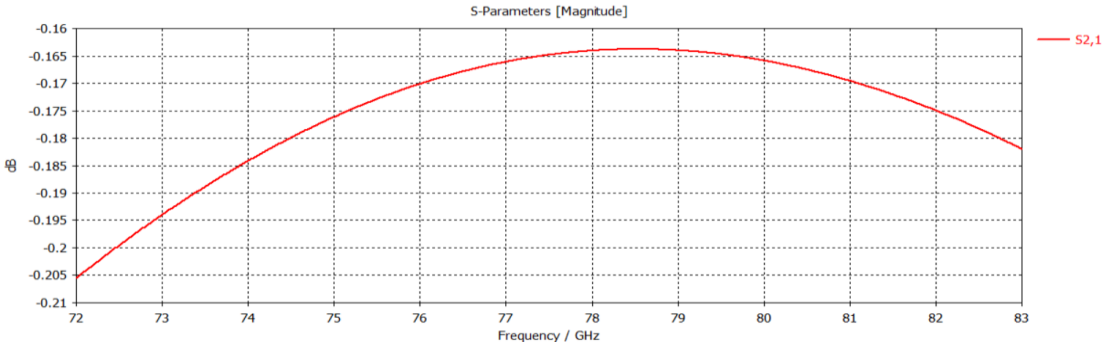

Figure 3.3 (b): S21 parameter result for the Microstrip to SIW topology.

3.1.2 Dielectric-filled waveguide to vacuum-filled rectangular waveguide transition

The next thing to do is to integrate a rectangular waveguide on the design, which will represent the waveguide of the slotted antenna. The signal will have to pass from the microstrip to the SIW and into the rectangular waveguide. For this reason, a transition from the SIW to the RWG is needed.

In order to design the correct antenna waveguide, for this initial step, the microstrip to SIW transition is replaced by a waveguide. This waveguide is filled with the same dielectric as the one used for the SIW, in order to mimic the characteristic of the signal going through the SIW. So, there will be a direct feeding of the first waveguide. After the antenna waveguide is verified to work correctly using this direct feeding, then the dielectric-filled waveguide will be replaced again by the microstrip to SIW transition. The SIW portion will have the same width as the waveguide that will be used.

This geometry is described in Fig. 3.4

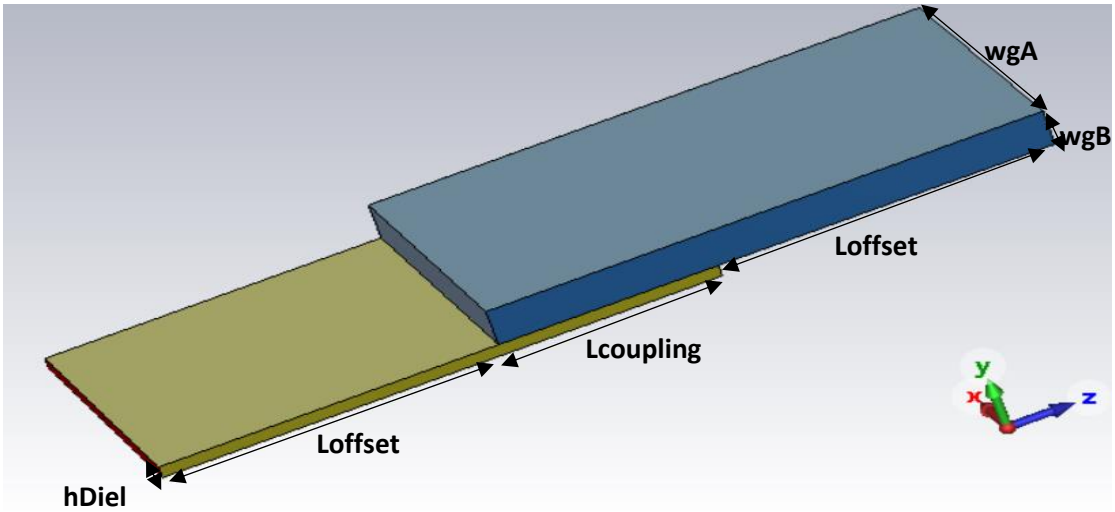

Figure 3.4: Dielectric-filled to vacuum-filled waveguide transition design in CST.

The yellow structure is the dielectric filled, whereas the blue one represents the vacuum filled waveguide (part of the final slotted antenna). They both have the same

length and width, but differ in height. They are set on top of each-other and have an overlapping region. The overlapping region has a length $\boldsymbol{L_{coupling}}$, across which, there is an aperture where both the dielectric and the vacuum meet. This aperture ensures the continuation of propagation from one waveguide to the other. There are 2 ports, one on each end of the rectangular waveguides.

When transitioning from one waveguide to the other, the change in the dielectric constant leads to a change in the propagation characteristics of the EM waves. In a dielectric filled waveguide, the field strength is reduced, since the electric field is partially stored in the dielectric material. When transitioning to the other waveguide the opposite happens, resulting in a much higher field strength within the waveguide. Moreover, the dielectric constant affects the cutoff frequency. Having a lower dielectric constant, the cutoff frequency will be higher, meaning that a higher frequency is needed to support the propagating mode.

The parameters that are adjusted in order to fit the desired outcome, are the coupling length and the height of the vacuum filled rectangular waveguide. The final parameters used are:

- $\boldsymbol{wgA = 2.54\ mm}$
- $\boldsymbol{h_{Diel} = 0.127\ mm}$
- $\boldsymbol{\varepsilon_r = 3}$
- $\boldsymbol{L_{offset} = 3\ mm}$
- $\boldsymbol{L_{coupling} = 1.95\ mm}$
- $\boldsymbol{wgB = 0.1\ mm}$

The modes on each port are shown in the figures below:

(a) Port 1 **(b) Port 2**

Figure 3.5: EM result of the ports

, whereas the resulting S11 parameter is given in the following.

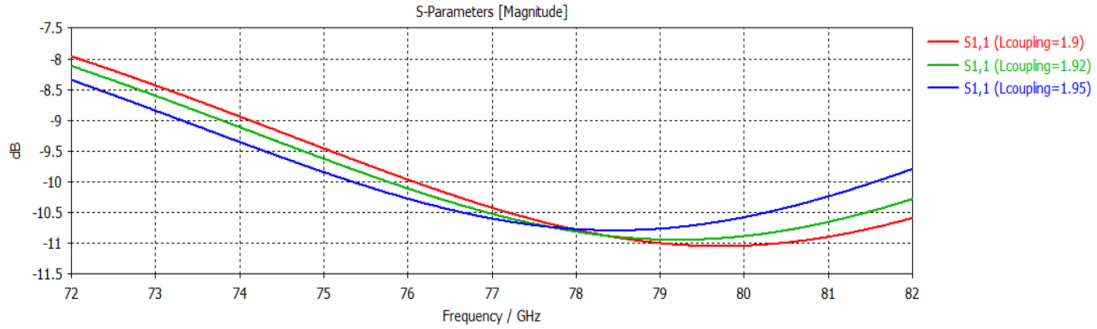

Figure 3.6: S11 results for varying $\boldsymbol{L_{coupling}}$ parameter.

As seen in the figure, the minimum is at around 78.5GHz. Nevertheless, its value on that point does not have a small enough value, which is what is needed. In fact, comparing to the previous stage, it is more than 15dB bigger, so it has to be adjusted if they are to be interfaced together. The way it can be adjusted to have a lower value is by introducing a double layer vacuum filled rectangular waveguide instead of the one used previously. This way, the first layer of the waveguide will act as an adapter for the wave before going on the second layer. This topology is presented in Fig. 3.7. It allows a smooth transition, which in turn reduces the reflection and loss of the signal at the interface between the two waveguides. It acts as an adapter by gradually changing the dimensions of the waveguide to match the dimensions of the connected component. This allows for an efficient transfer from the first waveguide to the second one, reducing the reflections that may occur at the junction.

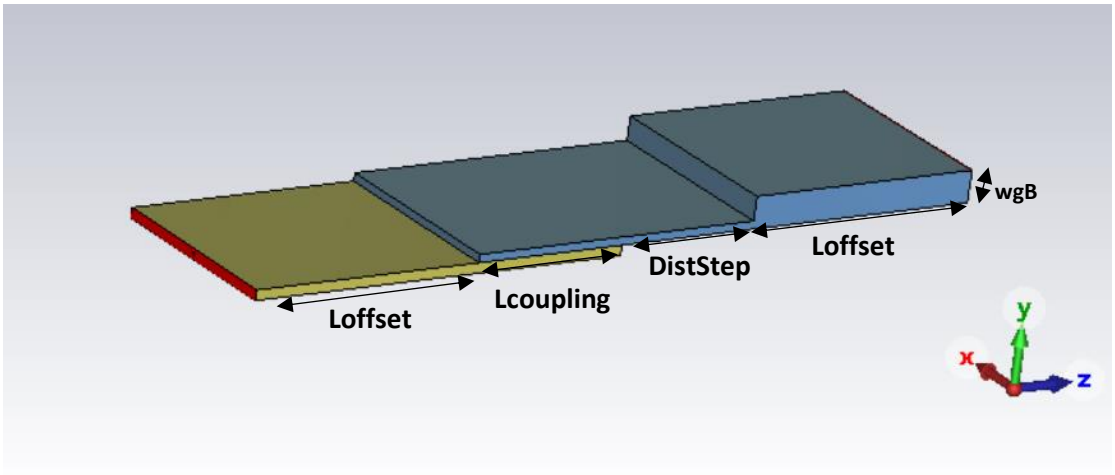

Figure 3.7: Double layer vacuum-filled waveguide design

The ports are the same as before. What changes is the fact that there is a portion of the second waveguide which has height ***wgBstep*** and the other portion which has total height ***wgB.*** The factor which will be modified on this design to have suitable results is the length ***DistStep***. It should be noted that when the length ***DistStep*** is positive, the first layer of the vacuum rectangular waveguide extends beyond the yellow waveguide. On the other hand, when this length is negative, the first layer and part of the second layer are both on top of the yellow waveguide as shown in Fig. 3.8.

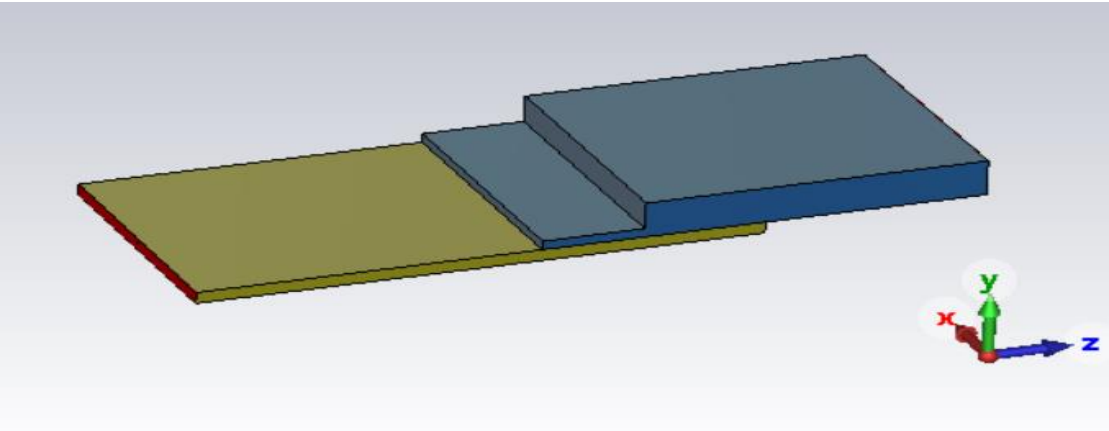

Figure 3.8: Double layer vacuum-filled waveguide design; negative ***DistStep*** parameter

The final parameters chosen for this design are:

- $\boldsymbol{CouplingLength = 1.95mm}$
- $\boldsymbol{DistStep = -1.06mm}$
- $\boldsymbol{wgBstep = 0.1mm}$
- $\boldsymbol{wgA = 2.54mm}$
- $\boldsymbol{hDiel = 0.127mm}$
- $\boldsymbol{Loffset = 3mm}$
- $\boldsymbol{wgB = 0.4mm}$

The resulting s11 parameter is shown in Fig. 3.9. The resonance frequency has a more visible peak around 78.5 GHz, and at the same time, the s11 value is around 10 dB lower than the previous case.

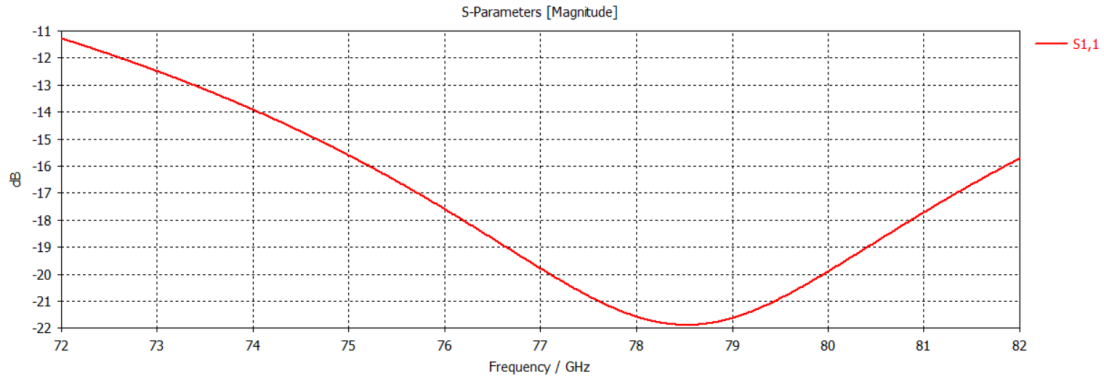

Figure 3.9 (a): S11 parameter result for the dielectric-filled to vacuum-filled waveguide transition.

Further optimizations and simulations have been done to have an even better result by modifying also the $\boldsymbol{CouplingLength}$ and the width of the first layer $\boldsymbol{wgBstep}$. Setting:

- $\boldsymbol{CouplingLength = 1.6742898541176\ mm}$
- $\boldsymbol{DistStep = -0.74966481481771\ mm}$
- $\boldsymbol{wgBstep = 0.109111\ mm}$

, the s11 parameter has a very good behavior as seen below.

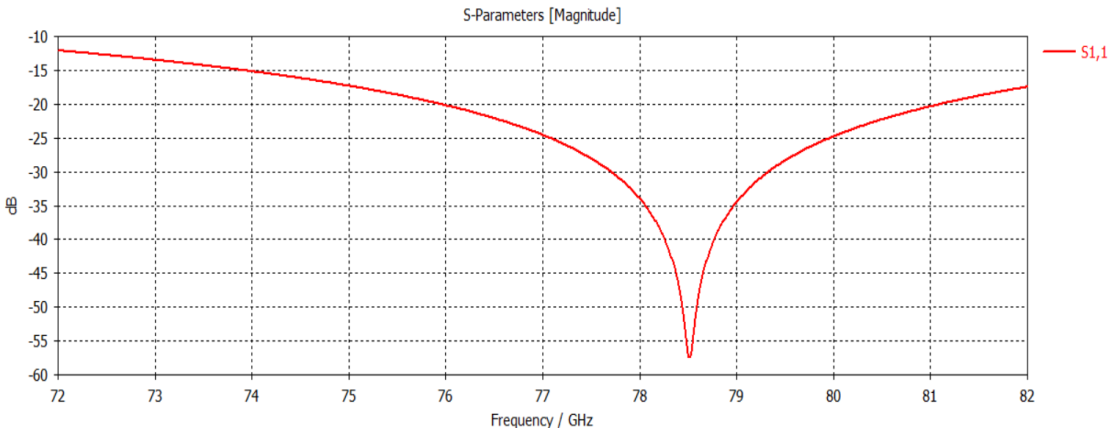

Figure 3.9 (b): Final S11 parameter result

It is fully centered around 78.5 GHz and has a value 47 dB lower than the previous design that had a single layer vacuum rectangular waveguide.

3.1.3 Microstrip to SIW integration

After achieving good results with the dielectric filled waveguide to vacuum filled waveguide transition, the next step that can be performed. The designed double layer waveguide can be used together with the Microstrip to SIW transition. The Microstrip to SIW stage will be used as a feeding for the double layer waveguide. Furthermore, a small portion of the final antenna enclosure will be integrated into the design. For now, there will not be any slotted antenna, but rather just a waveguide to test the operation frequency. The design is shown in Fig. 3.10.

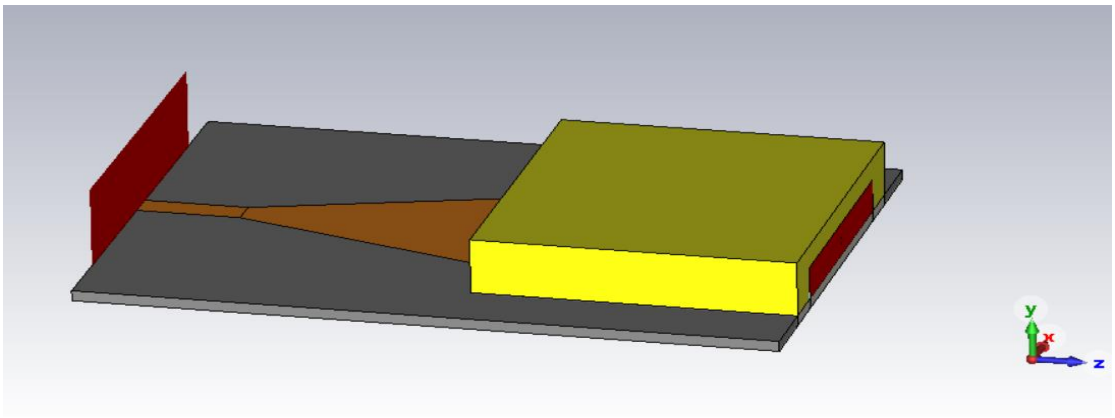

Figure 3.10: Integration of the Microstrip to SIW design

The yellow portion represents the antenna enclosure, which is a gold casing. It is mounted on top of the SIW portion and has an aperture at the point of contact, which is necessary for the feeding. It has walls of 0.5mm thickness on the x-direction. On the y direction, it follows the shape of the double layer rectangular waveguide described in the previous sub-chapter. Gold is a highly conductive metal with low resistivity that results in low loss and high-power handling, as well as in a good transition efficiency, which of course will also depend on the feeding stage. As a metal, it has high a reflectivity, which in turn translates to a high radiation efficiency, meaning it can keep more efficiently the EM wave inside the waveguide. Another benefit, which is purely due to its strength, is the fact that it can provide durability, longevity and protection against environmental factors such as wind, dust, temperature, humidity, corrosion etc., which is perfect for applications such as automotive radars.

Some changes have been made on the SIW structure with respect to what was discussed in the Microstrip-to-SIW transition. An aperture is created in the middle, which will act as a way to feed the signal to the waveguide. These changes are shown in Fig. 3.11.

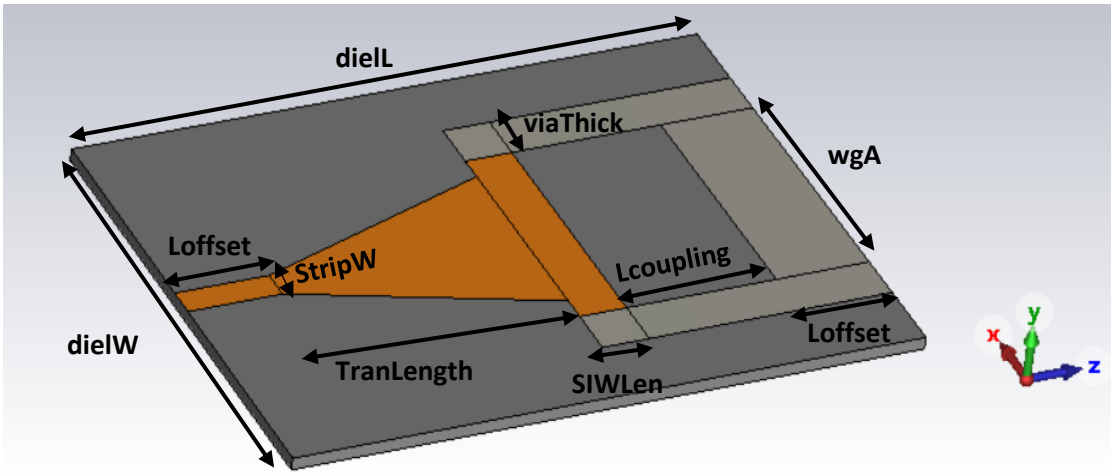

Figure 3.11: Changes in the Microstrip to SIW structure

The grey structure is the dielectric, whereas the orange ones are the microstrip lines which are used to feed the energy. The light grey structures are perfect electrical conductors, which are used to confine the wave. The wave will be guided through the microstrip line, it will transition to the SIW portion, where it will be confined, and then, through the aperture of length $\boldsymbol{L_{coupling}}$ and width $\boldsymbol{wgA}$, it will be transferred to the waveguide, which in turn will guide it towards the full antenna.

A cross-section view of the gold casing is given in Fig. 3.12.

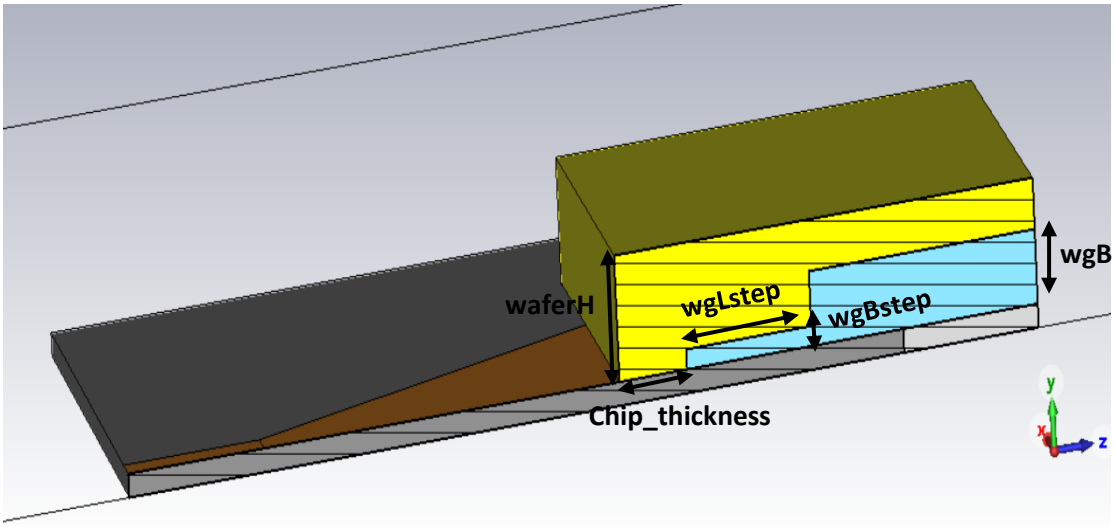

Figure 3.12: Cross section view of the Microstrip to SIW integrated with the gold casing.

It has a height $\boldsymbol{waferH}$ and a hollow region corresponding to the double layer rectangular waveguide studied in the previous sections. It should be noted that the casing has been made in such a way that the outer walls in the x-direction fit perfectly with the metals' layout of the SIW, leaving open only the middle space.

There are 2 ports as seen in Fig. 3.13, one on the microstrip input and the other one on the gold case end.

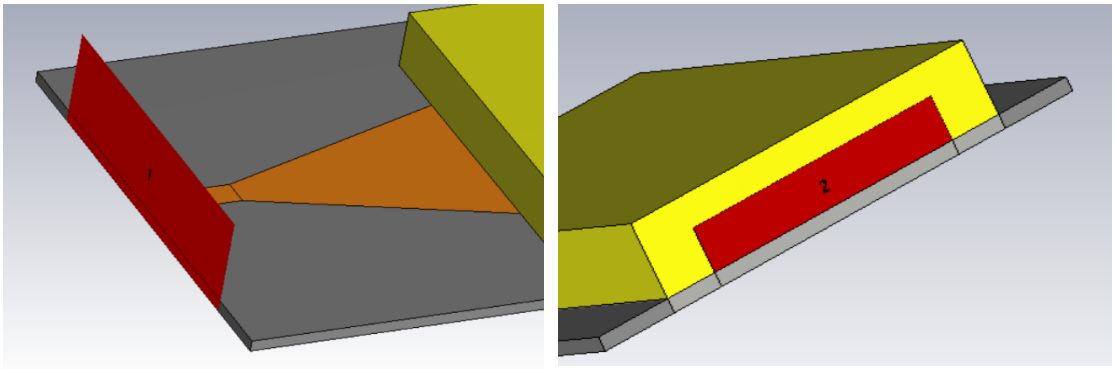

Figure 3.13: View of the ports for this design

Initially, the following parameters have been used:

- $\varepsilon_r = 3$
- $DielW = 5\ mm$
- $DielL = 2 * L_{offset} + Tran_{Length} + L_{coupling} + SIW_{Length}$
- $L_{offset} = 1\ mm$
- $Tran_{Length} = 2.624\ mm$
- $wgA = 2.54\ mm$
- $DielH = 0.127\ mm$
- $StripW = 0.3\ mm$
- $ViaThick = 0.5\ mm$
- $tandelta = 0.001$
- $EndRatio = 0.8$
- $CouplingLength = 1.674\ mm$
- $SIWLength = 0.5\ mm$
- $WGThick = 0.5\ mm$
- $wgB = 0.475\ mm$
- $WaferH = 0.675\ mm$
- $wgBStep = 0.109\ mm$
- $wgLstep = 0.924\ mm$

The results for the s-parameters are shown in Fig. 3.14.

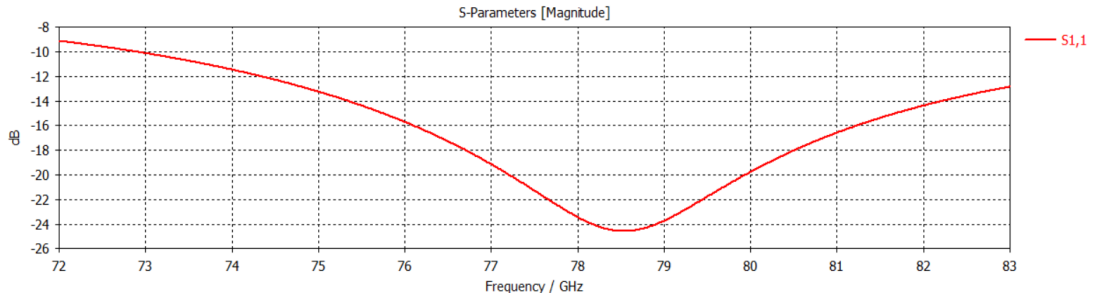

Figure 3.14 (a): S11 parameter result

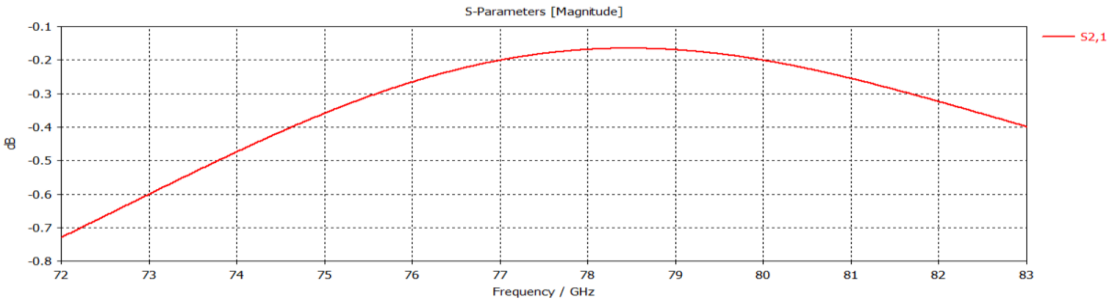

Figure 3.14 (b): S21 parameter result

A good resonance frequency is achieved, with the value of s11 being around -24.5 dB and centered on 78.5 GHz. This value is dependent a lot on the Microstrip to SIW stage, which alone yielded a much better s11 parameter than the SIW to RWG stage.

3.1.4 Full antenna

Since the feeding of only a portion of the waveguide antenna is tested to be correct, this next step focuses on incorporating the entire slotted waveguide antenna. To do so, the dielectric layer will be extended for an extra *DielL2* length. The gold casing will extend as well but it will have a little tolerance from the end. In this initial step, the whole casing is gold filled. Both ends are closed and there will be only a single port of excitation, that on the microstrip input.

Fig. 3.15 shows the substrate portion.

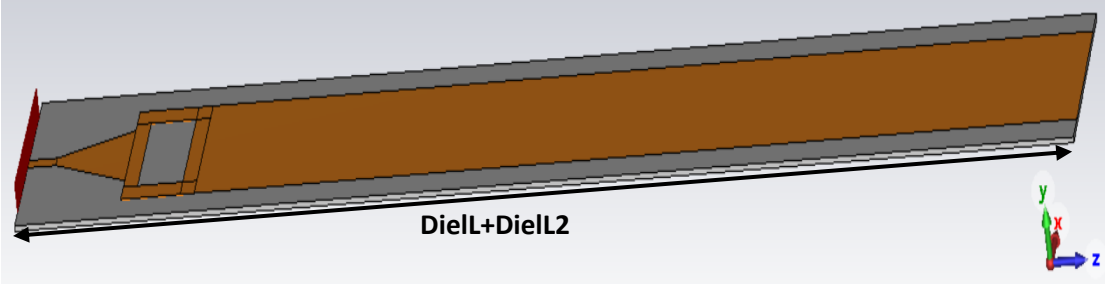

Figure 3.15: Substrate of the full antenna design. Orange = Copper

It can be noticed that along with the dielectric, also a layer of metal (copper annealed) has been extended to cover the lower portion of the slotted waveguide. Moreover, the perfect electrical conductor in the SIW has also been replaced with copper, in order to have a more realistic design and results. The bottom metal layer, being copper and having a low resistivity, is ideal to be used as a ground plane and enhance the antenna's performance. The copper layer helps to reduce the wave propagation on the dielectric substrate, thus reducing the loss and improve antenna's radiation efficiency. It can also reduce the mutual coupling between the antenna elements acting as an isolation. Moreover, it can provide shielding against EM interference, by reducing the amount of EM energy radiated or conducted outside of the antenna.

The SIW aperture is kept open as the microwave feeding point from the microstrip line. A front and back view of the slotted waveguide antenna gold casing, which is put on top of the dielectric, is given in Fig. 3.16.

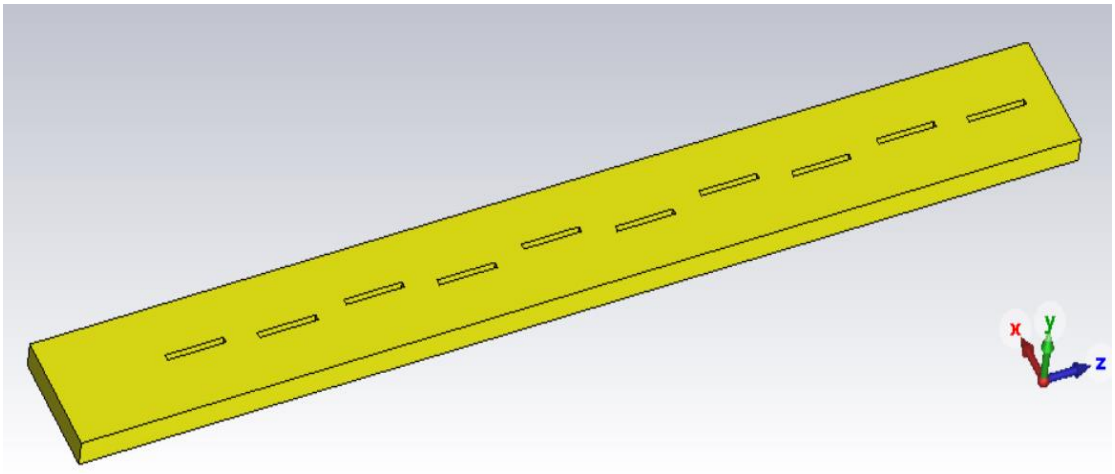

Figure 3.16 (a): Top view of the gold chip

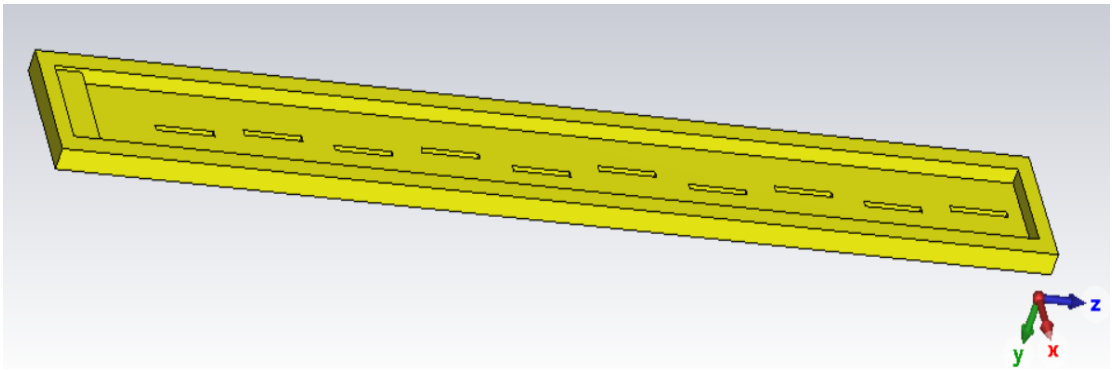

Figure 3.16 (b): Inner view of the gold chip

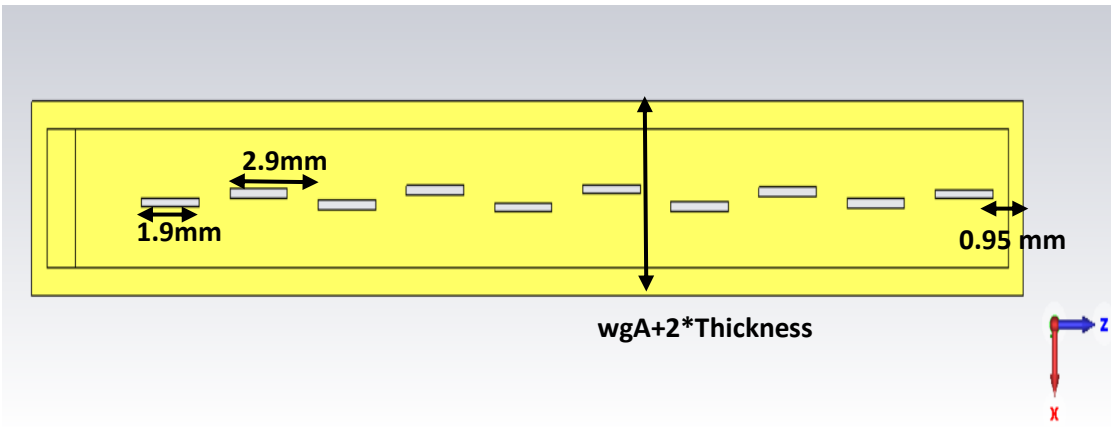

Figure 3.16 (c): Bottom view of the gold chip

The design of the slotted waveguide antenna is based on the travelling-wave feed slotted waveguide antenna design by Robert S. Elliot [8].

As it can be seen, there are 10 slots on the waveguide. To design this type of slotted antenna, the slots should be equidistant by a $d \neq \frac{\lambda_g}{2}$, with the last slot being terminated by a matched load (short-circuited). The distance between adjacent slots is chosen to be $\boldsymbol{d = \frac{3\lambda_g}{4} \approx 2.87mm}$. By matched load, it is intended that the last slot center should be at a distance $\boldsymbol{m * \frac{\lambda_g}{4}}$ from the waveguide end, with m being an odd number. This distance is based on the quarter-wavelength matching, to ensure that the impedances are matched and that the signal reflection is minimized. For this design, m=1 has been chosen. λ_g is the guiding wavelength, which in this case is the simple wavelength in vacuum. Moreover, to ensure that the antenna has the best possible radiation characteristics, the slots in the antenna are chosen to be at a resonance length, which is usually selected to be approximately half the wavelength ($\frac{\lambda_g}{2}$) that the antenna is designed to transmit. Choosing this length or a multiple of it, ensures that the induced current in the metal surface around the edges of the rectangular slots is in phase with the electromagnetic waves of the waveguide.

Doing some calculation, you achieve:

$$\boldsymbol{\lambda_g = \frac{c}{f} = \frac{3e8\ m/s}{78.5e9\ Hz} = 3.82\ mm} \qquad \boldsymbol{\frac{\lambda_g}{2} = 1.91\ mm}$$

$$\frac{\boldsymbol{\lambda_g}}{\mathbf{4}} = \mathbf{0.95}\ \boldsymbol{mm}$$

The slot width can be calculated by the following formula [9]:

$$slot\ width = a * \frac{0.0625}{0.9}$$

It comes from the fact that the most common used slot width is around 0.0625in equal to 1.5875 mm corresponding to a waveguide of width 0.9in equal to 22.86 mm. By proportionality, the width of a slot for a waveguide of width $\boldsymbol{a}$ is given by the above formula. For a width $\boldsymbol{a = 2.54\ mm}$, the slot width will be equal to **0.171 mm.** The slot width affects the frequency of operation and the bandwidth of the antenna. Having a wider slot allows to operate at lower frequencies, while narrower slots provide higher frequency of operation. This because for lower frequencies, the wavelength of the EM waves is larger, so the slots need to have a wider opening to allow them to pass through. The contrary can be said for high frequencies.

The slot height has been chosen to be **0.2mm,** which good enough to have a good radiation and to be in concordance with the thickness of the gold chip on the upper part. The slot height affects more the radiation pattern of the antenna. It affects the polarization in the y-direction, so the vertical one. Having taller slots, provides better vertical polarization and can result in a narrower beam.

The space between the center line of the slot and the center line of the waveguide is referred as slot displacement. It is possible to position the slots at an equal distance from the centerline, however this results in a SLR in the directivity pattern of around 13 dB. To achieve higher SLR, non-uniform displacements are used in the placement of the slots. The slots, have a two-by-two symmetrical displacement with respect to the waveguide centerline. The symmetrical displacement goes like this: the first and the last slot have the same displacement from the centerline, however the displacement of the first slot is positive, whereas that of the last slot is negative; the same goes on for the second and penultimate slot, and so on. In fact, from the figures alone, it can be noticed that the slots are not in a direct line, but rather are a bit shifted.

The displacement of the n-th slot is related to its normalized conductance g_n by: [10]

$$d_n = \frac{a}{\pi}\arcsin\left(\sqrt{\frac{g_n}{2.09 * \frac{\lambda_g}{\lambda_0} * \frac{a}{b}\cos^2\left(\frac{\pi * \lambda_0}{2 * \lambda_g}\right)}}\right)$$

$$g_n = \frac{c_n}{\sum_{n=1}^{N} c_n}$$

, where N is the number of slots, and c_n are the coefficients of the Chebyshev distribution that have to be determined to reach the desired SLR.

There are ready tables with the desired SLR and the corresponding slot displacement and Chebyshev taper coefficients. The displacements used for this slotted waveguide antenna are shown in Table. 1.

Slot Number	Displacement
1	0.0771 mm
2	-0.0907 mm
3	0.1190 mm
4	-0.1472 mm
5	0.1659 mm
6	-0.1659 mm
7	0.1472 mm
8	-0.1190 m
9	0.0907 mm
10	-0.0771 mm

Table 1. Displacement factor of each slot with respect to the centerline of the waveguide which is located on the plane x=0.

The final design, including everything is given in Fig. 3.17.

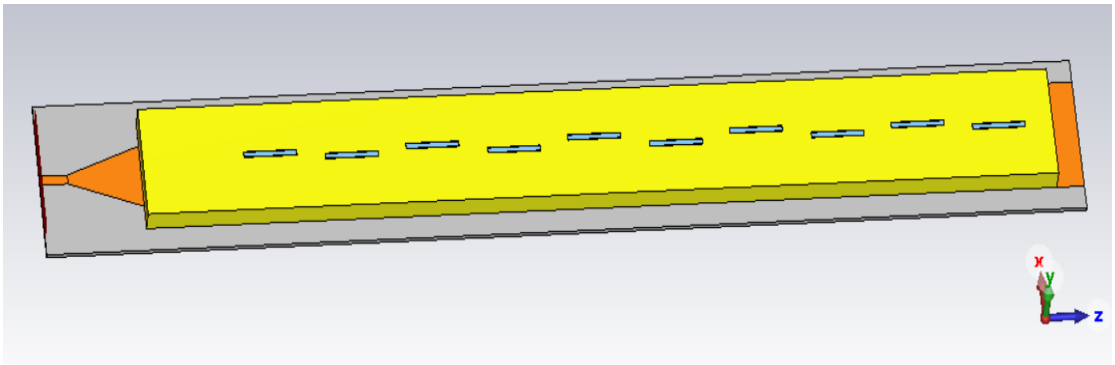

Figure 3.17: Full antenna view, with all the different transition stages

Copper(annealed) has been used for the metallic parts on the dielectric. The final length of the gold casing is:

$$Gold_{Len} = DielL + DielL2 - Tran_{Length} - 2 * L_{offset} = 32.6\ mm$$

Its height is $waferH = 0.675mm$, used in the previous chapter, as well as the width equal to $wgA + 2 * Thickness = 3.54\ mm$.

The full parameter list is given below:

- $epsR = 3\ mm$
- $DielW = 5\ mm$
- $DielL = Loffset + TranLength + Lcoupling + SIWLen + distTransAnt$
- $Loffset = 1\ mm$
- $TranLength = 2.624\ mm$
- $wgA = 2.54\ mm$
- $DielH = 0.127\ mm$
- $StripW = 0.3\ mm$
- $ViaThick = 0.5\ mm$
- $tandelta = 0.001\ mm$
- $EndRatio = 0.8\ mm$
- $CouplingLength = 1.602\ mm$
- $SIWLength = 0.5\ mm$
- $WGThick = 0.5\ mm$
- $WaferH = 0.675\ mm$
- $wgB = 0.475$ mm
- $wgBStep = 0.12\ mm$
- $wgLStep = 0.927\ mm$
- $AntStepLength = 29.003\ mm$
- $DistTransAnt = 1\ mm$
- $DielL2 = AntStepLength + ViaThick + Loffset$

Now it is time to review the results of this topology, including the s-parameter, radiation efficiency and directivity. They are shown in Fig. 3.18.

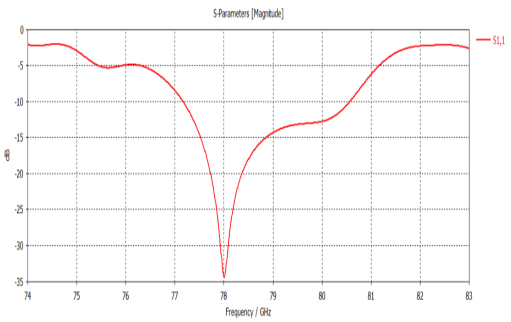

Figure 3.18 (a): Resulting S11 parameter

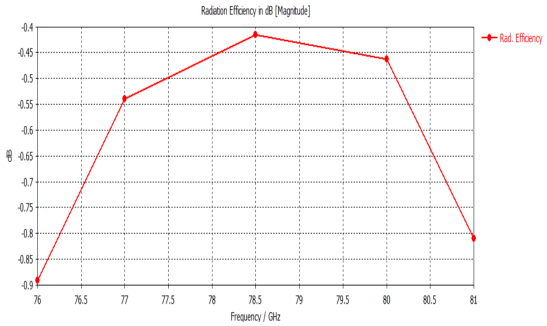

Figure 3.18 (b): Resulting S11 parameter

The resonance frequency is 78 GHz, which is very close to the desired frequency of 78.5 GHz. It has a good central behavior and a small value of nearly -35dB. Its bandwidth is around 1.5 GHz at the -15 dB level.

Moreover, a good radiation efficiency is achieved, with level between -0.9 and -0.42 dB is achieved in the range of interest, which means that the antenna converts around 80%to 90% of its input fed power into radiated power, with the maximum being on 78.5 GHz.

Furthermore, the directivity pattern gives the following results for the 78.5 GHz frequency of operation and an angle $\varphi = 90°$.

NOTE FOR THE DIRECTIVITY PATTERN STUDY
This type of antenna has a linear horizontal polarization, since the electric field is horizontal to the direction of propagation in the antenna. Being so, the E-plane ofthe antenna relates to the azimuth plane, whereas the H-plane of the antennacoincides with the elevation plane. Being a highly directional antenna in the vertical direction, the most interesting directivity plane for this study is the elevation one (H-plane). So all thefollowing descriptions of the directivity pattern will be actually referring tothe elevation plane directivity pattern for an angle phi=90° and varying angles theta.

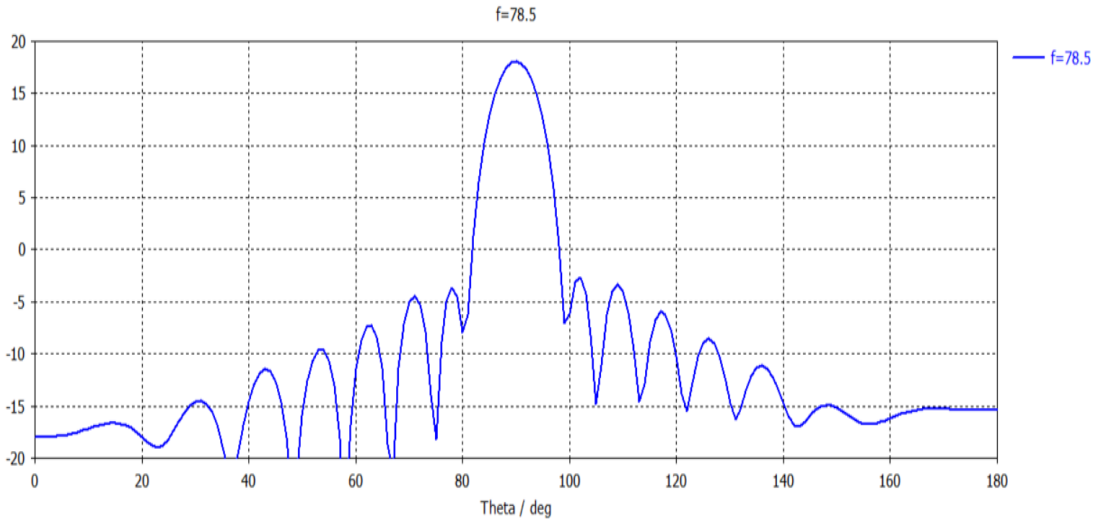

Figure 3.26 (c): Resulting directivity pattern for the full antenna.

The value of the main lobe reaches 18.07 dB, with the side lobe reaching at most -2.95 dB. This is a difference of at least 21 dB and is all attributed to the displacement of the slots of the antenna. Without the displacement, as discussed before, a slotted waveguide antenna can reach a maximum difference of around 13 dB.

3.1.5 Full antenna + vias

Up until now, the antenna has used as the SIW delimiters some simple rows of metal, in this case Copper (annealed). What can be done is to use vias instead of the rows. Vias are small, drilled holes, which serve as electrical conductors and go through 2 or more layers. They are made of copper, and as before, delimit the propagation of the waves. The vias are reliable and at the same time save some material, as the metal used in the metallic rows is much more than the one used with the vias. They are depicted in Fig. 3.19.

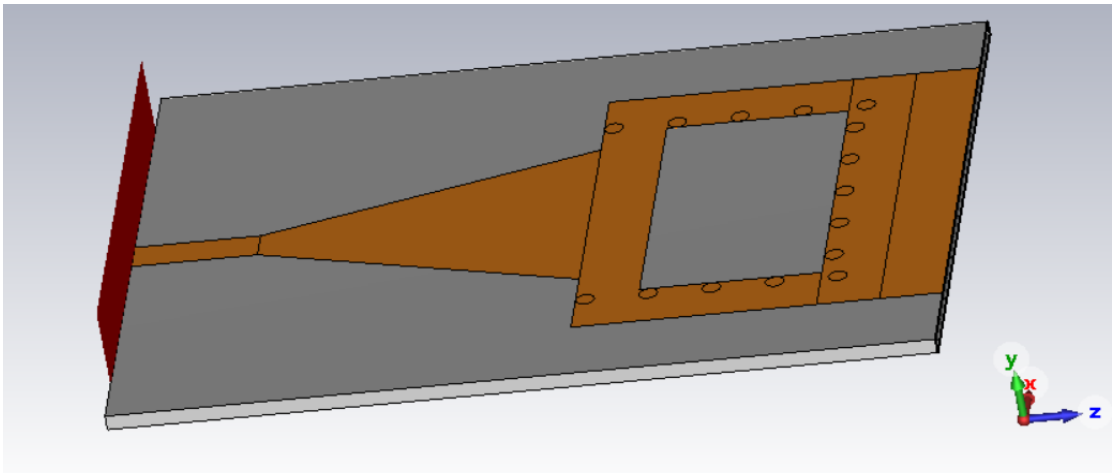

Figure 3.19 (a): View of the Microstrip to SIW transition with the inclusion of vias

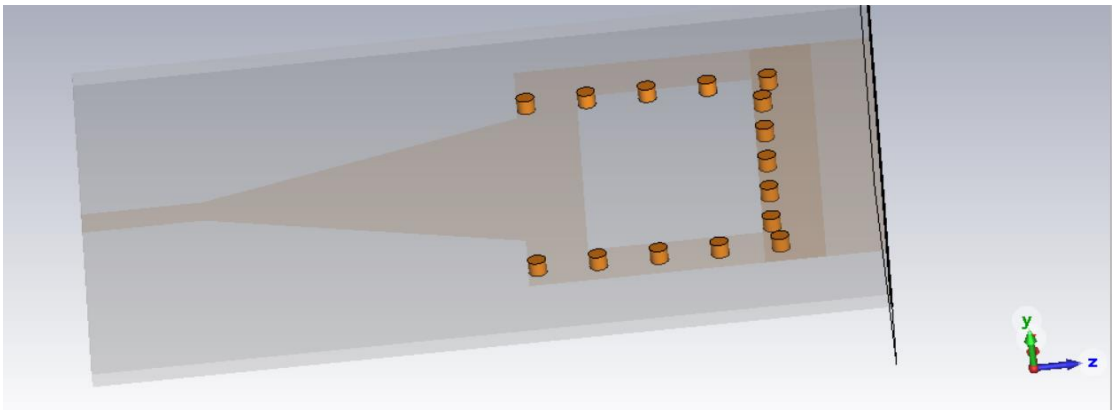

Figure 3.19 (b): View of the vias only

The vias have a diameter of around 0.15 mm and are separated from each other by a distance of 0.5 mm. It can be noticed that there are 2 parallel rows and an orthogonal one, all of them used to guide the wave into the slotted waveguide antenna. The achieved results are very similar to the previous case. Actually, the resonance frequency is a little bit more shifted to the right, getting even closer to 78.5 GHz. Its

minimum value is also a bit smaller, even though it doesn't differ by much, but by around 8 dB in values which are already very small. These results can be seen in Fig. 3.20.

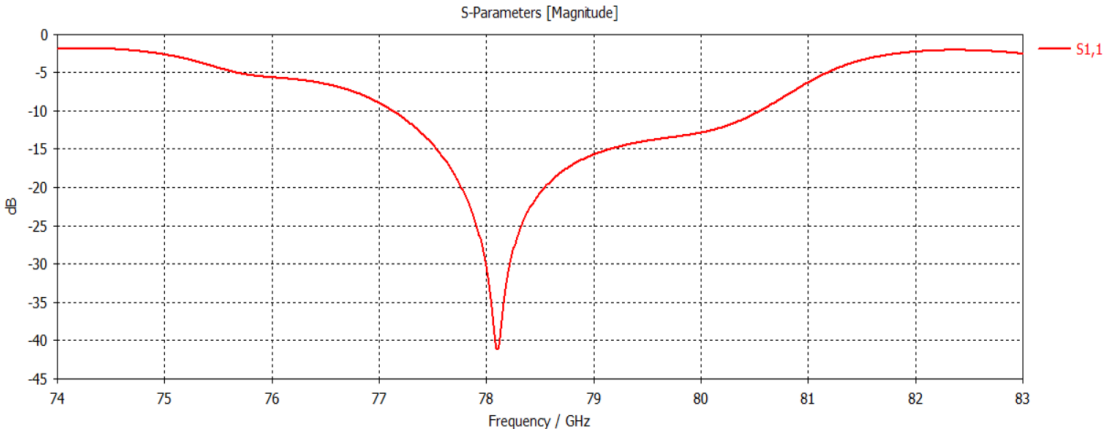

Figure 3.20 (a): Resulting S11 parameter for the full antenna + vias.

The radiation efficiency is nearly the same, with this case being around 0.02 dB smaller.

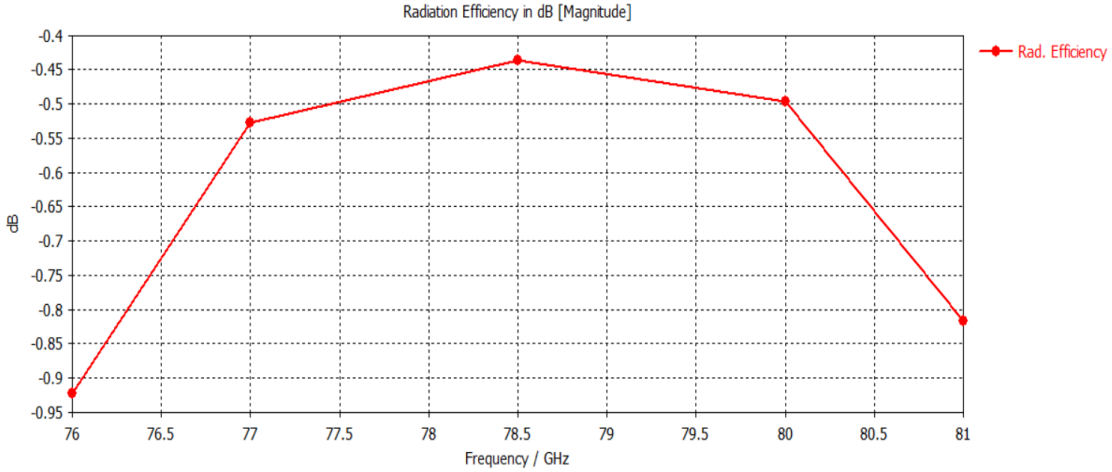

Figure 3.20 (b): Resulting radiation efficiency for the full antenna + vias.

As for the directivity pattern, it also has minimal changes with respect to the previous case.

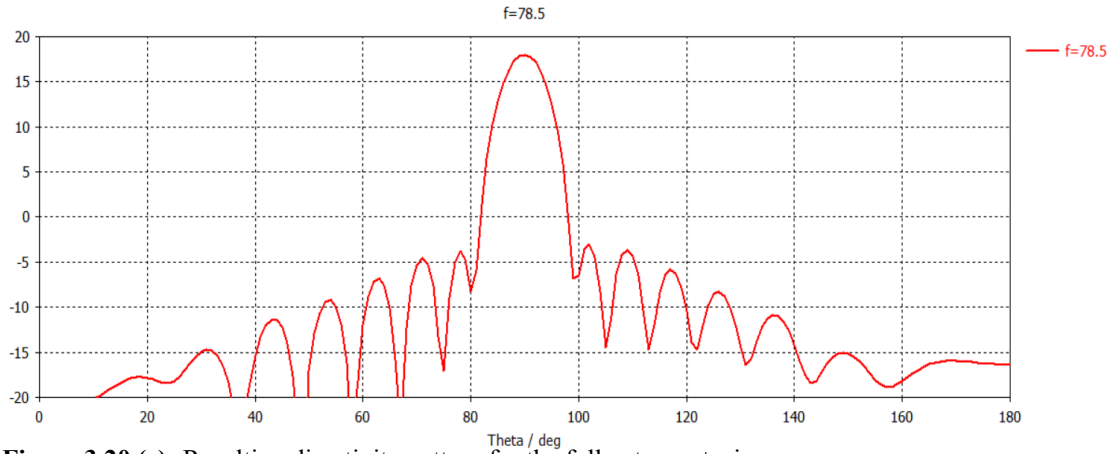

Figure 3.20 (c): Resulting directivity pattern for the full antenna + vias.

3.1.6 Silicon filled with a gold layer all around the antenna

For the next point, a way to reduce the usage of gold is to be found, as gold is an expensive metal. Taking in consideration the price for commercially available gold as of December 2022, it oscillates around 55 Euros per each gram. To find the volume of used gold, the following calculation can be made:

$$V = V_{central} - 10V_{slot} + V_{wgLstep} + 2 * V_{side1} + 2 * V_{side2}$$

$$= [slot\_depth * (DielL + DielL2 - 2 * Thickness - 2 * L_{offset} - TranLen) * wgA]$$

$$-10 * slot_{width} * slot_{length} * slot_{depth} + wgLstep * (wgB - wgBstep) * wgA$$

$$+2 * [(DielL + DielL2 - 2 * L_{offset} - TranLen) * waferH * Thickness]$$

$$+2[Thickness * waferH * wgA]$$

$$= 16.0553\ mm^3 - 0.1899\ mm^3 + 22.008\ mm^3 + 1.715\ mm^3$$

$$= 39.58\ mm^3$$

The density of gold is $0.019\ g/mm^3$. That means that for one single antenna, a mass of 0.7522 grams of gold has to be used. Its price amounts to around 41 Euros, which is not very comfortable after adding all the manufacturing costs.

The solution employed for this case is to have only a thin layer all around made of gold, and have the inside filled with silicon. The total volume of the casing will not change, but there will be less gold involved as most of it will be exchanged with silicon. As an example, having a gold thickness of around 0.06 mm, the resulting gold volume (measured using the in-built tools of CST Microwave Studio) is of around 17.8975 mm^3, which is much lower than what was used before.

Silicon is a semiconductor material, which conducts electricity, but not as good as a metal like gold. However, when depositing a thin layer of gold on the silicon surface, it creates a Schottky barrier (potential energy barrier for electrons formed at a metal–semiconductor junction) that increases the electron mobility of the silicon. The electrons can move more easily and efficiently, improving the total performance of the antenna.

A cross section view of this configuration is given in Fig. 3.21.

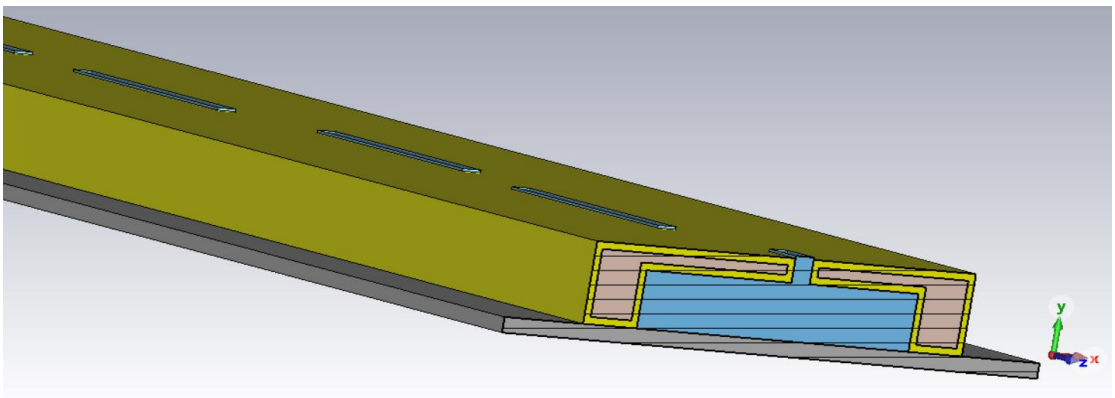

Figure 3.21: View of the silicon filled gold chip.

As it can be seen, there is gold (yellow) all around including the antenna slots, whereas on the inside there is silicon (light orange). Different thicknesses of the casing gave different results. Some of them will be studied below.

- gold thickness=0.018 mm

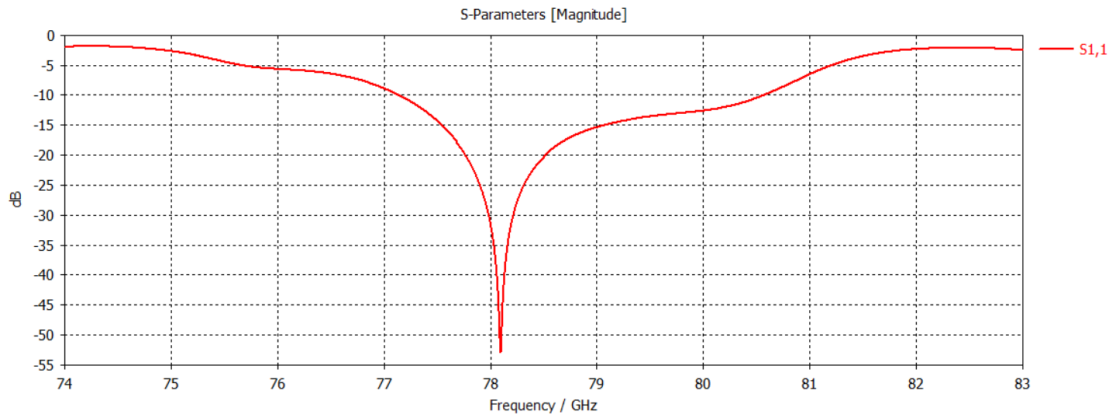

Figure 3.22 (a): S11 parameter result

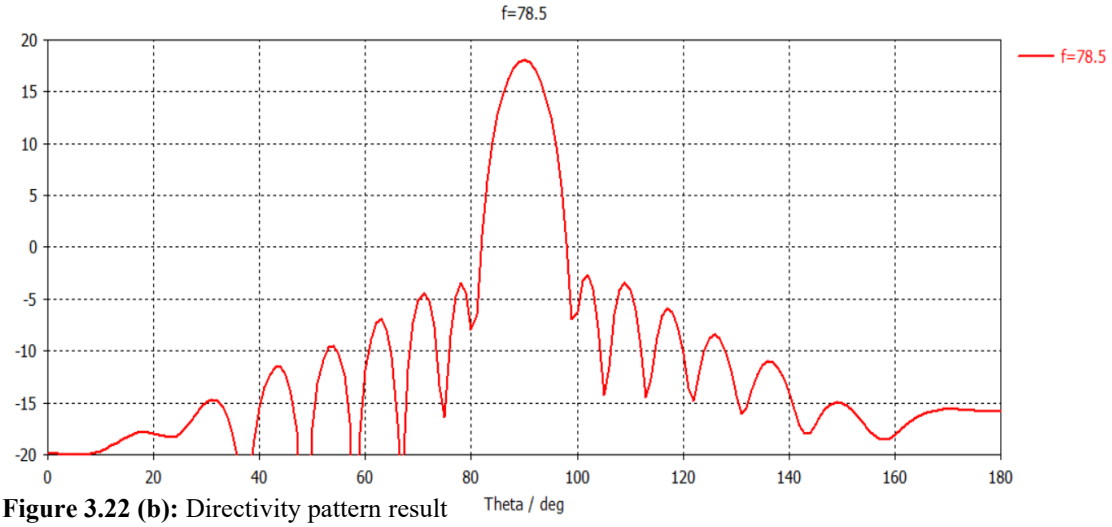

Figure 3.22 (b): Directivity pattern result

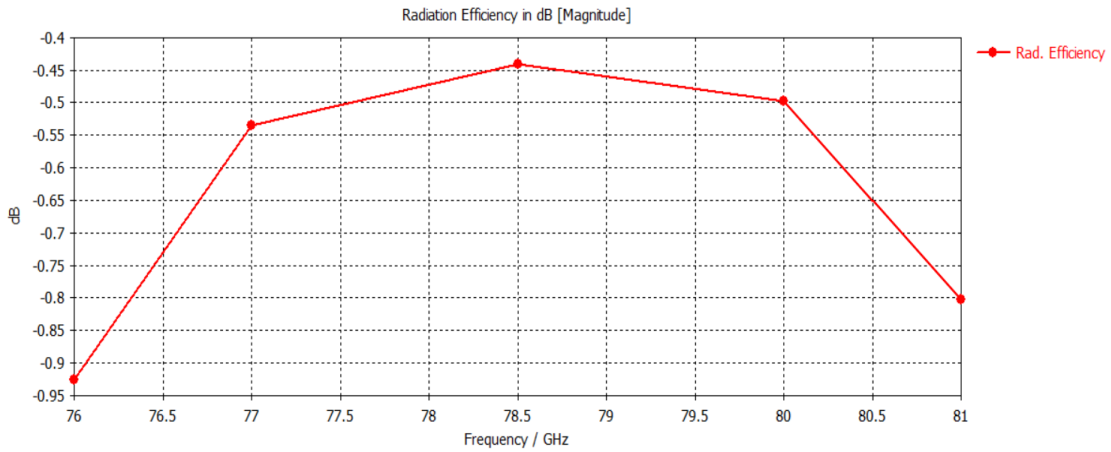

Figure 3.22 (c): Radiation efficiency parameter result

- gold thickness=0.06 mm

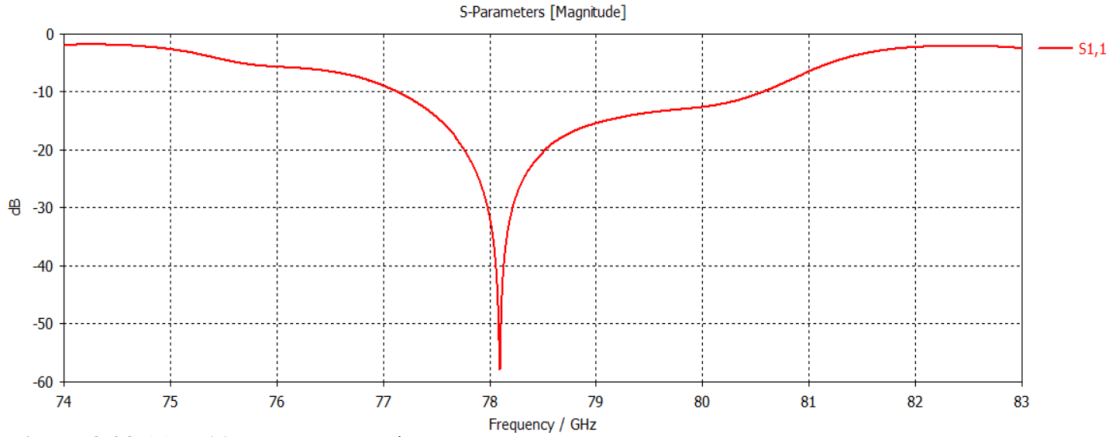

Figure 3.23 (a): S11 parameter result

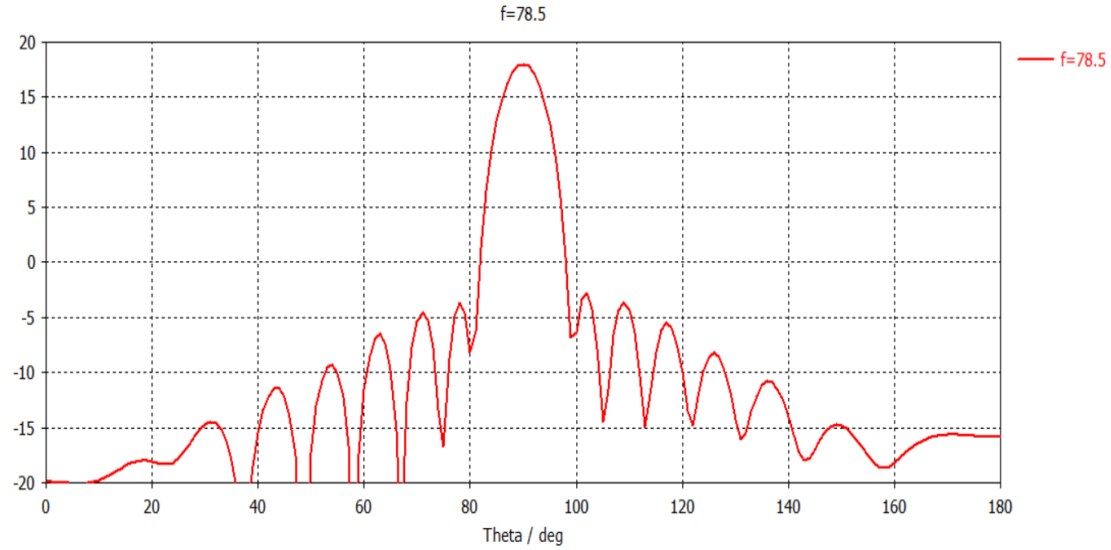

Figure 3.23 (b): Directivity parameter result

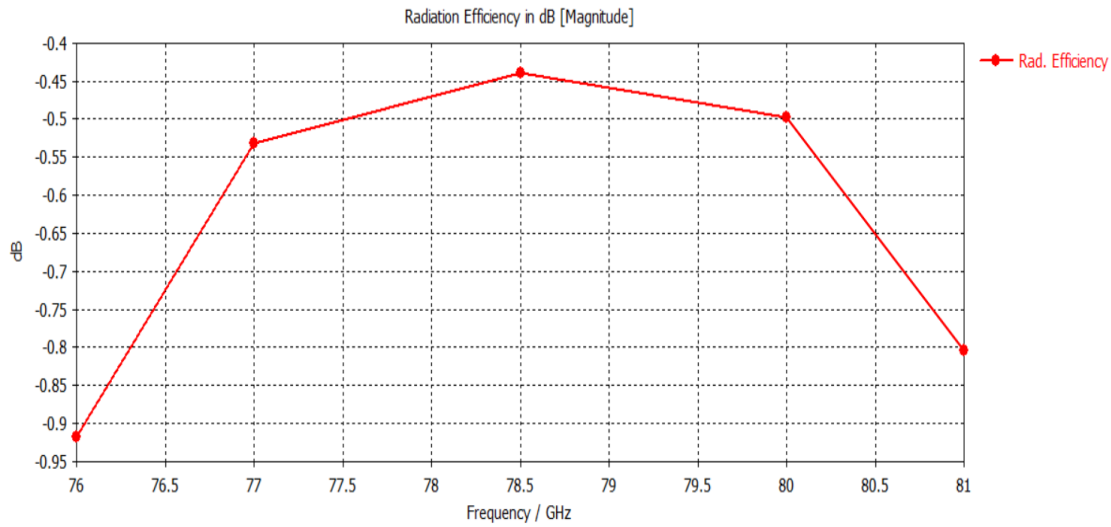

Figure 3.23 (c): Radiation efficiency parameter result

It can be noticed that the result is almost identical to the case in which the casing was totally gold-filled. The resonance frequency is the same, and there are some

differences on the minimum amplitude of the s-parameter, depending on the gold layer thickness. As for the directivity, no noticeable differences can be observed. Same thing goes also for the radiation efficiency. So, this structure can be used to replace the full gold casing, since it has no noticeable differences during the simulations.

3.1.7 Silicon filled with a gold layer at the bottom of the antenna

A further change is made in order to have even less gold involved. This time, only the lower part of the chip and the slots are surrounded by gold. All the other parts are silicon only. A cross section of this design and the gold casing only are shown in Fig 3.24.

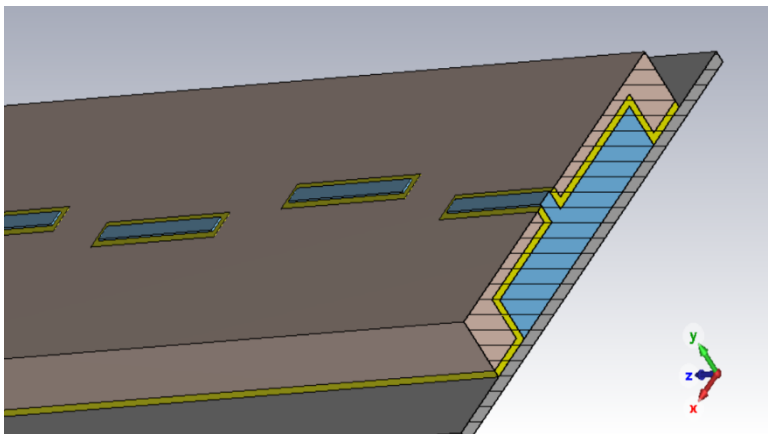

Figure 3.24 (a): Cross section view of the design with a gold layer only at the bottom

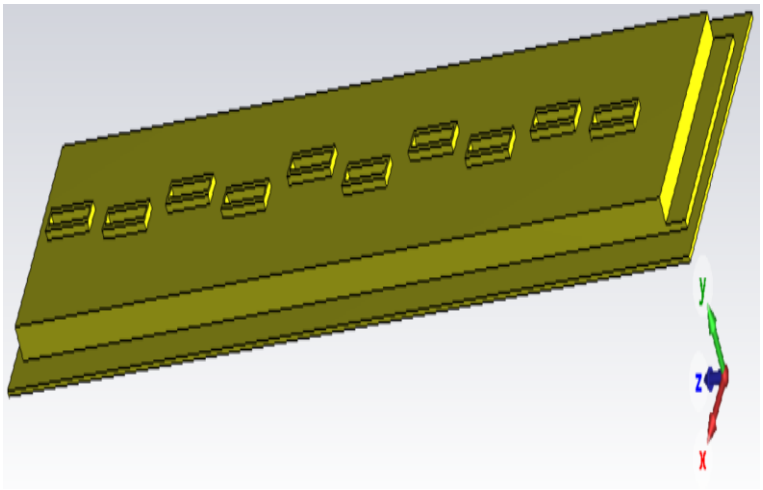

Figure 3.24 (b): View of only the gold layer at the bottom

Some results of different thicknesses of gold are given below to verify the operation of this design.

- gold thickness=0.02 mm

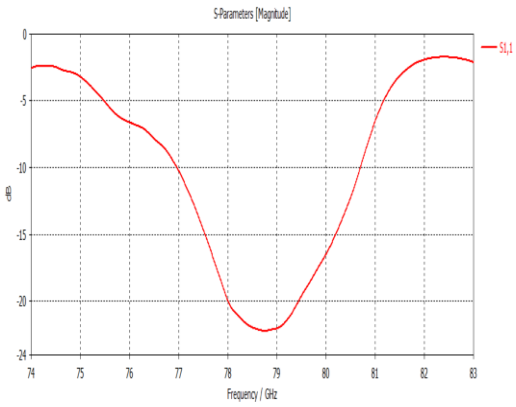

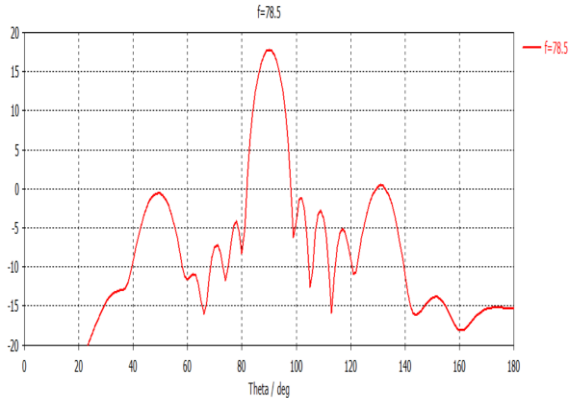

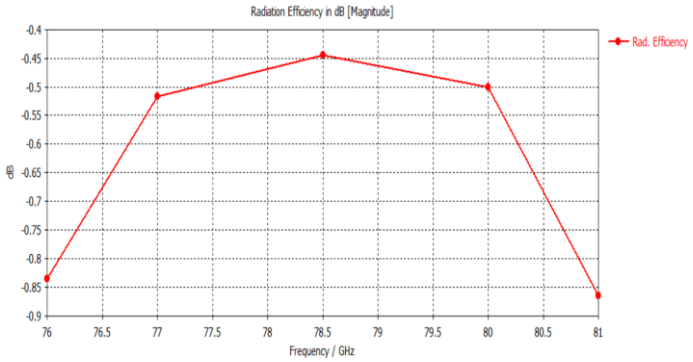

Figure 3.25: Results for a gold layer of 0.02mm thickness

- gold thickness=0.04 mm

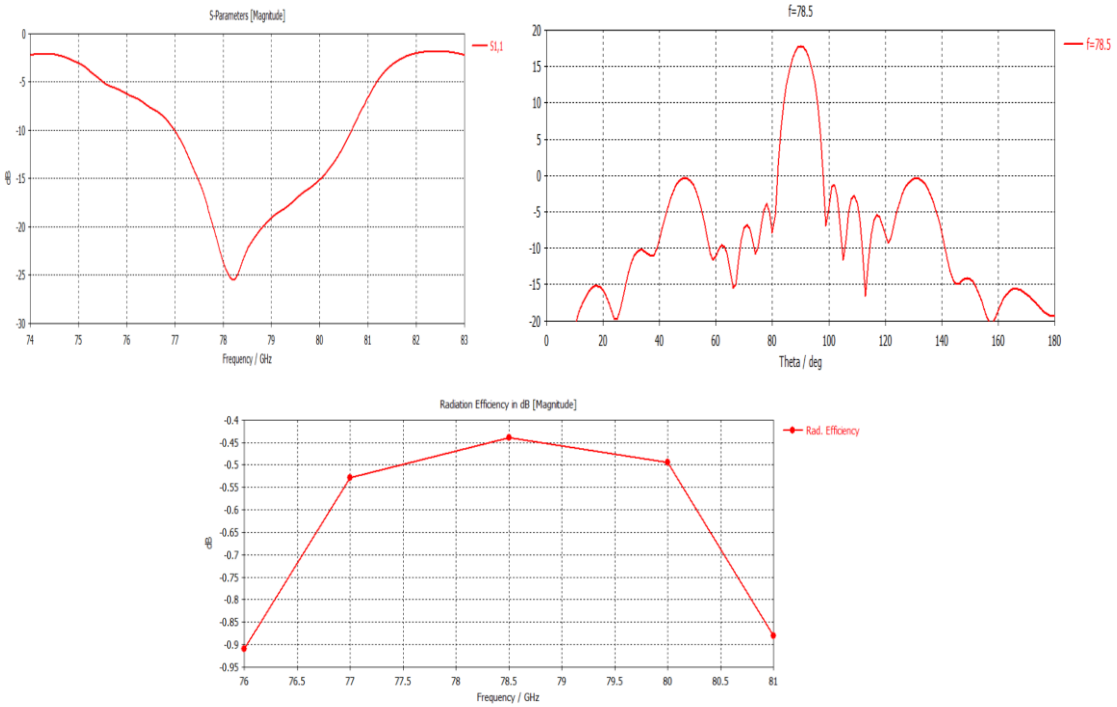

Figure 3.26: Results for a gold layer of 0.04mm thickness

- gold thickness=0.06 mm

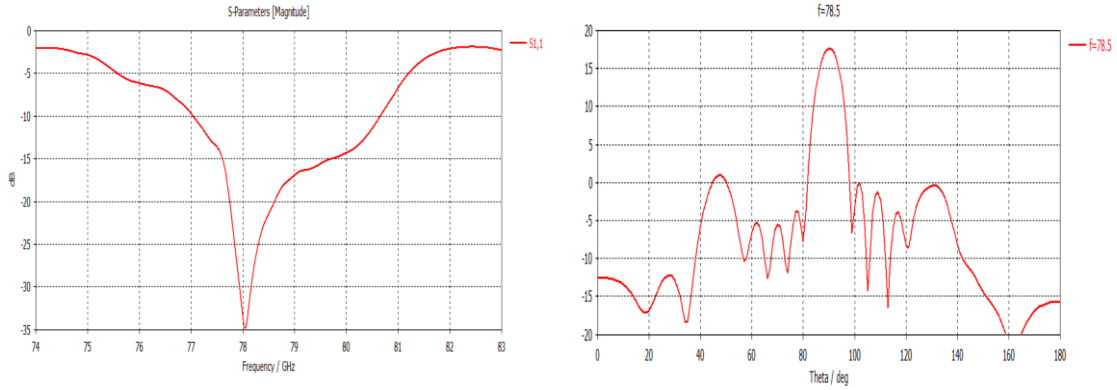

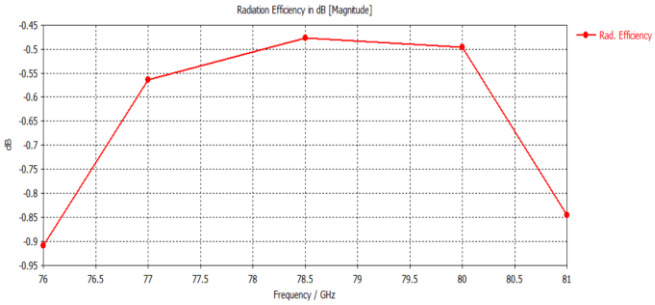

Figure 3.27: Results for a gold layer of 0.06mm thickness

- gold thickness=0.08 mm

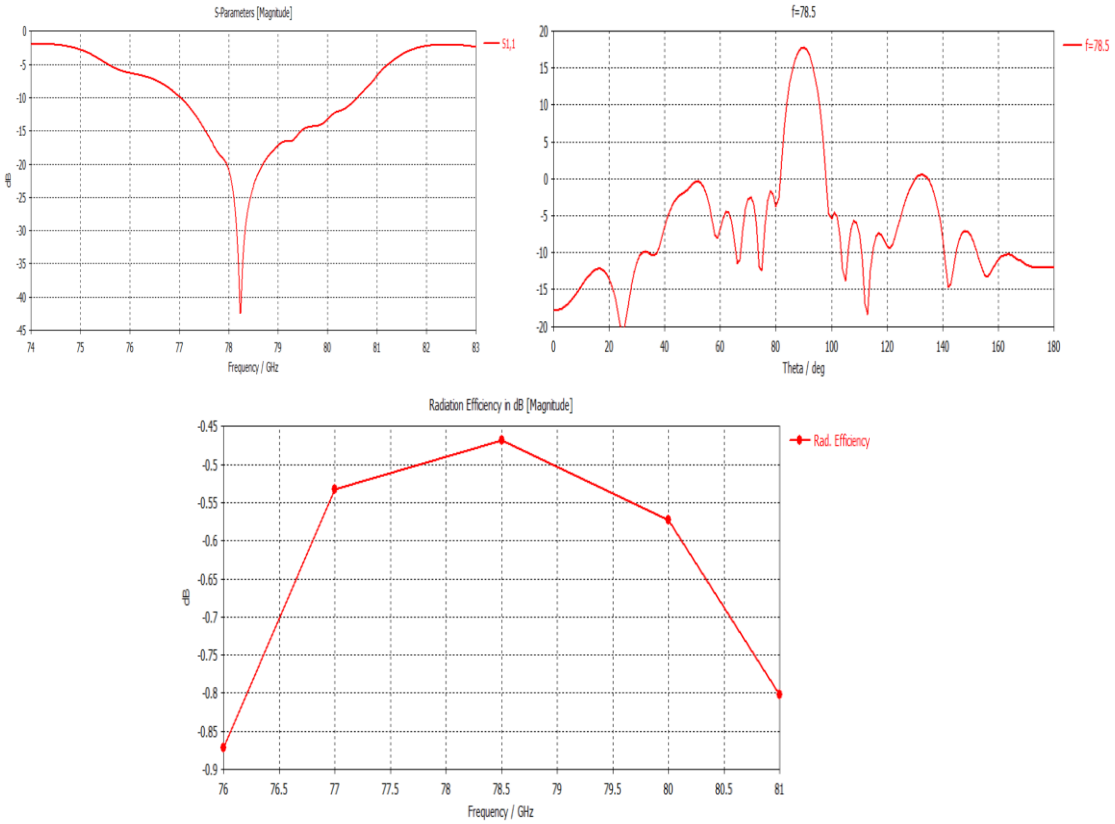

Figure 3.28: Results for a gold layer of 0.08mm thickness

It can be noticed that for this design, the s-parameter results can be acceptable. They vary a lot depending on the gold thickness, differing in minimum value as well as in bandwidth. The radiation efficiency, on the other hand, is not affected by this change and is almost the same as the previous design. However, the directivity is a little irregular, having side lobes which have a big value for some angles θ.

Finally, it was decided to opt out of this design and use either the full gold pack antenna, or the silicon pack with the surrounding gold layer. In the following chapters, the fully gold antenna has been used, as it is more compact, easy to fabricate and easy to combine when working with antenna arrays.

3.2 Waveguide fed antenna

In this upcoming design, the feeding method of the antenna is changed. Instead of a microstrip feeding, another rectangular waveguide will be used to feed the slotted waveguide antenna. In this type of feeding, a separate waveguide is used to excite the main antenna. This type of feeding has some advantages, which include:

- high power rating compared to microstrip lines for the fact that rectangular waveguides have a larger section area, that allows to handle high powers without the worry of losses or damage. It is important for high-power applications such as radar.
- the TE10 dominant mode supported by the rectangular waveguide has low-loss transmission characteristics.
- support of a wide range of frequencies
- the use of a transition section between the feeding and the slotted waveguide antenna can ensure a smooth impedance matching, reducing the reflection coefficients and improving the efficiency.
- ease of fabrication and maintenance. The rectangular shape is easy to manufacture and assemble through machines. Moreover, it is less prone to damage and wear compared to the microstrip counterpart.

The waveguide feeding is an essential part of this thesis work for this slotted waveguide antenna. For that reason, the waveguide has to be excited in a proper way to achieve a good performance for the desired application and it needs to be designed in a way that there is a matching between the impedances of the two structures. The physical dimensions also play a significant role in the design process. The waveguide and the antenna should be designed to have appropriate dimensions to achieve the desired operating frequency range and gain for the application of interest. In the end, the fabrication needs precision machining and assembly techniques to ensure proper functioning and continuation of the simulation results.

3.2.1 Direct waveguide feeding – Single Antenna

For now, a very straightforward design will be discussed. The slotted waveguide antenna will be fed directly from the WR10 of reduced height, which is the waveguide on which the slotted antenna has been built. The full antenna used in the previous chapters, has been cut before the slots and given enough length to have a good feeding such that it does not have perturbations. This structure is shown in Fig. 3.29.

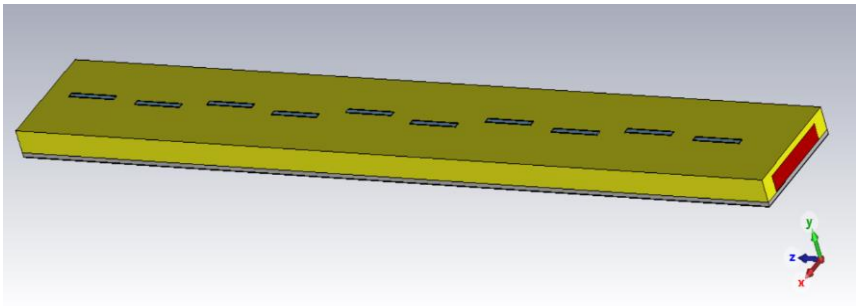

Figure 3.29 (a): Direct feeding of a slotted waveguide antenna

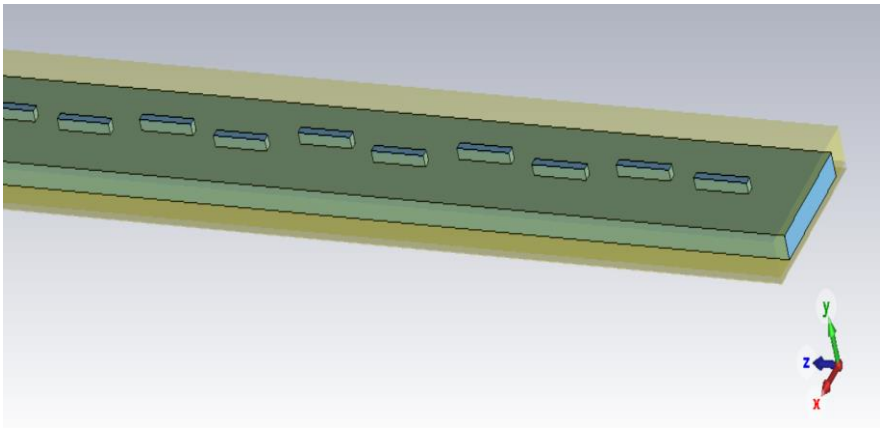

Figure 3.29 (b): Inner view of the slotted waveguide antenna

As displayed in the figures above, this configuration basically studies the extension of the waveguide of the slotted antenna, using it directly as a feeding point. The results of the s-parameter, directivity and radiation efficiency are given in Fig. 3.30.

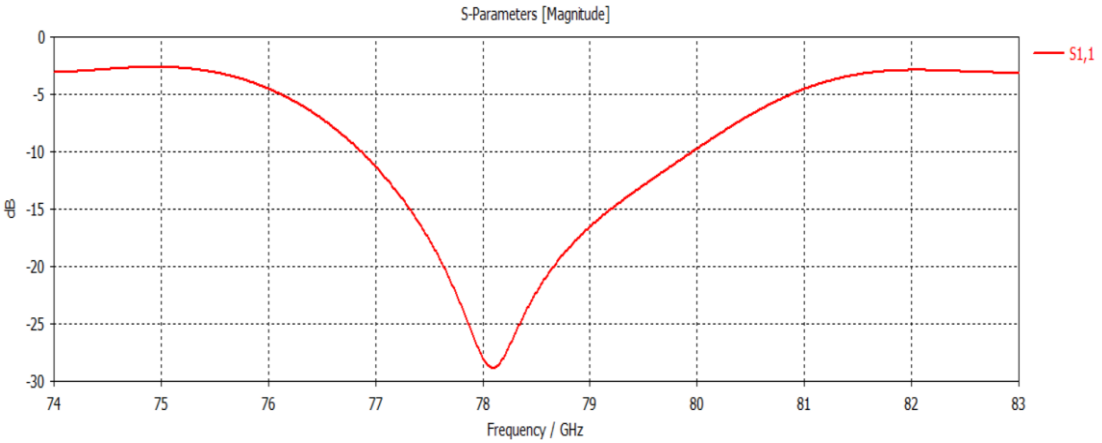

Figure 3.30 (a): S11 parameter

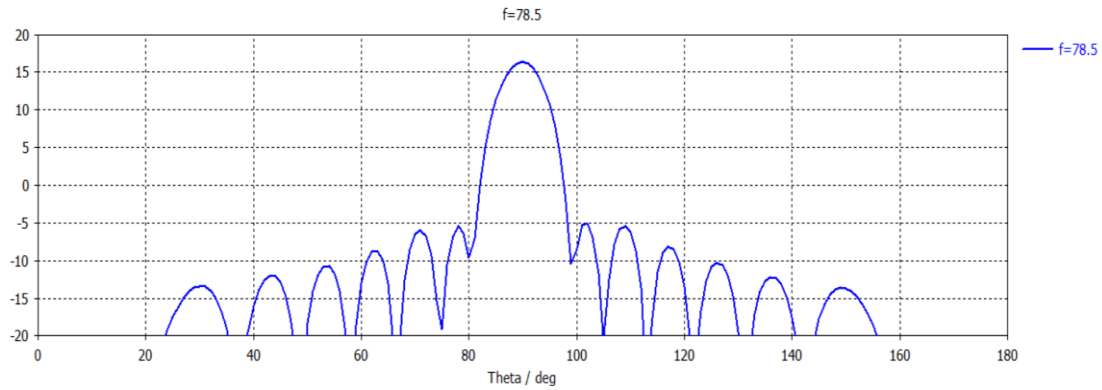

Figure 3.30 (b): Directivity pattern for $\boldsymbol{\varphi = 90°}$

NOTE FOR THE DIRECTIVITY PATTERN STUDY

This type of antenna has a linear horizontal polarization, since the electric field is horizontal to the direction of propagation in the antenna. Being so, the E-plane of the antenna relates to the azimuth plane, whereas the H-plane of the antenna coincides with the elevation plane. Being a highly directional antenna in the vertical direction, the most interesting directivity plane for this study is the elevation one (H-plane). So all the following descriptions of the directivity pattern will be actually referring to the elevation plane directivity pattern for an angle phi=90° and varying angles theta.

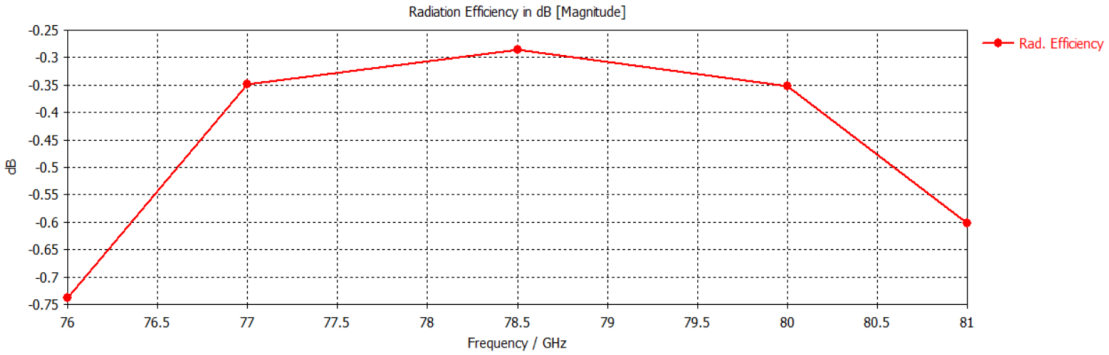

Figure 3.30 (c): Radiation efficiency

This design has been used to basically test the function of the antenna, since it doesn't have many constraints on the feeding. It can be seen that the operating frequency is around 78 GHz, just like the antenna with microstrip feeding. However, in this case the bandwidth is bigger for the -15dB and -10dB level, which is an upgrade with respect to the previous case. The directivity pattern is almost the same, with a main lobe of around 16.3 dB and side lobes lower than the -5dB level. The radiation efficiency is also good for the range of interest, with a peak at the range of interest of around -0.28dB, which corresponds to a radiation efficiency of 93.8% in linear scale.

These results give a good insurance that the slotted waveguide antenna works well while being directly fed through its waveguide. Now, further steps into the design can be made.

3.2.2 Two waveguides in an L-transition

For the next steps, it was decided to have a "Launcher On Package" technology for the antenna, in which the launcher (the feeding) is integrated directly into the module substrate allowing for a compact and low-loss solution for feeding the antenna. LOP technology has been developed for primary use in applications where space and cost play a huge role in the design. The signal is coupled from the RFIC to the 3D antenna (normally through a waveguide) mounted above the package. The external 3D antenna then radiates the signal to the environment. The external 3D antenna is not limited to the package size, so the antenna can be designed for high performance usage. Having this solution can bring to a reduced number of components for the antenna as well as an improvement of the overall antenna efficiency. Doing so, the feeding waveguide has to be fixed to a WR12, which is the most commonly used one for automotive radar application. Since it has to be connected directly to the module, the feeding waveguide will have to feed the main antenna from the bottom an L-transition form in the y-direction. An idea of this L topology is given in Fig. 3.31.

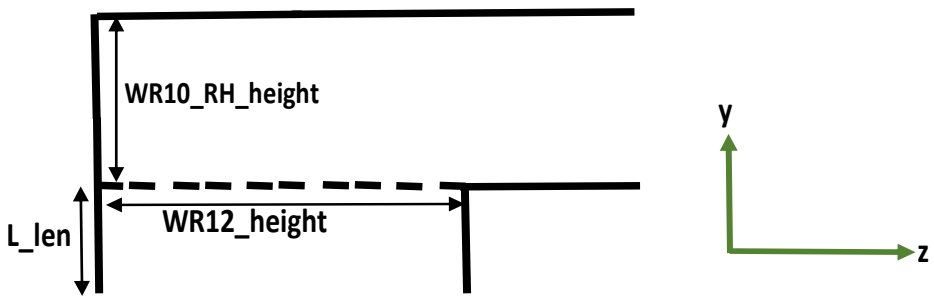

Figure 3.31: Side view of a simple L-transition structure idea

In this figure, an illustration of an x-cut cross section is shown. Everything below the dashed line is the waveguide used to feed the slotted waveguide antenna. One of the key advantages of using the WR12 waveguide for LOP technology is its ability to efficiently transfer power from the radar transceiver to the antenna element. The waveguide's rectangular shape allows for a good impedance match between the transceiver and the antenna, which minimizes signal loss and improves overall performance. However, there is the need to have a transition stage from the WR12 to the WR10 of reduced height, which is connected to the slotted waveguide antenna. The two structures, as seen in Fig. 3.32, have the following dimensions:

- **WR10-RH: 2.54mm x 0.475mm (width x height)**
- **WR12: 3.0988mm x 1.5494mm (width x height)**

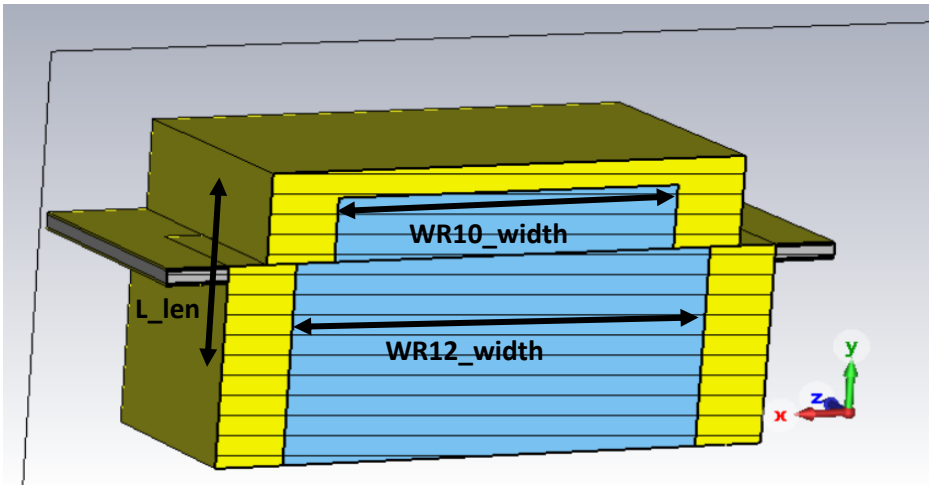

Figure 3.32: Inner view of the designed L-transition structure

The L transition is used to couple energy between the two waveguides with different dimensions. It is designed to have an impedance matching and to minimize the reflection coefficient and losses. The “L” in the name refers to its shape. It is widely used in millimeter wave systems for antenna feed networks as the one being designed in this thesis. This type of adapter is not hard to fabricate and can provide good matching for a wide frequency range. For now, a study of only the transition stage between the two waveguides will be discussed. The slotted antenna will be added later, after achieving suitable results in this preliminary case. The antenna is cut right before the first slot.

The idea implemented in the designing of this L-transition is that of having a gradual passage from one waveguide to the other, which can be done by introducing steps. They are designed to have a specific height, width and step size, based on the operating frequency requested. Moreover, the usage of steps helps minimize the unwanted EM modes, which can be generated at sharp corners and cause interferences. Initially, the idea to use steps rose from a different design. In that design, the setting was the same,but the WR12 height was free to change. It was noticed that at a certain WR12 height,there was no need for many adjustments of the structure, as there was already a relatively good matching.

Going back to the current design, using a step is a good transition stage which gradually shifts the passage from one waveguide to another. It gradually reduces the

height of the lower waveguide to match the height of the upper one. This multi-step transition provides good impedance matching and minimizes the reflections over a wide frequency range.

The material used for this design is gold. To reach a good outcome, the results of each modification on the structure were studied through CST Microwave Studio tools, constructing a pattern, and choosing the best parameters to have the best transition and matching between the 2 waveguides.

The steps' structure is shown in Fig. 3.33.

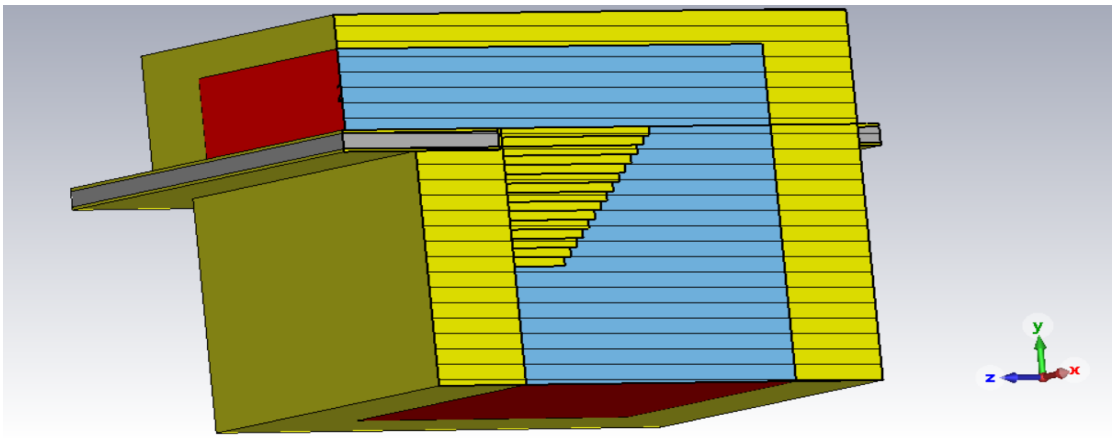

Figure 3.33 (a): Side view of the steps used as the L-transition together with the two waveguides.

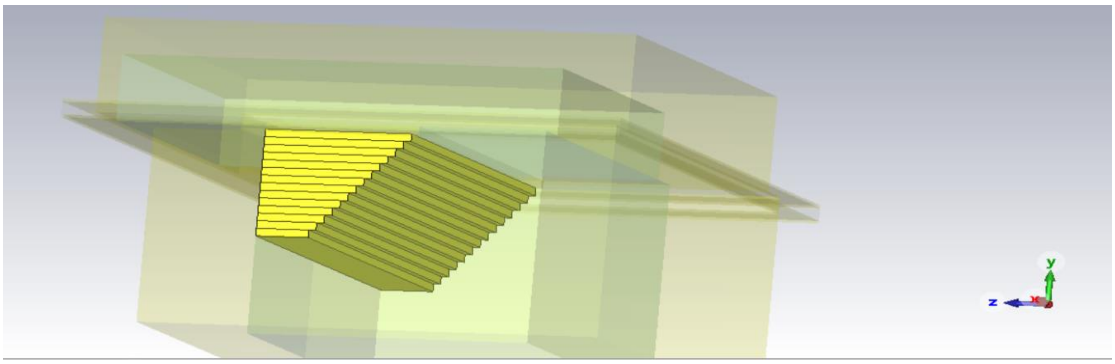

Figure 3.33 (b): Full view of the steps used as the L-transition.

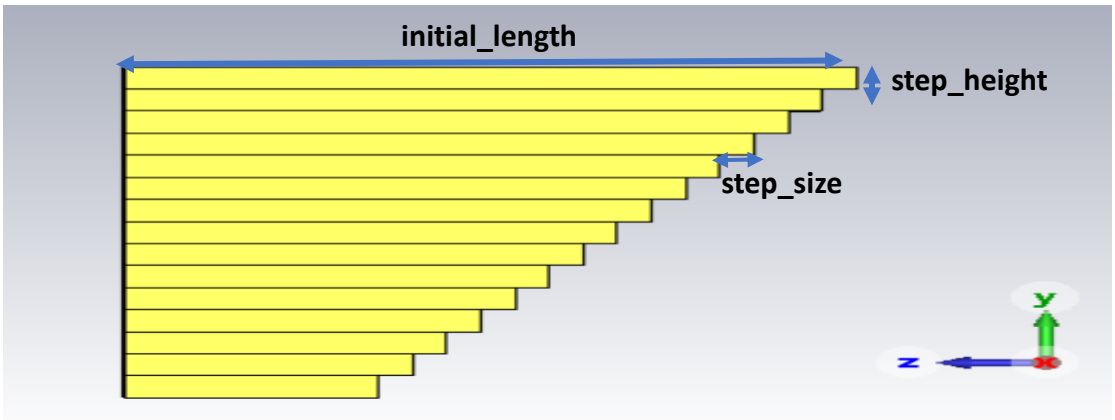

Figure 3.33 (c): Side view of only the steps used as the L-transition.

It should be noted that the steps width is equal to the width of the WR12 waveguide. Moreover, the number of steps was chosen based on the change in results after each

new step was introduced. Depending on the number of steps, the step size required to have a good transition would change. Mainly, having less steps, the step size required was also smaller. So, in order to have a good result, such that small tolerances in the step dimensions would not affect the final outcome, the number of 14 steps was chosen, with a relatively high step size with respect to the tolerances. After some simulations and optimizations, the final parameters chosen are the following:

- **L_len=1.5mm**
- **initial_length=0.875mm**
- **step_height=3*metal_thick=3*0.018mm**
- **step_size=0.04mm**

The result of the s-parameter in this design, in which port 1 is the WR12 port (below) and port 2 is the WR10 port (above), is given in Fig. 3.34 below.

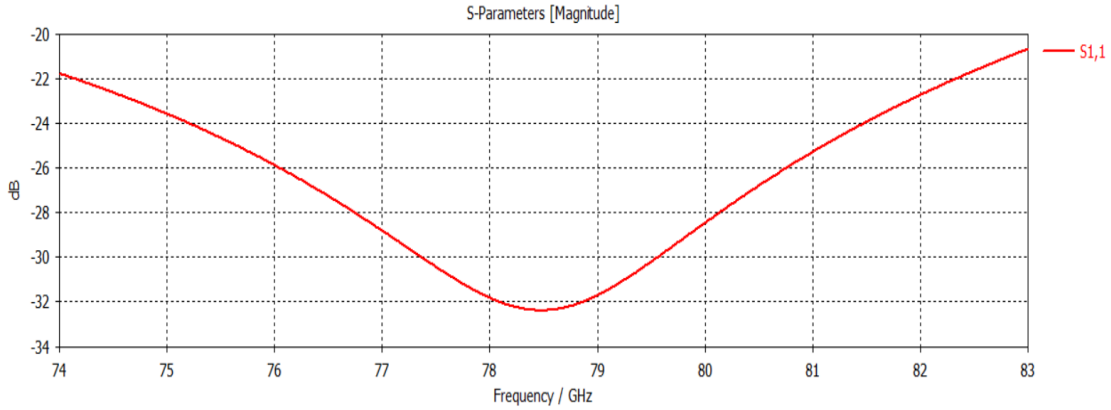

Figure 3.34 (a): S11 parameter for the L-transition structure

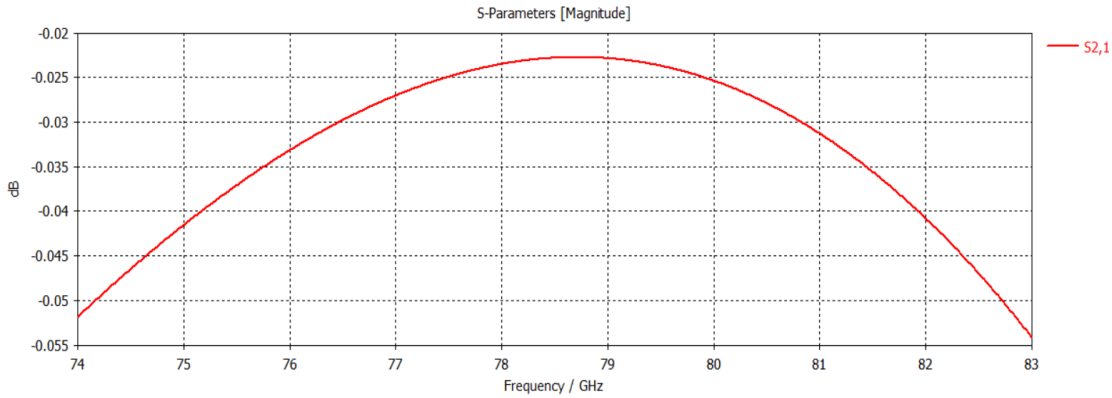

Figure 3.34 (b): S21 parameter for the L-transition structure

It can be noticed that the s11 parameter is centered around 78.5 GHz, has a very small value and a large bandwidth of operation. The s21 parameter, on the other hand is very close to 0 dB or 1 in linear scale, which means that there is minimal interference or coupling between the input and output port of the waveguide.

3.2.3 Full antenna L-transition

Now it is the time to include the whole antenna. Before going to the multiple antennas, a single antenna will be studied. The slotted waveguide antenna is added after the L-transition. A view of this design is given in Fig. 3.35. The antenna has one feeding port, which is that on the WR12 waveguide on the L-transition.

It must be noted that both the L-transition and the slotted waveguide antenna should be carefully designed and matched in order to achieve optimal performance. If one of the two is poorly designed or has limited bandwidth or efficiency, the system's performance may degrade. For example, a poorly designed L-transition stage can introduce unwanted reflections and degrade the system's performance. Similarly, a poorly designed slotted waveguide is inefficient and may limit the performance of the whole system, despite having a high-quality transition stage.

The slotted waveguide is the one used before, which is covered by gold and on the bottom has the PCB metal and a dielectric layer. The addition of the L-transition stage to the slotted waveguide antenna will act as a tool for improving the overall antenna performance. By using the optimized L-transition structure discussed in the previous point, the final efficiency of the antenna can be maximized for the requested operation.

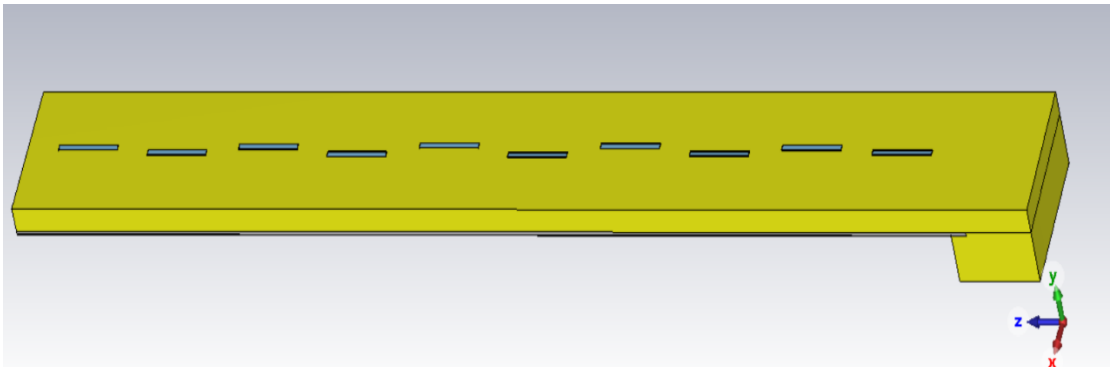

Figure 3.35: Full antenna + L-transition strucutre

A cross section view is shown in Fig. 3.36.

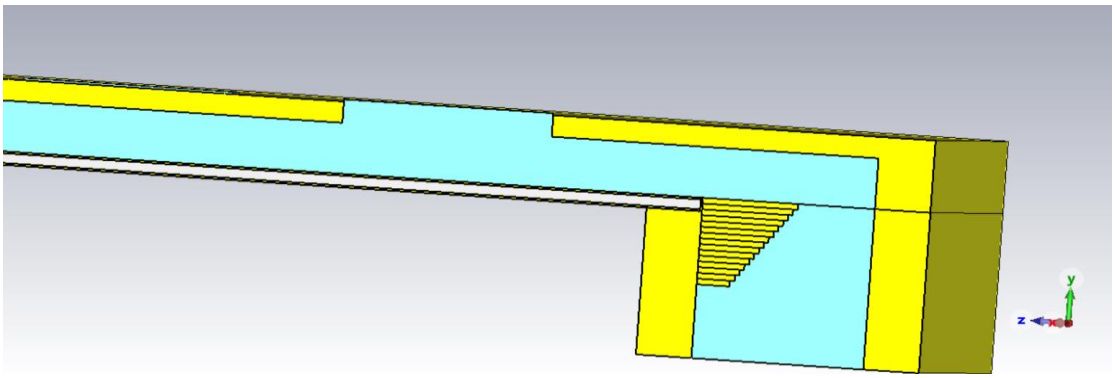

Figure 3.36: Side view of the full antenna + L-transition

Using the parameters of the slotted waveguide antenna, which were described in the previous chapters and the parameter of the L-transition, which was just now designed, the following s-parameter result, shown in Fig. 3.37. is achieved.

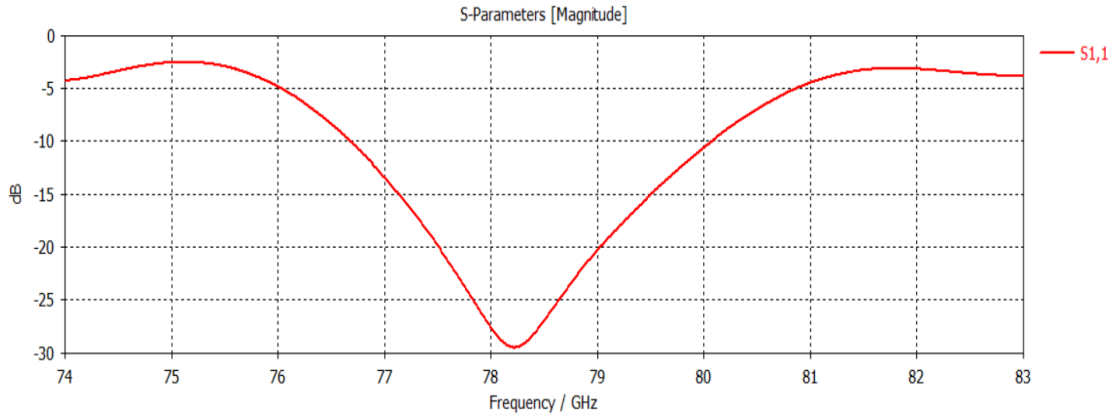

Figure 3.37 (a): S11 parameter of the full structure

The result of the s-parameter from the simulations shows a wide bandwidth of around 3.5 GHz at the -10dB level and around 2.5 GHz at the -15dB level, with a bottom of -29.5dB at 78.22GHz. On the other hand, as illustrated below, the directivity pattern for a frequency of 78.5 GHz, a theta from 0 to 180°, with a phi of 90°, shows a main lobe of 16dB and side lobes below the -5 dB mark.

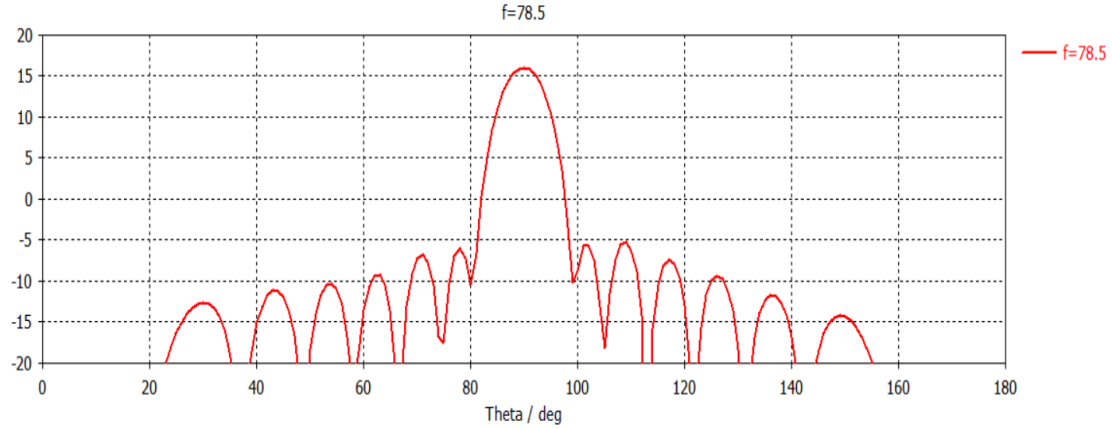

Figure 3.37 (b): Directivity pattern of the full structure; $\boldsymbol{\varphi = 90°}$

As for the radiation efficiency, it has a good result for the frequency range of interest, with the lowest value being around -1dB for 76GHz and the highest being -0.3dB, corresponding to 93.3% radiation efficiency for 78.5GHz, as shown below.

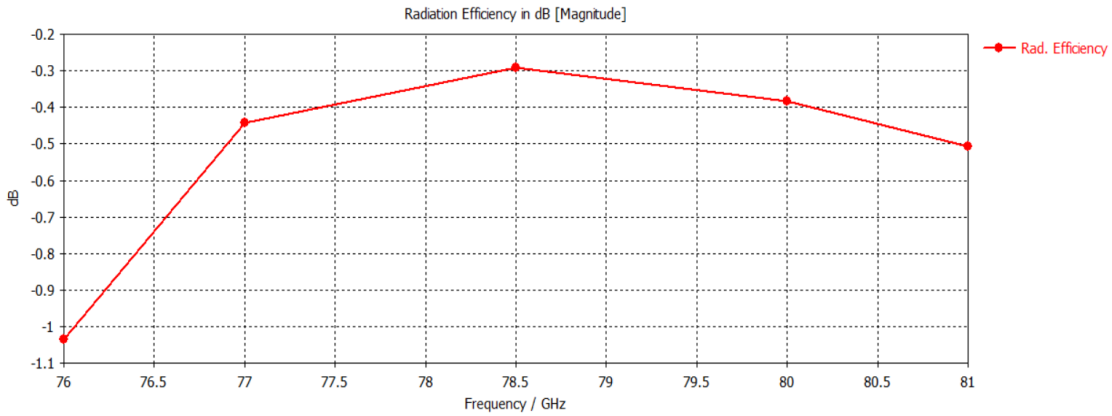

Figure 3.37 (c): Radiation efficiency of the full structure

3.2.4 Antenna array

The previous results of the L-transition and the antenna are promising and good for the application field of interest. Based on these results and designs, an antenna array can now be built.

In a radar antenna array, the antennas should have a distance $\frac{\lambda_g}{2}$ between one another. That distance, in this case, has been measured from the centers of the antennas. However, there is a problem. The half-wavelength is equal to 1.91mm, but the distance of the built antenna from the center to the edge where the metal starts is equal to $\frac{wgA}{2} = 1.27mm$. That means that antennas of these lengths and operating frequency cannot be set into the same plane to build an array for radar application, since the inner parts of the antennas would overlap. For it to work, the maximum half-length of the antenna (center to edge) would have to be $\frac{\lambda_g}{4} = 0.955mm$. One way to overcome this problem is to have the antennas one on top of the other, in a way that the inner part of top one doesn't overlap with that of the first antenna and vice versa.

3.2.4.1 Direct waveguide feeding

The main goal of this sub-chapter is to test the correct functioning of the antenna array, while having a direct feeding of the WR10-RH waveguides like it was done in Ch. 3.2.1. This way, the directivity pattern can be analyzed to see if the antennas are working as a combination, increasing the final value of this parameter.

As for the design part, since the antennas must be put one on top of each other, a down-shift in the y-direction will be present, such that there will not be any superposition of the inner parts of different waveguides. A good parameter for the y-shift is "***y_shift***"*=0.675mm*. At the same time, as discussed before, there will be the x-direction shift equal to half-wavelength. A preliminary design, up to this point, with only 2 antennas is shown in Fig. 3.38.

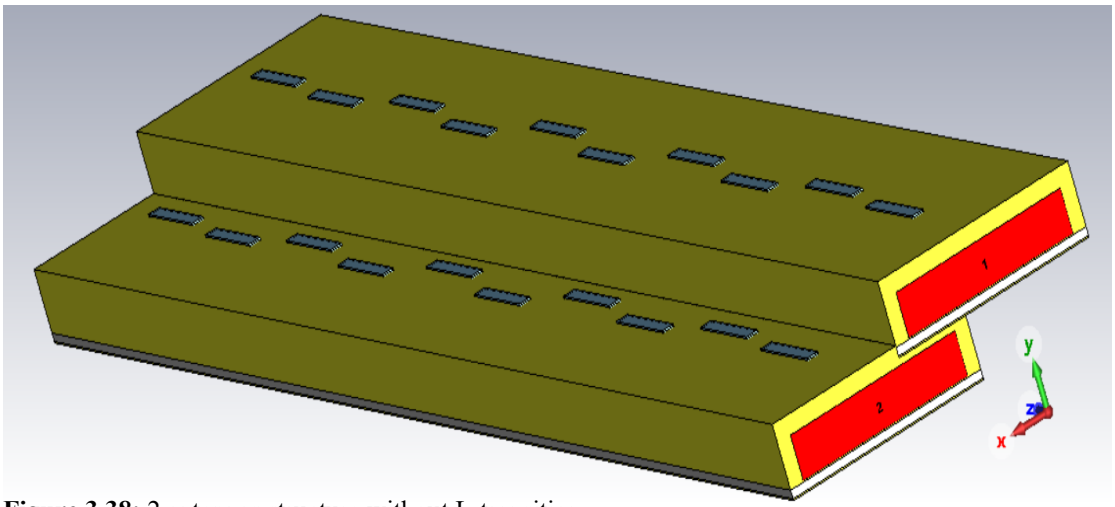

Figure 3.38: 2 antennas structure without L-transition

It can be noticed that there needs to be an adjustment of the bottom antenna, to have its slots at the same level as the top antenna. This adjustment is needed in order to have the desired beamforming, which means having the antennas work together to

produce a strong and focused beam in a certain direction, rather than radiating in different directions. Moreover, having them not on the same plane, can lead to reduced antenna gain and distorted radiation patterns. The adjustment can be done by extending the upper gold layer and the slots up to the level of the top antennas. The extension will have a value equal to the y-direction downshift, which is 0.675mm. However, this adjustment leads to another problem, which is that of having very high and narrow slots of the bottom antenna. This will lead to a decrease in efficiency due to the large distance between the slots and and top of waveguide, meaning that there will be a decrease in coupling between slots and free space. Moreover, the s-parameters will not be on the desired position and the bandwidth of the antenna decreases due to changes in effective aperture of antenna, since the energy will be confined to a narrow beam. To overcome this problem, the following tactic can be used: have a double width along the slots of the bottom antenna, which means having a certain width of the slot for a height *"**height1**"* and then have an extension of the width for the remaining height "***y_shift-height1***". This will bring to an increased bandwidth due to an increase on the effective aperture of the antenna and an improved radiation efficiency improving the coupling between slots and free space. By changing the width of the slots, the radiation pattern can be shaped to achieve high gain in a particular direction. A note on the effect of the slot width and height will be given below.

The slot width affects the frequency of operation and the bandwidth of the antenna. Having a wider slot allows to operate at lower frequencies, while narrower slots provide higher frequency of operation. This because for lower frequencies, the wavelength of the EM waves is larger, so the slots need to have a wider opening to allow them to pass through. The contrary can be said for high frequencies.

The slot height affects more the radiation pattern of the antenna. It affects the polarization in the y-direction, so the vertical one. Having taller slots, provides better vertical polarization. Moreover, higher slots can result in a narrower beam.

Fig 3.39 (a) and (b) show the adjusted antenna.

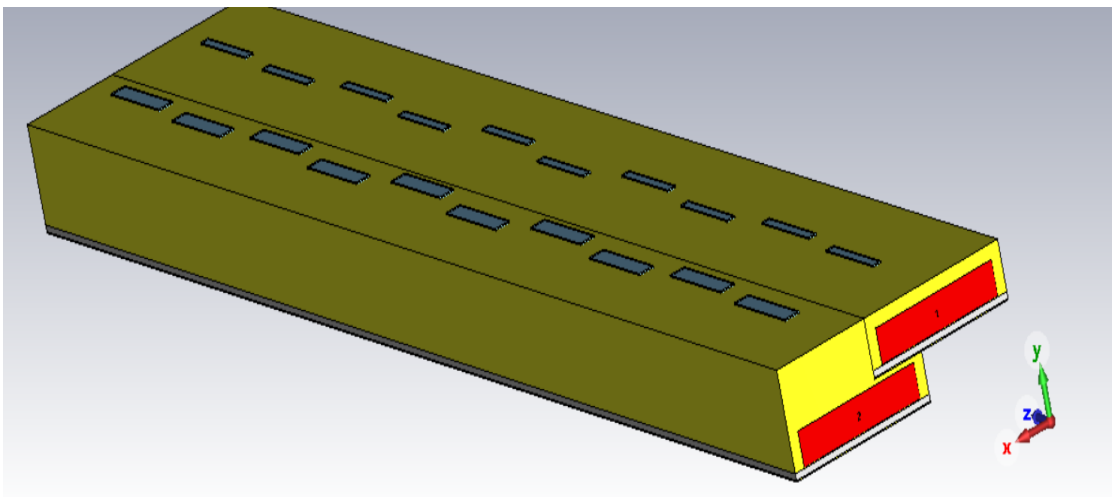

Figure 3.39 (a): 2 antennas structure with adjusted height and width

It can be noticed that despite the fact that the bottom antenna is downshifted by a certain value, its upper part has been compensated by the same value. Moreover, the

width of the slots can be clearly seen to be wider for the bottom antenna as discussed previously.

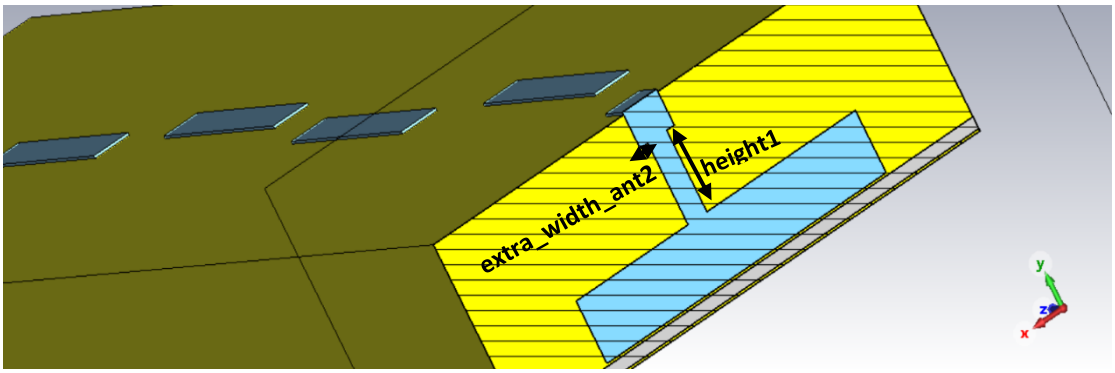

Figure 3.39 (b): Inner view of the adjusted antenna in height and width

A simulation of only the elongated antenna only, seen in Fig 3.41 (b), was done to check its operation. The following parameters have been used:

- **extra_width_ant2=0.07 mm**
- **height1=0.4mm**

The results for the s-parameter and the directivity pattern are given in Fig 3.40 (a) and (b)

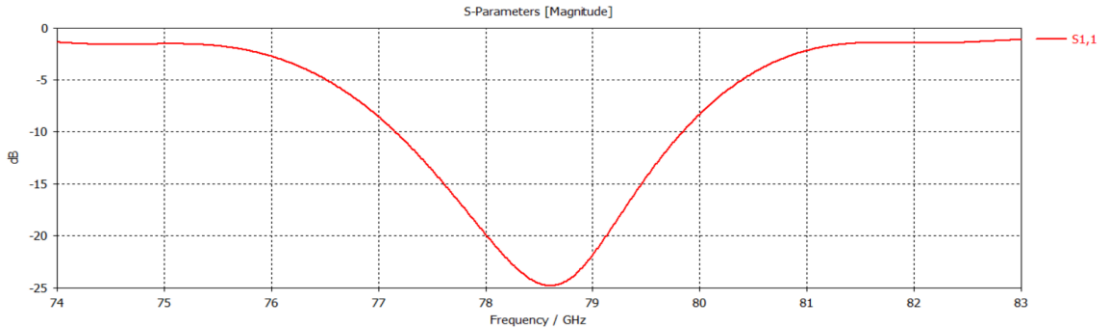

Figure 3.40 (a): S11 parameter of the adjusted antenna only without L-transition

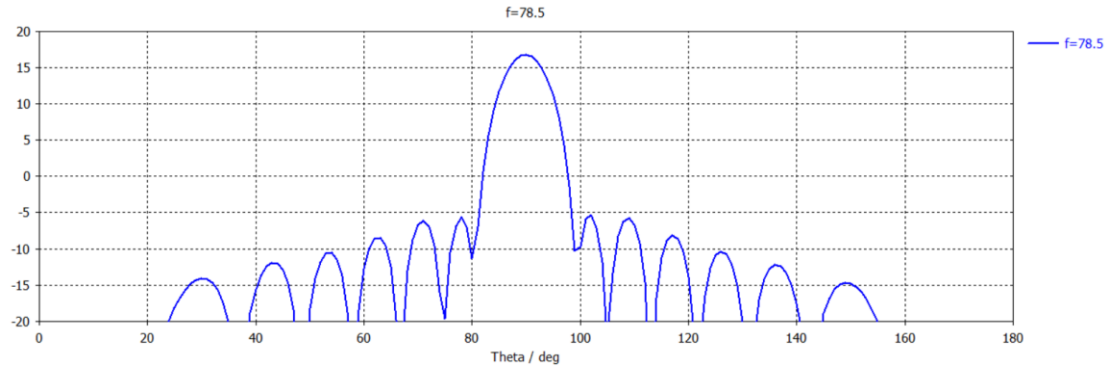

Figure 3.40 (b): Directivity pattern of the adjusted antenna only without L-transition; $\boldsymbol{\varphi = 90°}$

It can be noticed that the s-parameter is centered on 78.5 GHz, with a bottom of -25 dB and has a bandwidth of around 2GHz on the -15dB level and 2.7GHz on the -10dB. These results are good for this application and are on a similar level to the single antenna result of chapter 3.2.1. As for the directivity pattern, it is also very similar to the previously mentioned case, with a main lobe of -16.3dB and side lobe

level below the -5dB mark. These results verify that this design can be used together with the default antennas to have a full antenna array.

The full array will consist of 8 antennas. There will be 4 top ones and 4 bottom ones. The port numbering will be odd for the top antennas and even for the bottom ones. As it was discussed up to now, the neighboring antennas are separated by the half-wavelength distance of 1.91mm. Everything is set in such a way that the inner parts of the different waveguides do not interfere with each other and that there is enough gold layer around them for separation as shown in Fig. 3.41.

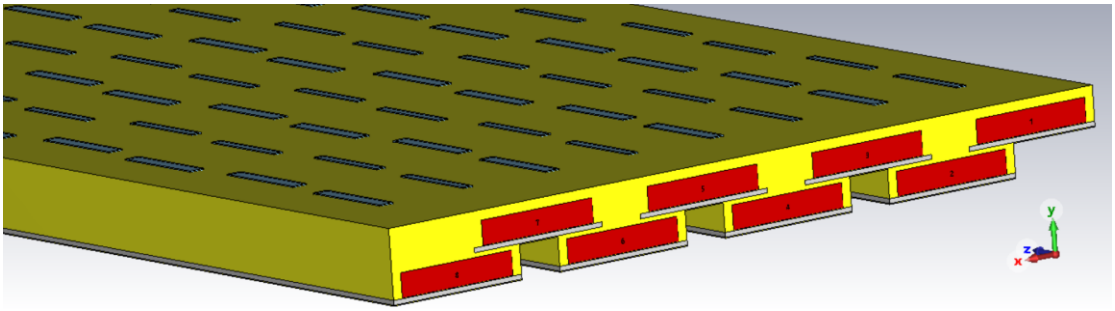

Figure 3.41: Antenna array; no L-transition

After some simulations, it was noticed that the s-parameter for the odd port antennas was affected by the newly added antennas and needed a little left-shift. So, in order to have even better results for all the antennas, such that they go good with each other, it was decided to have an enlargement of the slot size also for the odd port antennas ("Top" antennas), similarly as it was done with the even port antennas. However, this time there will be only an enlargement of the width of the slots, rather than also of the height. This parameter will be called ***"extra_width_ant1"***. As it was discussed, the enlargement of the slot width gives way to lower frequencies. Some results will be shown below:

- **extra_width_ant2=0.07 mm**
- **height1=0.3mm**
- **extra_width_ant1=0.016 mm**

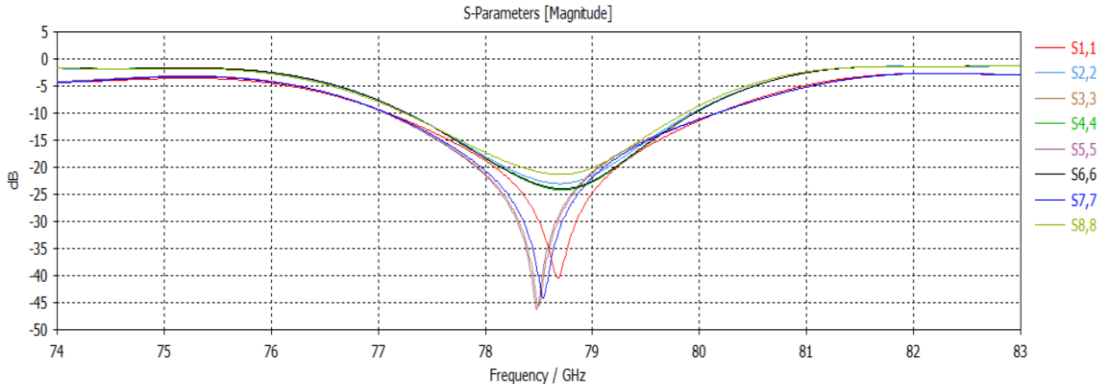

Figure 3.42 (a): S11 parameter for the first case

The different curves show the s-parameters of each port. It can be noticed that the odd port antennas have a deeper bottom on the s-parameter compared to the even port antennas. This is mainly due to having the higher slots in the even port antennas. Some other parameters have been tried and the result are shown in Fig. 3.42.

- **extra_width_ant2=0.07 mm**
- **height1=0.3mm**
- **extra_width_ant1=0.02 mm**

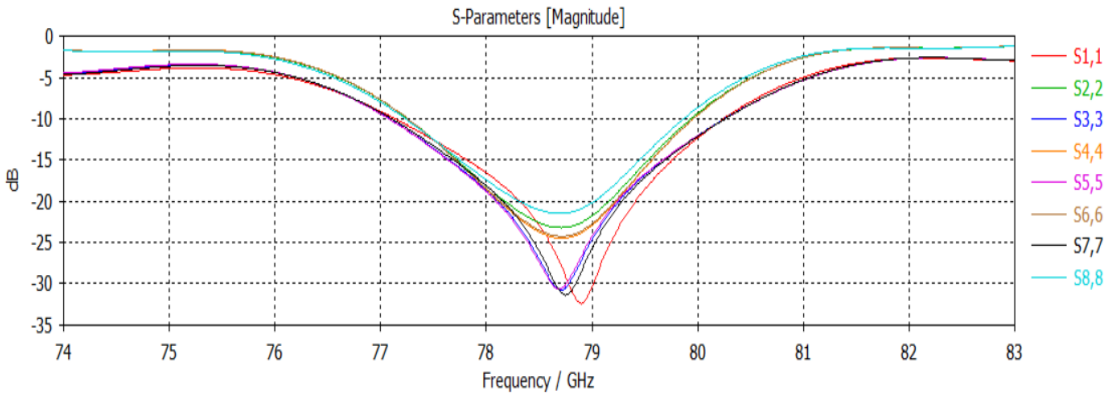

Figure 3.42 (b): S11 parameter for the second case

The s-parameters this time are nearly on the same level. The bottom of the s-parameter is on around 78.5 GHz for all antennas and their value is quite similar. The bandwidth is of around 2 GHz for the -15dB level and around 2.7 GHz for the -10 dB level.

In order to test the directivity pattern, the feeding phase shift should be adjusted for the different ports. The phase shift depends on the distance between the ports of the different antennas. More concretely, the phase difference is given by $\theta = k * L$, where k is the propagation constant, and L is the distance between ports. This formula can be rewritten as $\theta = \frac{2\pi}{\lambda} * L$, which gives a result in radians. Ultimately, it will be used to multiply the amplitude with the value $e^{-2j\theta}$. The distance on the x-direction is equal to half-wavelength. This means that it will not affect the phase shift, whereas the distance in the y-direction is -0.675mm. That gives a phase shift of around -63.6°. Using this value for the even ports, a combination of the result for the directivity pattern of all single antennas was made. The final directivity pattern result is shown in Fig. 3.43 in three types: 3D, 2D cartesian and 2D polar plot.

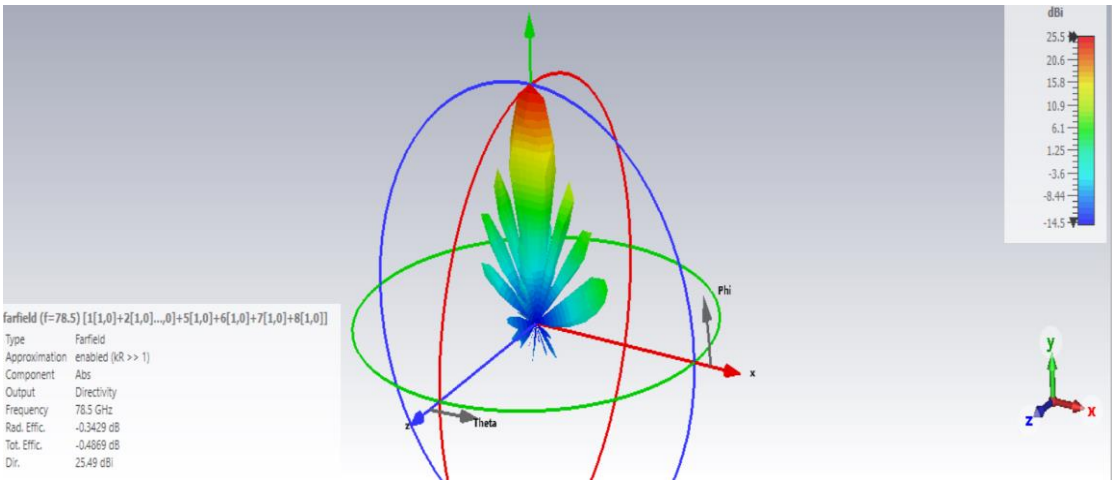

Figure 3.43 (a): 3D Far-field directivity pattern for antenna array without L-transition

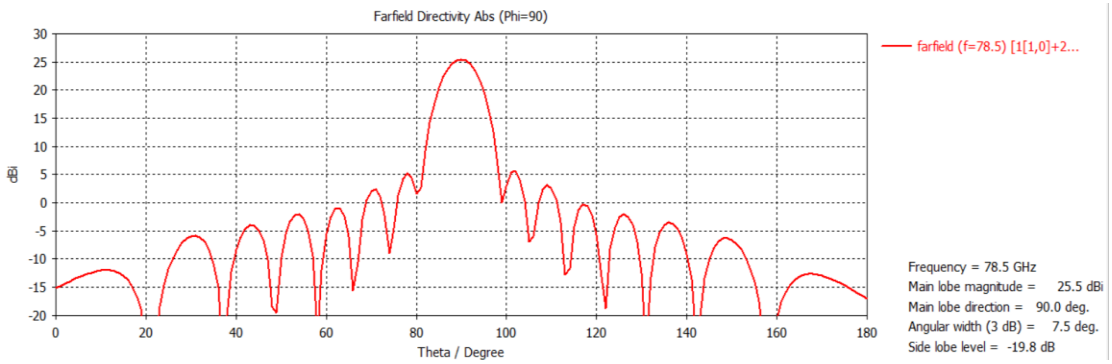

Figure 3.43 (b): 2D cartesian Far-field directivity pattern for antenna array without L-transition; $\boldsymbol{\varphi = 90°}$

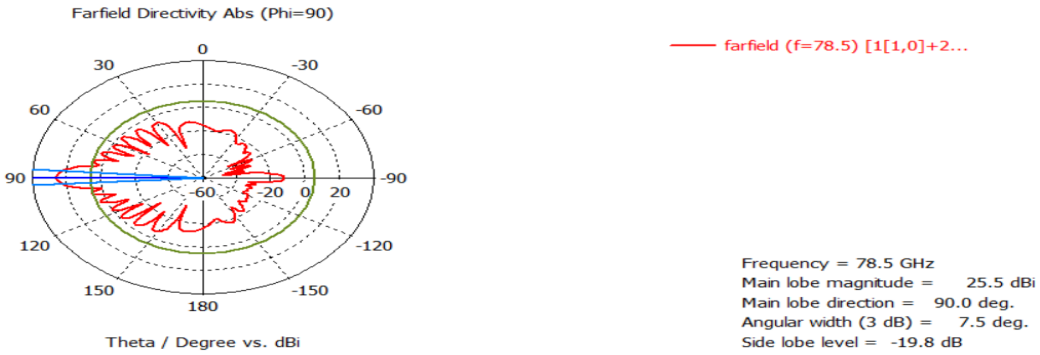

Figure 3.43 (c): 2D polar Far-field directivity pattern for antenna array without L-transition; $\boldsymbol{\varphi = 90°}$

The single antenna is known to have a main lobe value on the directivity pattern equal to around 16.3dB. That means that having 8 antennas together, the main lobe in theory should increase by around 9dB. Every double in the number of antennas gives a 3dB increase (double power gain) in the main lobe. Here it can be seen that the main lobe magnitude is 25.5 dB, which is in correspondence to the theoretical hint. On the other hand, the side lobe level is -19.8dB below the main lobe peak, which is around 100 times smaller (using the linear scale).

The combined radiation efficiency is given in fig.3.44.

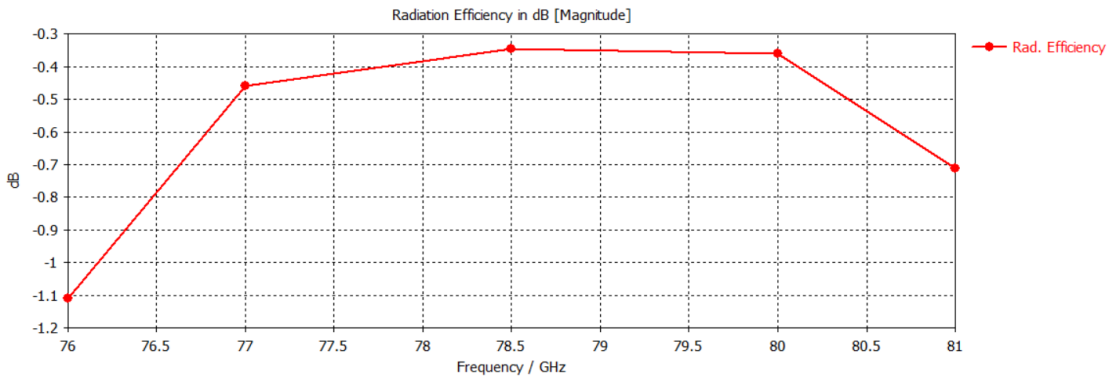

Figure 3.44: Radiation efficiency for antenna array without L-transition

The radiation efficiency for the frequency range of interest, which is that around 78.5 GHz, gives a result of around -0.346 dB, which corresponds to around 92.3% efficiency in the linear scale.

With these results, the antenna array is verified to function well, and the next step is that of building the L-transition antenna array.

3.2.4.2 WR12 waveguide feeding through an L-transition

Similar to the previous case, in order to not have an intersection between the different waveguides, a shift of the antennas has to be made. However, since an L-transition is present, there will not only be a down-shift in the y-direction by ***"y_shift"***, but also a shift in the z-direction, by ***"WR12_height+2*Lchip_tol"***. The design up to this point is shown in Fig. 3.45.

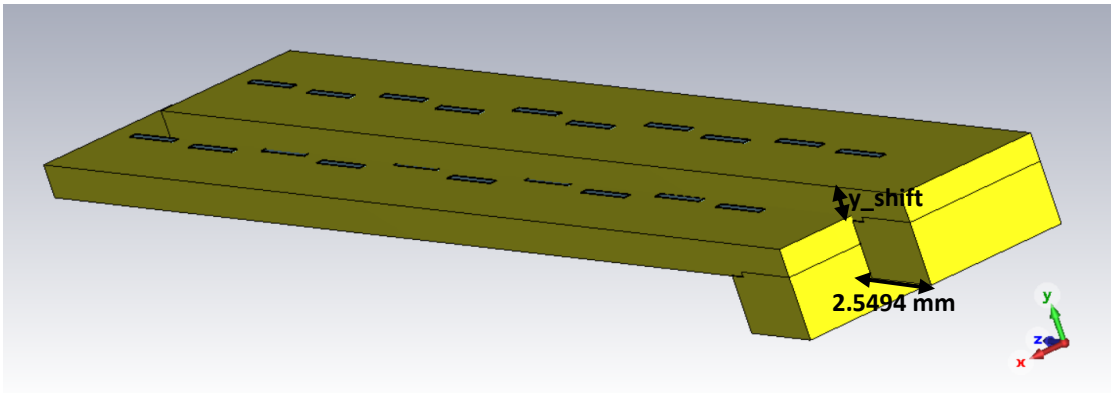

Figure 3.45: 2 antennas structure with L-transition

The next step is the adjustment of the bottom antenna to have its slots at the same level as the top antenna, by extending the upper gold layer and the slots up to the level of the top antennas by a value ***"y_shift"***. Differently from the previous case, now the slots of the two antennas will be not aligned due to the shift in the z-direction. An alignment is needed to have a good beamforming, which means having the antennas work together to produce a strong and focused beam in a certain direction. To have this alignment, an adjustment on the length of either the top or the bottom antenna must be done. The bottom antenna would have to be trimmed whereas the top antenna would have to be elongated. The first case is not feasible, since that way, the antenna would be too short and the slots of the antennas would start where the L-transition happens, meaning that it would not work. On the other hand, the second solution is feasible and involves the elongation of the top antenna by the same length that the bottom antenna was shifted in the z-direction. The elongation starts before the slots and involves in extending the waveguide. The design after these adjustments is shown in Fig. 3.46 below.

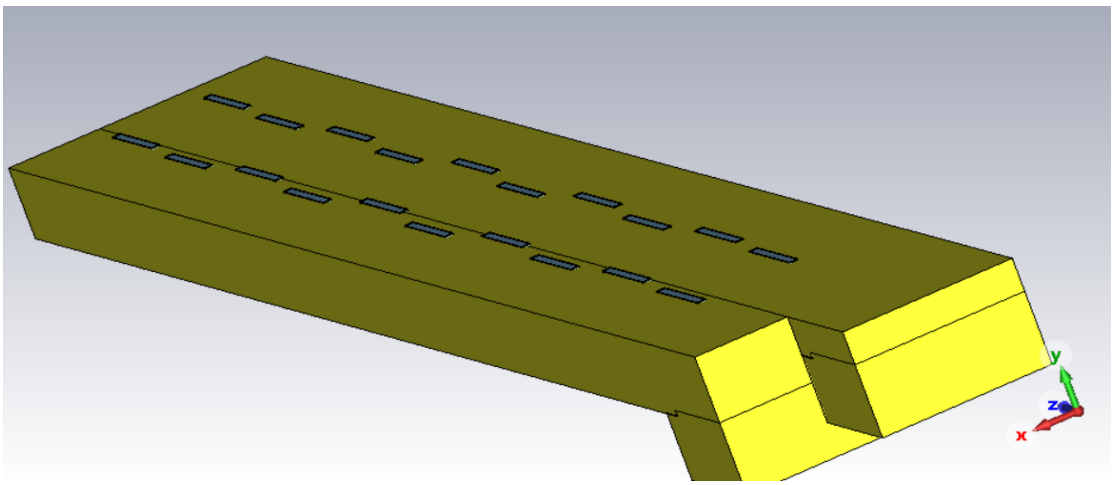

Figure 3.46 (a): 2 antennas structure with L-transition

The next step is the same as the one done in the previous sub-chapter. A double-width slot topology is applied, doing the same adjustments as before.

Fig 3.46 (b) shows this design.

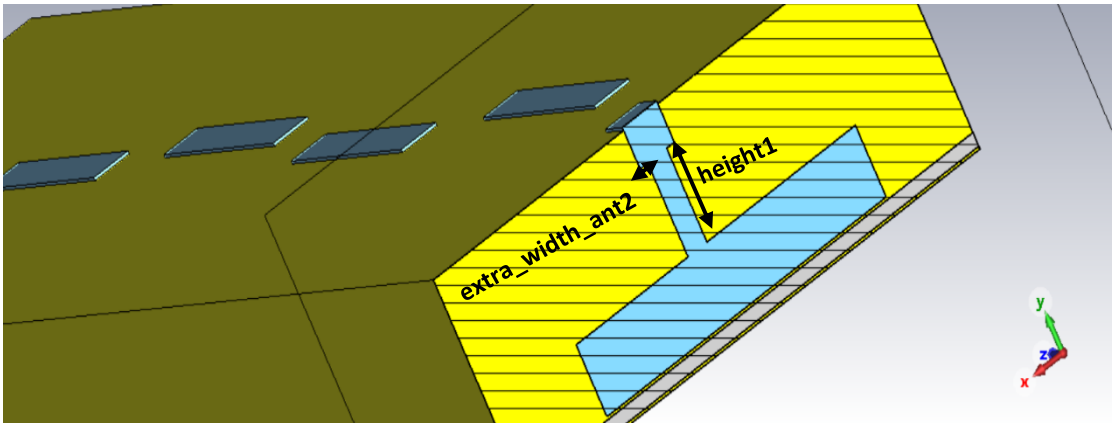

Figure 3.46 (b): 2 antennas structure with L-transition

There can be noticed the slots that have a certain width up to a certain height and another width on the remaining height. The parameters ***height1***, ***extra_width_ant2*** are the ones which will be adjusted in order to have the desired result. The outcome of this double width structure for dimensions equal to:

- **extra_width_ant2=0.07mm**
- **height1=0.4mm**

is given in figure 3.47 (a), (b) and (c).

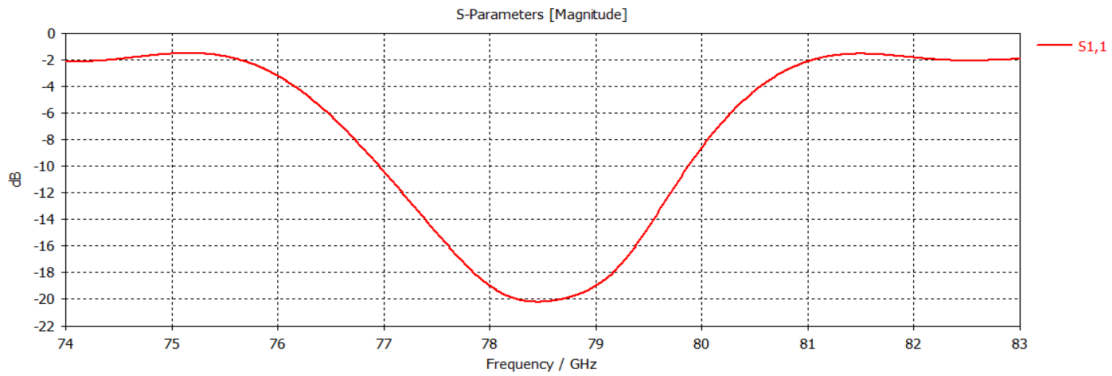

Figure 3.47 (a): S11 parameter of the adjusted antenna only without L-transition

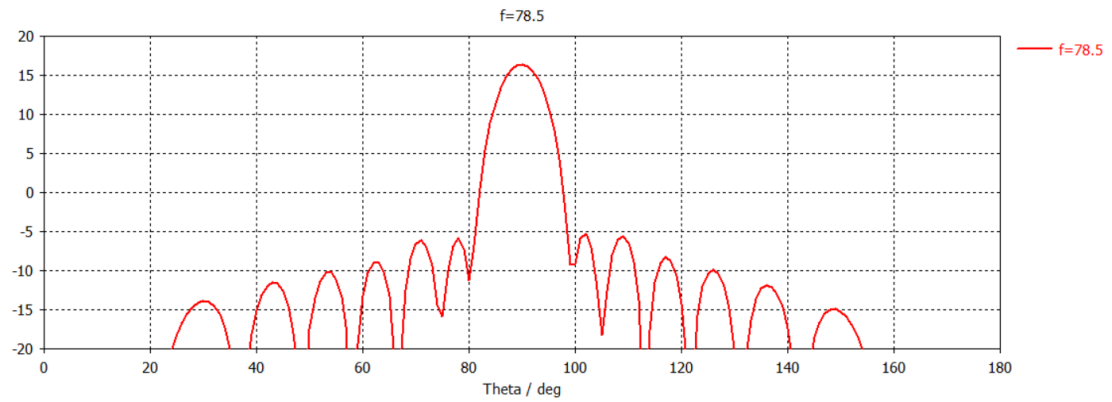

Figure 3.47 (b): Directivity pattern of the adjusted antenna only without L-transition.

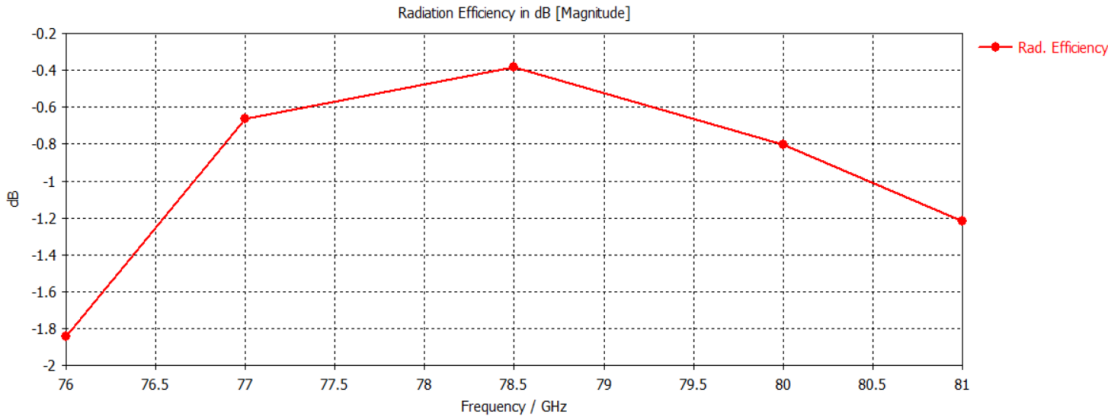

Figure 3.47 (c): Radiation efficiency of the adjusted antenna only without L-transition

The results show that the antenna has a bandwidth of around 2GHz at the -15dB mark and a bandwidth of around 3GHz at the -10dB mark. The minimum value is around -20 dB. The radiation pattern, affected by the slotted waveguide shows again a main lobe of around 16.3 dB and side lobes lower than the -5dB mark, which is very similar to the result of the single antenna in the L-transition and the antenna without the transition at all. As for the radiation efficiency, it has a peak at the 78.5GHz of around -0.4dB.

Finally, a full array of 8 antennas has been designed, consisting of 4 top ones and 4 bottom ones. Based on what was designed up to now, the two antennas were translated by the half-wavelength distance of 1.91mm. Everything is set in such a way that the inner parts of the different waveguides do not interfere with each other and that there is enough gold layer around them for separation as shown in Fig. 3.48.

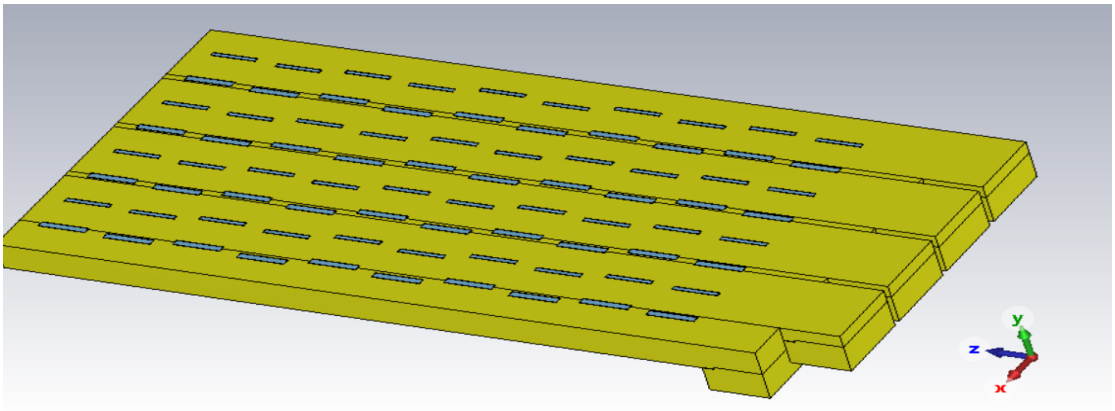

Figure 3.48: Antenna array with L-transition

The ports have been set in the following way: the top antennas are the odd ports, whereas the bottom antennas are the even ports. A bottom view of the array of antennas, in order to see the port configuration, is shown in Fig. 3.49.

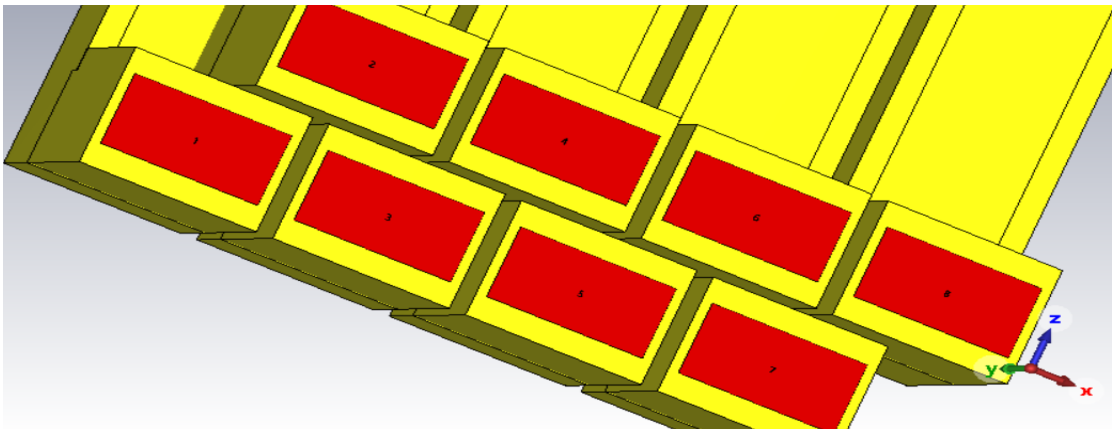

Figure 3.49: Antenna array with L-transition ports view

Different dimensions were simulated, and as in the case of array without the L-transition, it was noticed that an additional change was needed in the upper antennas. The s-parameter of the odd port antennas needed a small shift to the left in order to be centered around the 78.5GHz mark. In order to achieve this, a similar change as on the last chapter is made and the width of the slots is directly changed and increased by a factor called ***"extra_width_ant1"***. To fit the operation and have it on the same band as the s-parameter result of the even port antennas, the value of *vacuum_tol_ant1=0.0225mm* was chosen. One result with this applied change is shown below in Fig. 3.50.

- **extra_width_ant2=0.07 mm**
- **height1=0.3mm**
- **extra_width_ant1=0.0225 mm**

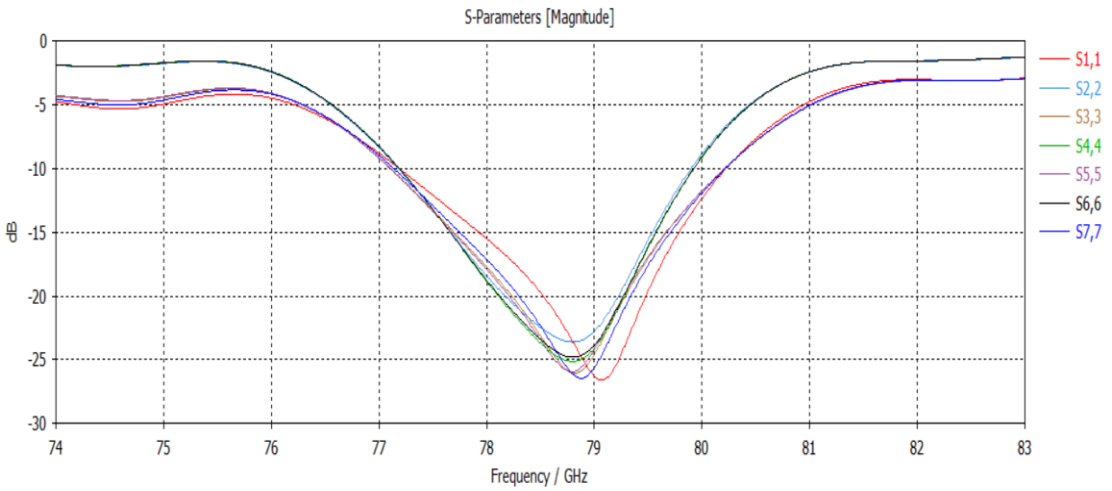

Figure 3.50: S11 parameter of the antenna array with L-transition

However, it can be noticed that the s-parameter for the antenna with port 1 needs some more adjustments. During the optimization process, it was noticed that the bigger the width adjustment is for the odd antennas, the more the corresponding s-parameter shifts to the right. Since, the s-parameter for the first port antenna is already shifted a lot to the right, it was decided to use a smaller width for that antenna and continue to use the same width adjustment for the other antennas. The result of this change is shown below in Fig. 3.51.

- **extra_width_ ant2=0.07 mm**
- **height1=0.3mm**
- **extra_width_ant1=0.0225 mm for antennas with port 3,5,7**
- **extra_width_ant1=0.018 mm for antenna with port 1**

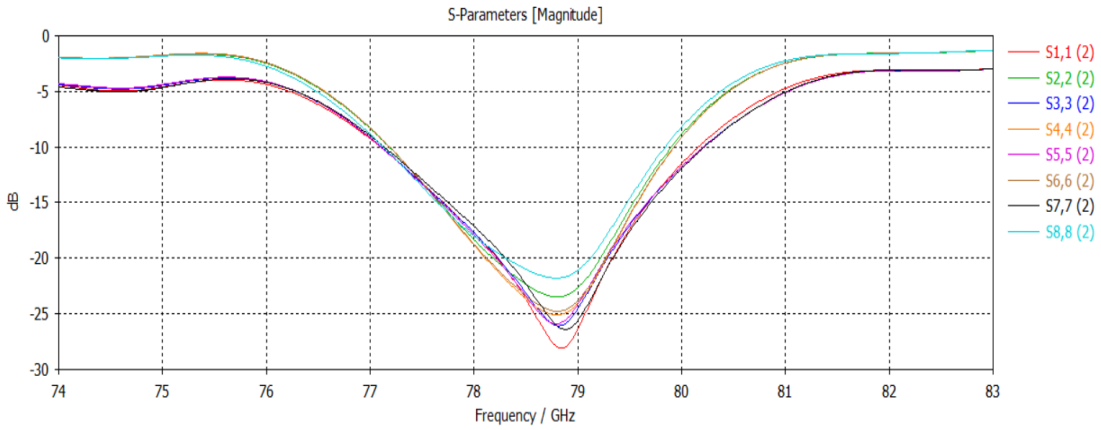

Figure 3.51: S11 parameter of the antenna array with L-transition with extra shift on antenna 1

Here, it can be noticed that the s11 parameter has been shifted more to the left and all the s-parameters are almost on the same band. There is a nearly 2GHz bandwidth for the -15dB level, and a nearly 3GHz bandwidth for the -10 dB level. This result is very similar to the previous case, in which there was the direct feeding of the antennas. This shows that the L-transition has been designed in a good way and is doing its job correctly.

As for the directivity pattern, the same discussion as the previous case can be made. The ports have been shifted in the y-direction and the z-direction. So, in order to have a correct showing of the directivity pattern, the ports should be fed with a certain phase shift from one another.

The y-direction shift is equal to -0.675mm, which corresponds to a phase shift of

$$k * L\_y = -1.1102\, rad = -63.6°$$

The z-direction shift is equal to 2.5494mm, which corresponds to a phase shift of

$$k * L\_y = 4.1933\, rad = 240°$$

The total phase shift is equal to 176.6°. The result of the directivity pattern after these adjustments is given in Fig.3.52 in three types: 3D, 2D cartesian and 2D polar plot.

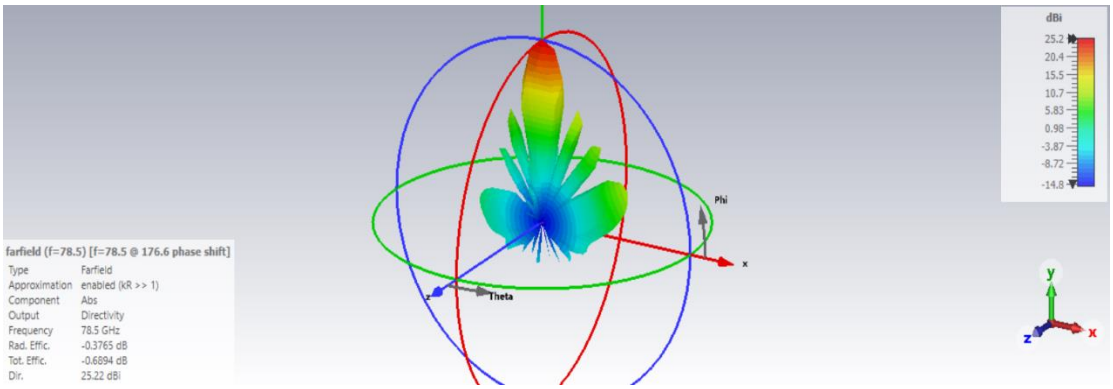

Figure 3.52 (a): 3D far-field directivity pattern for antenna array with L-transition

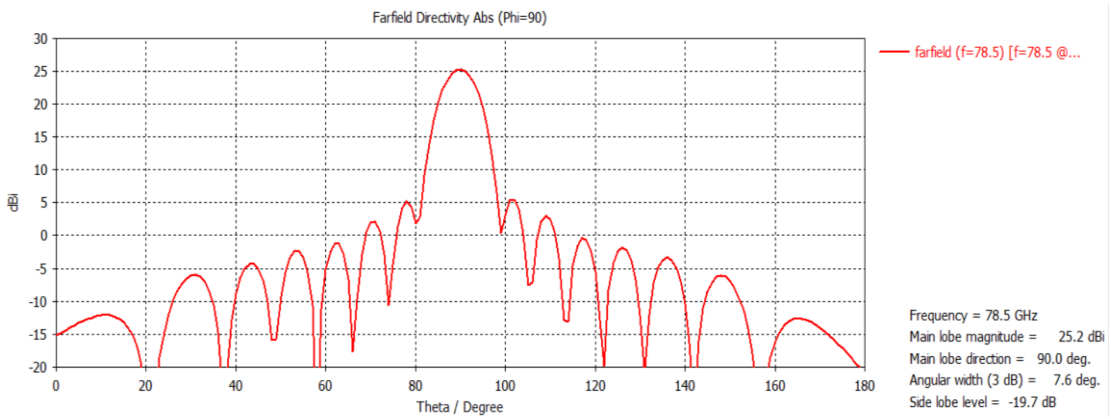

Figure 3.52 (b): 2D cartesian far-field directivity pattern for antenna array with L-transition; $\boldsymbol{\varphi = 90°}$

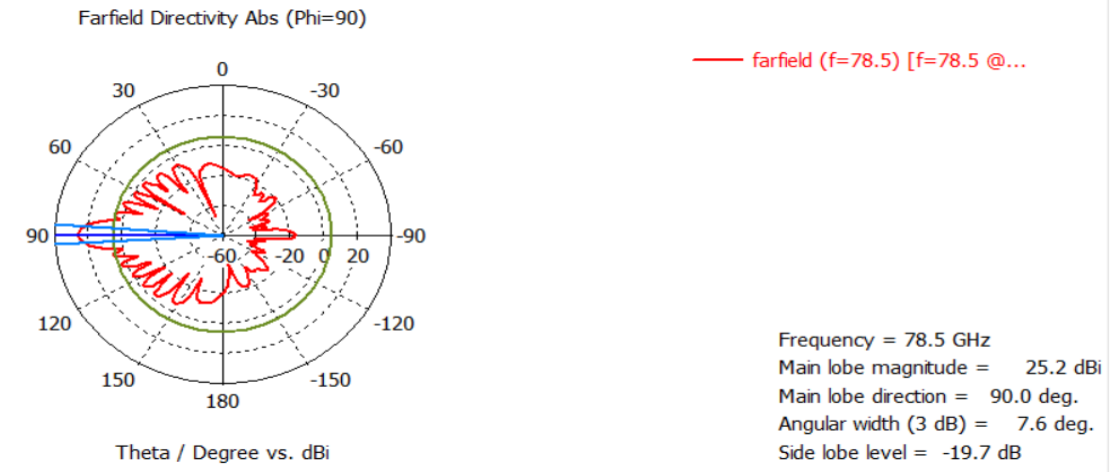

Figure 3.52 (c): 2D polar far-field directivity pattern for antenna array with L-transition; $\boldsymbol{\varphi = 90°}$

The directivity pattern shows that a good beamforming has been achieved. Almost all the power from all the single antennas has been combined with each-other and have reached a main lobe level of 25.2dB, which is 8.9 dB higher than the single antenna main lobe level. As for the side lobes, they are on a level which is -19.7 dB lower.

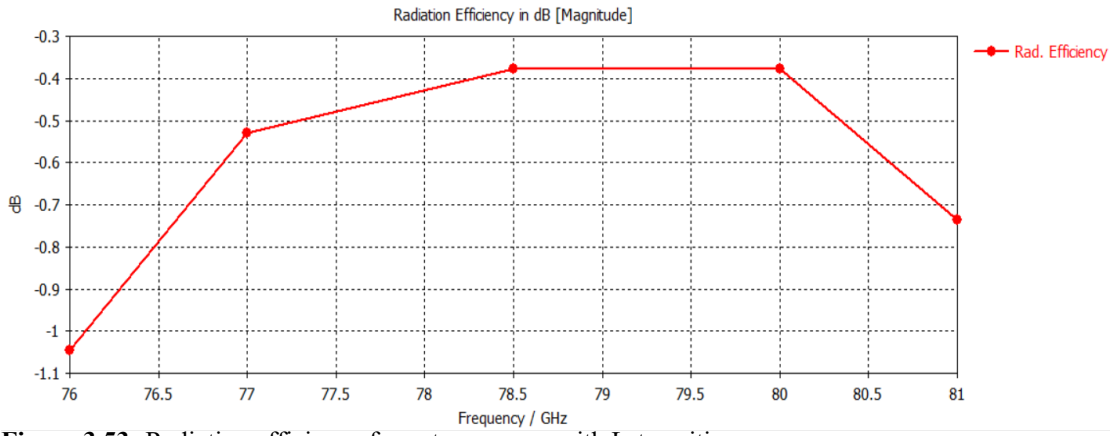

Figure 3.53: Radiation efficiency for antenna array with L-transition

A combination of the radiation efficiency is given in Fig. 3.53. It shows that for the frequency of interest, the radiation efficiency is -0.376dB, which corresponds to 91.7% efficiency in the linear scale.

A further step has been made, in order to have a more compact design and to remove the PCB dielectric from the bottom part of the antennas. Everything has been made in gold. The design is shown in Fig. 3.54.

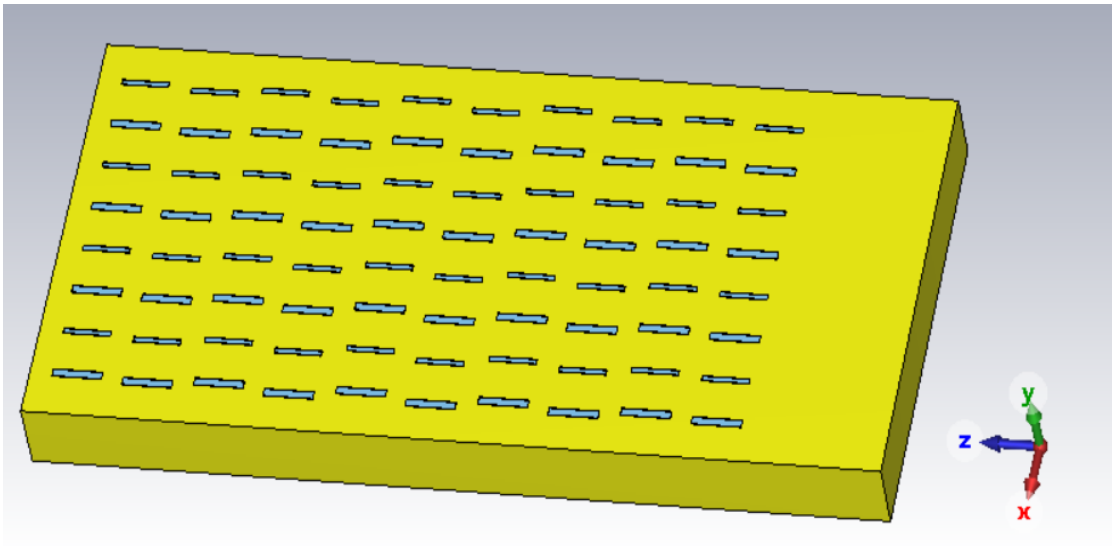

Figure 3.54 (a): Top view of the antenna array pack

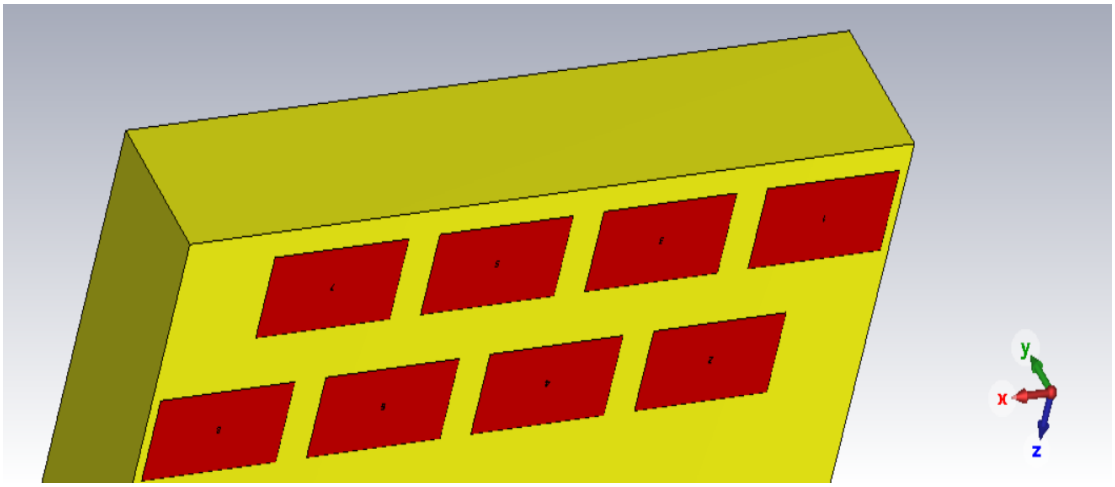

Figure 3.54 (b): Bottom view of the ports of the antenna array pack

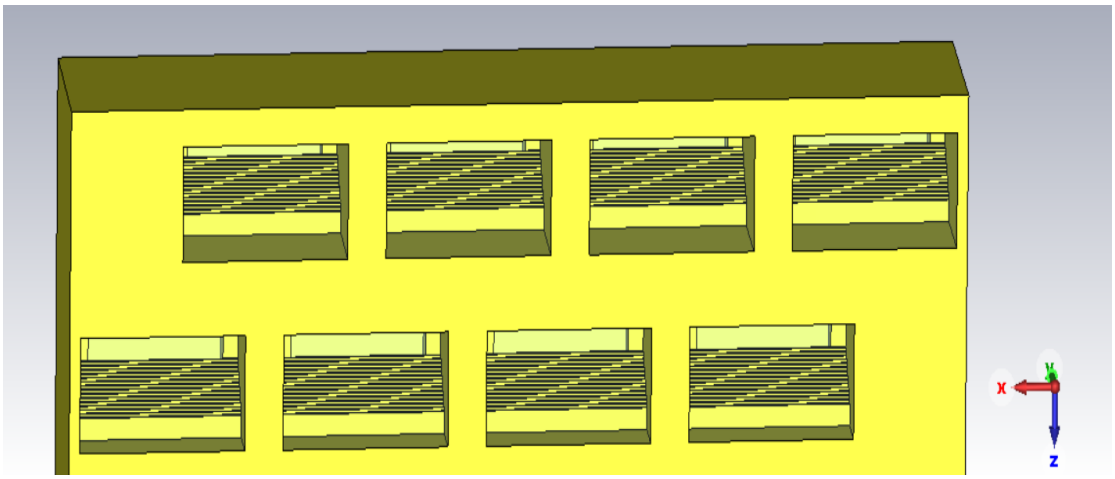

Figure 3.54 (c): Bottom view of the L-transitions of the antenna array pack

Using the following parameters:

- **extra_width_ant2=0.07 mm**
- **height1=0.3mm**
- **extra_width_ant1=0.0225 mm**

The resulting s-parameters are shown in Fig. 3.55.

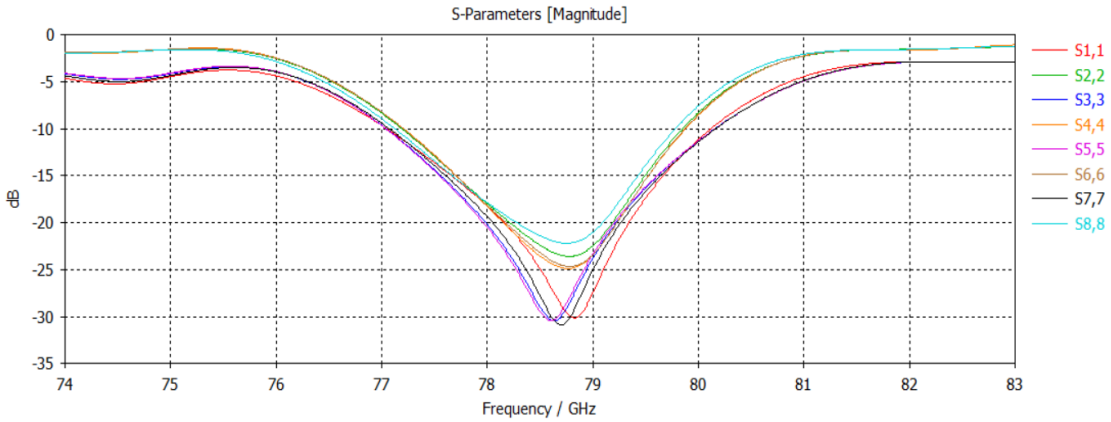

Figure 3.55: S-parameter result of the full antenna array pack.

They are centered around 78.5GHz and have similar bandwidth properties as the previous case which included the dielectric. For the directivity, the same phase shift manipulation has to be done at the port signal. The result is the following, given in Fig. 3.56 in 2D Cartesian, Polar, and 3D.

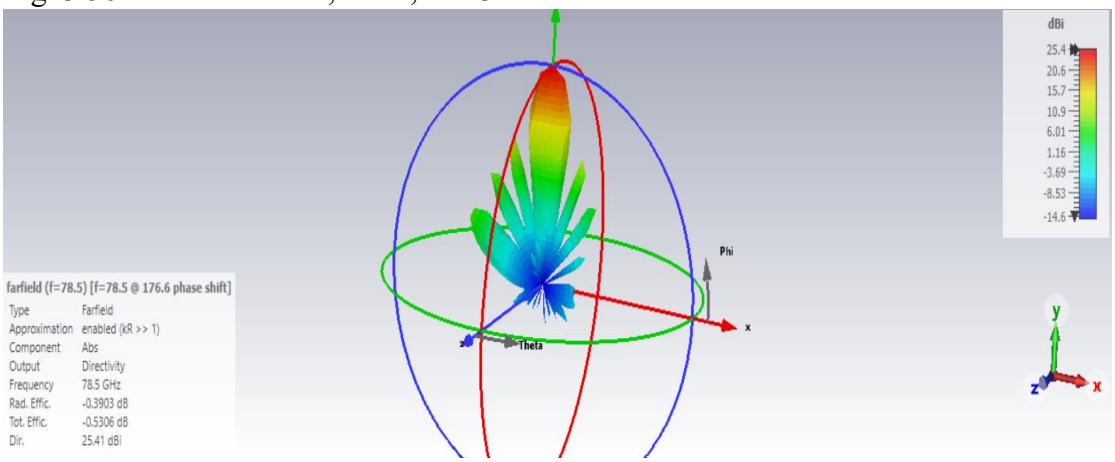

Figure 3.56 (a): 3D far-field directivity pattern for the full antenna array pack

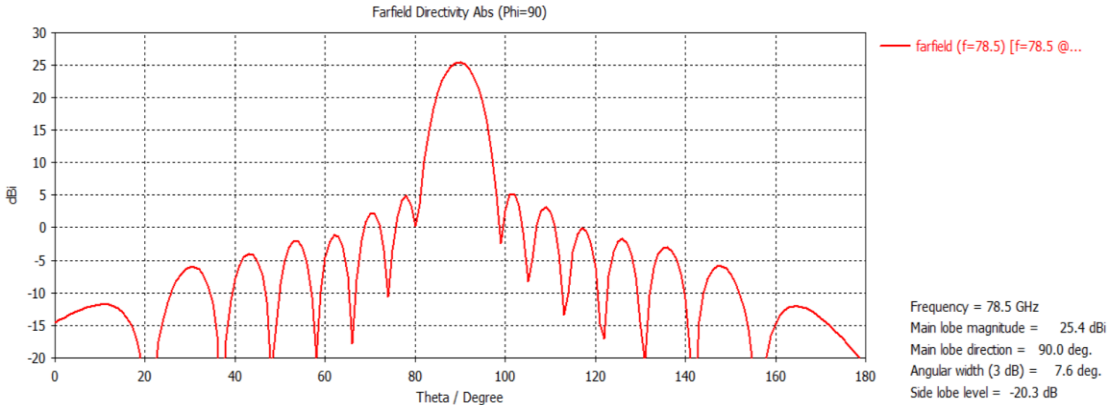

Figure 3.56(b): 2D cartesian far-field directivity pattern for the full antenna array pack; $\boldsymbol{\varphi = 90°}$

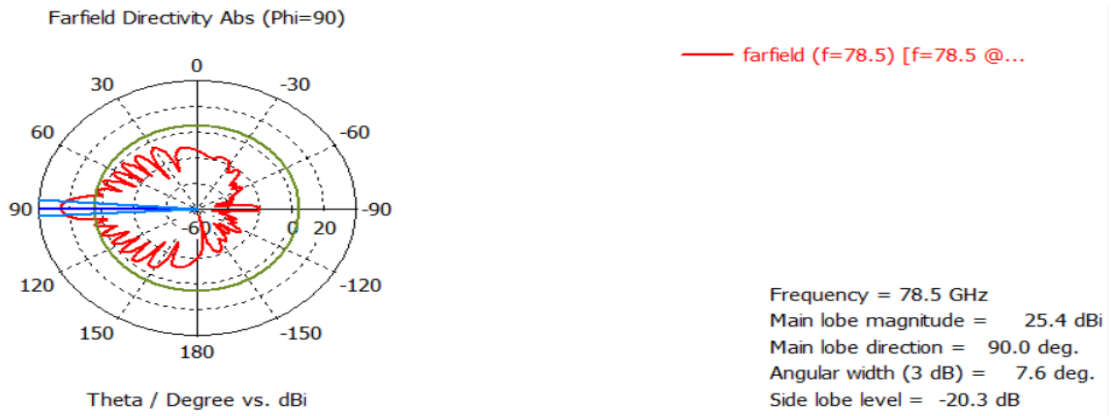

Figure 3.56 (c): 2D polar far-field directivity pattern for the full antenna array pack; $\boldsymbol{\varphi = 90°}$

The beamforming qualities are maintained and are on a similar level to the previous case which included the PCB dielectric on the bottom of the antennas. More in detail, the main lobe level is around 25.4 dB, whereas the side lobes are 20.3dB lower than this level.

The combined radiation efficiency is given in Fig.3.57.

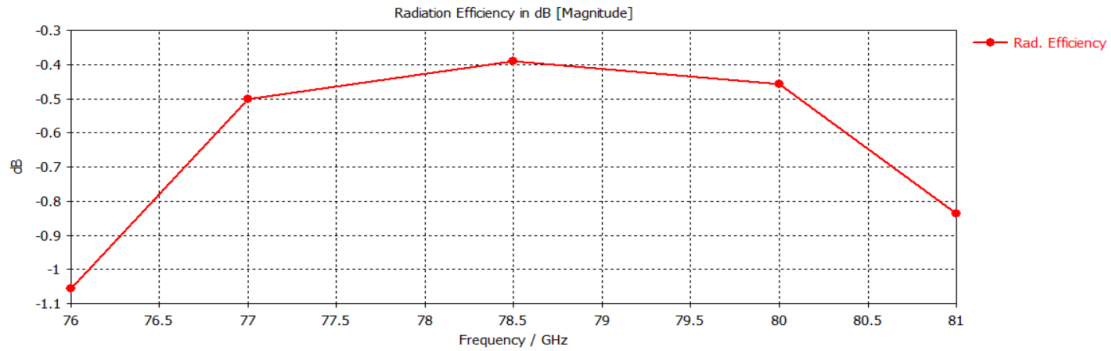

Figure 3.57: Radiation efficiency for the full antenna array pack

The radiation efficiency level for the frequency of interest is of around -0.39dB, which corresponds to 91.4% radiation efficiency in linear scale.

A final adjustment can be made, in order eliminate the elongation of the top antennas. This adjustment consists of having the bottom antennas rotated with respect to the top antennas. So, the feeding port of the odd antennas will be on the ending side of the top antennas, hence there won't be an overlap of the L-transition segments. This topology is shown in Fig.3.58.

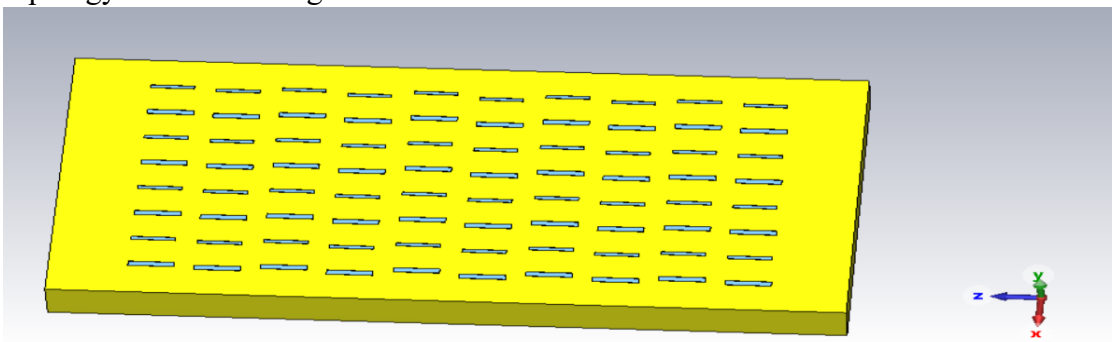

Figure 3.58 (a): Top view of the readjusted full antenna array pack

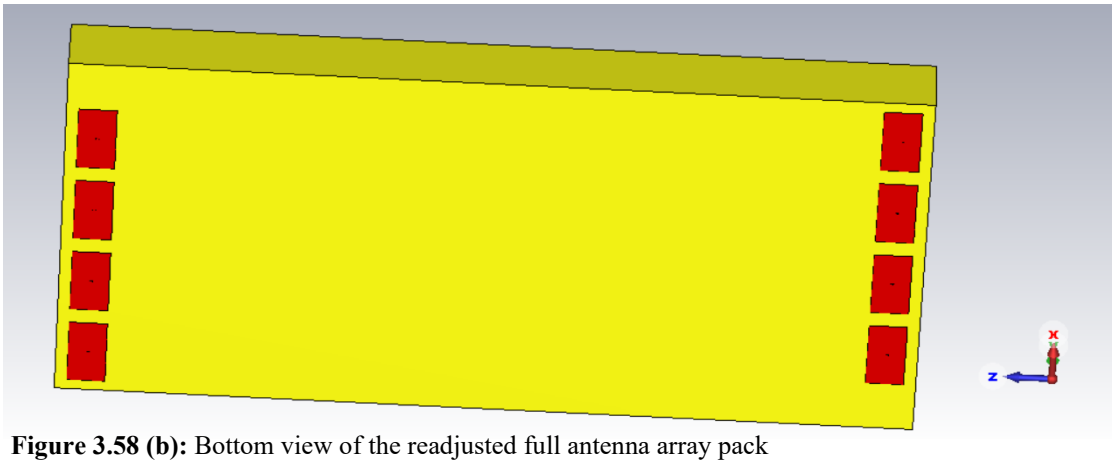

Figure 3.58 (b): Bottom view of the readjusted full antenna array pack

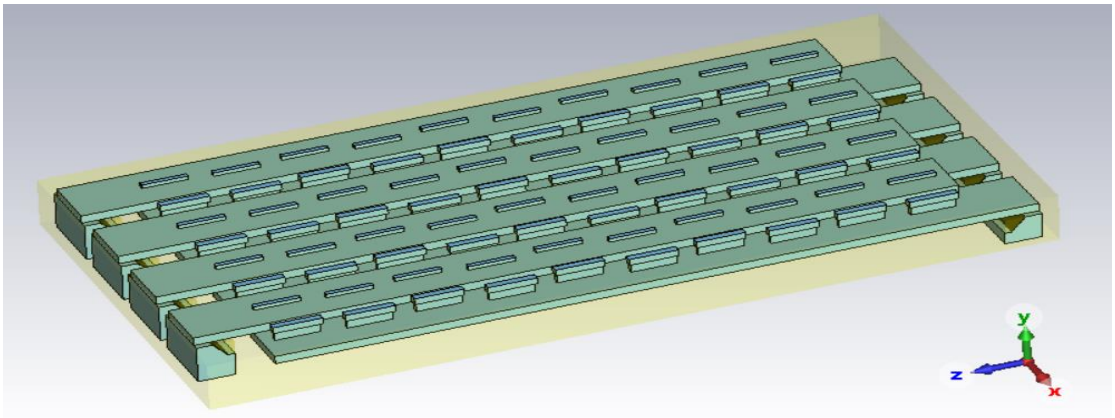

Figure 3.58 (c): Inner view of the readjusted full antenna array pack

After some simulations, it was decided that in order to adjust the s-parameters, the technique used in the previous chapter where the first antenna had a different width adjustment with respect to the other odd antennas will be applied. The final parameters are the following and the result is given in Fig. 3.59:

- **extra_width_ant2=0.07 mm**
- **height1=0.3mm**
- **extra_width_ant1=0.0225 mm for antennas with port 3,5,7**
- **extra_width_ant1=0.018 mm for antenna with port 1**

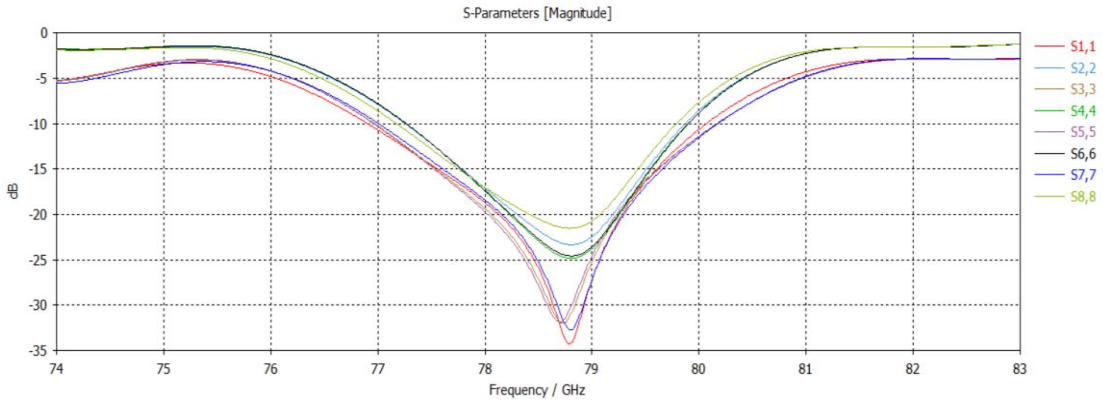

Figure 3.59: S-parameter result of the readjusted full antenna array pack.

For the directivity, only the phase shift for the y-direction will be applied, which is equal to -63.6°. This is because there is no more an elongation of the upper antennas, which would increase the phase difference. In this case, the slots are aligned with each other, and even though the feeds are in opposite positions, having antennas wihch are symmetrical in terms of slot tapering and a short circuited last slot, helps maintain the good beamforming qualities. The results in 3D, 2D cartesian and 2D polar plot are given in Fig.3.60.

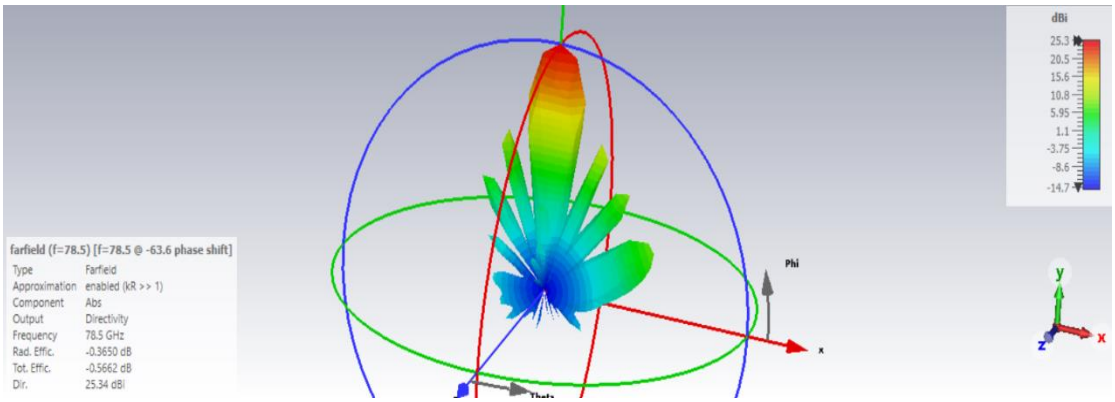

Figure 3.60 (a): 3D far-field directivity pattern for the readjusted antenna array pack

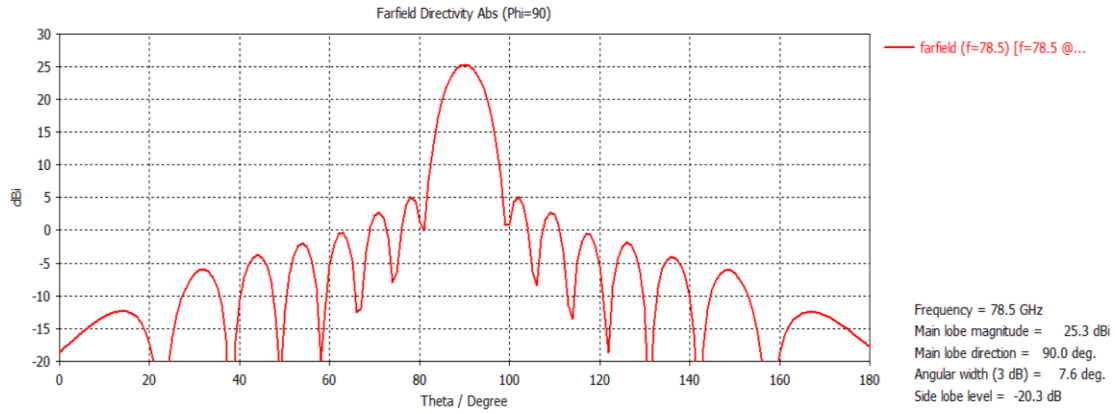

Figure 3.60 (b): 2D cartesian far-field directivity pattern for the readjusted antenna array pack; $\boldsymbol{\varphi = 90°}$

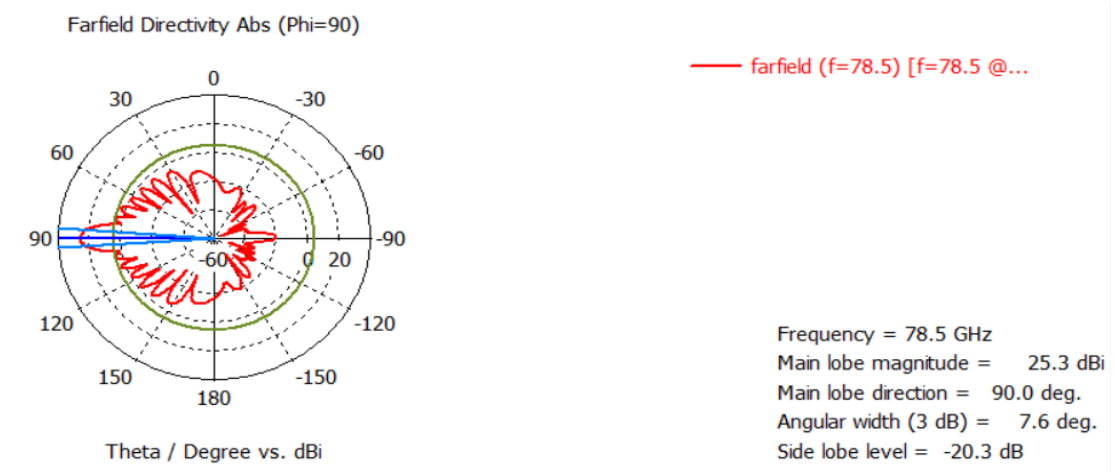

Figure 3.60 (c): 2D polar far-field directivity pattern for the readjusted antenna array pack; $\boldsymbol{\varphi = 90°}$

This result goes in line with the previous cases and the theoretical results. The main lobe is on a level of 25.3dB, whereas the side lobes are on a level 20.3dB lower.

As for the radiation efficiency, its result is given in Fig. 3.61.

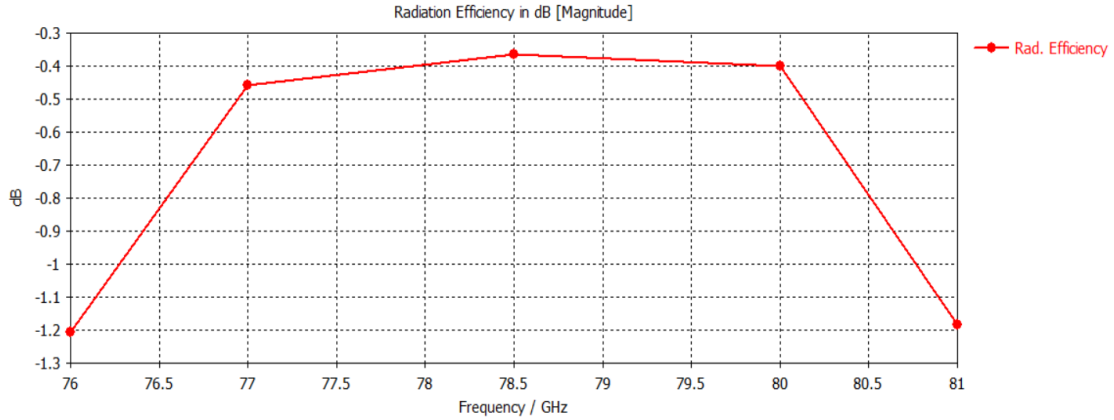

Figure 3.61: Radiation efficiency for the readjusted antenna array pack

It has a value of -0.36dB on the range of interest, which corresponds to around 92% radiation efficiency on a linear scale.

3.2.5 Conclusion

To conclude, the design of the 3D waveguide antenna array has shown great promise in simulations, with good results obtained in several keys. The S-parameters of the antenna array demonstrate a good impedance matching within the antenna, indicating high efficiency and signal quality. The simulations also show that the antenna array has a high directivity, meaning it can transmit and receive signals with high precision and accuracy, making it ideal for automotive radar applications. Currently, the antenna is in the mechanical workshop for the fabrication stage and the next step will be the measurement and comparisons with the simulated results. Although the fabrication of the antenna was not possible within the time frame of this thesis, the simulation results suggest that the proposed design has great potential to improve the performance of automotive radar systems.

The success of this thesis can be attributed to the careful design of the antenna array, taking into account the characteristics of automotive radar systems. All the different results and design steps offer a good insight and can be used as a guide for future works in the field. It is recommended to have further research, to fabricate and test the proposed antenna design to provide valuable feedback on the actual performance of the antenna, offering further optimization possibilities. In the end, it can be finally integrated within a radar system to evaluate its performance in a realistic environment.

References

[1] G. Rollmann, V. Schmid; *Advanced Microsystems for Automotive Applications* 2003 (215-221), 2003

[2] Naresh K. Darimireddy, U. Mohan Rao, Chan-Wang Park, I. Fofana, M. Sujatha and Anant K. Verma; *Perspectives of Convertors and Communication Aspects in Automated Vehicles, Part 2: Printed Antennas and Sensors for Automotive Radars*, 2021

[3] Antenna Patterns and Their Meaning. CISCO White Paper, 2007

[4] S. Drabowitch,A. Papiernik, H. Griffiths, J. Encinas, Hugh Griffiths & Bradford L. Smith; *Printed antennas and Modern Antennas, 117-139,* 1998

[5] M. T. Sebastian, *Dielectric Materials for Wireless Communication*, 11-47, 2008

[6] Nassir Guellil, Chemseddine Zebiri, Djamel Sayad,I.T.E. Elfergani, Farid Djahli, Abdalfettah Asharaa, Jonathan Rodriguez, and Raed Abd-Alhameed; *Design of Optimum Microstrip to Substrate Integrated Waveguide Transition,* 2021

[7] Optimum compact H- and E-plane corners in rectangular waveguide July 2004 Authors: Alicia Casanueva Jose Antonio Pereda Angel Mediavilla

[8] Robert S. Elliott; *The Design of Waveguide-Fed Slot Arrays, 16-20, 1988*

[9] Hilal M. El Misilmani, Mohammed Al-Husseini, Karim Y. Kabalan; *Design procedure for planar slotted waveguide antenna arrays with controllable sidelobe level ratio for high power microwave applications,* 2020

[10] H. El Misilmani, M. Husseini, K. Y. Kabalan; *Design of slotted waveguide antennas with low sidelobes for high power microwave applications*, 2015

Sitography

https://www.britannica.com/technology/radar/Doppler-weather-radar

https://www.elprocus.com/radar-basics-types-and-applications/

https://www.everythingrf.com/community/automotive-radar-basics

https://electriciantraining.tpub.com/14183/css/Waveguide-Modes-Of-Operation-Continued-39.htm

https://www.everythingrf.com/tech-resources/waveguides-sizes/wr10

https://www.everythingrf.com/tech-resources/waveguides-sizes/wr12

https://pixabay.com/